Aus dem Medizinischen Zentrum für Innere Medizin
Aus der klinischen Forschergruppe „Chronische Atemwegserkrankungen“ in der Klinik für Pneumologie
Geschäftsführender Direktor: Prof. Dr. med. Claus Vogelmeier

des Fachbereichs Medizin der Philipps-Universität Marburg
in Zusammenarbeit mit dem Universitätsklinikum Gießen und Marburg GmbH, Standort Marburg

Histopathological Morphometry of Human Endobronchial Biopsies – a Comparison of Conventional Quantitative Analyses and Stereological Designs

Inaugural-Dissertation zur Erlangung des Doktorgrades der gesamten Humanmedizin
dem Fachbereich Medizin der Philipps-Universität Marburg
vorgelegt von

Vlad Antonio Bratu

aus Bucureşti, România

Marburg, 2008

Angenommen vom Fachbereich Medizin der Philipps-Universität Marburg am: 17.08.2009

Gedruckt mit Genehmigung des Fachbereichs.

Dekan: Prof. Dr. med. Matthias Rothmund

Referent: Prof. Dr. rer. nat. Heinz Fehrenbach

Korreferent: Prof. Dr. med. Roland Moll

To my parents, my friends and the family Fehrenbach

To err is human, to forgive is divine – but to include errors in your design is statistical.

Leslie Kish

TABLE OF CONTENTS

LIST OF TABLES

LIST OF FIGURES

LIST OF ABBREVIATIONS AND SYMBOLS

2D	Two-Dimensional
2D cell	Two-dimensional count of cell profiles (with and without nucleus)
2D nucleus	Two-dimensional count of nuclear profiles
3D	Three-Dimensional
α	Probability of type I error
a_p	Area-per-Point
ABC	Avidin-Biotin Complex
AHR	Airway Hyperresponsiveness
ATS	American Thoracic Society
BA	Block Advance
BAL	Bronchoalveolar Lavage
B.C.	Before Christ
CD##	Cluster of Differentiation
CE	Coefficient of Error
COPD	Chronic Obstructive Pulmonary Disease
CV	Coefficient of Variation
d	Difference
dim	Dimensions
DAB	3,3'-Diaminobenzidine
EGF	Epithelial Growth Factor
EGFR	Epithelial Growth Factor Receptor
ERS	European Respiratory Society
est	Estimator of
F	Female
FEV_1	Forced Expiratory Volume in the first second
FVC	Forced Vital Capacity
GOLD	Global Initiative for Chronic Obstructive Lung Disease
Ig	Immunoglobulin
IHC	Immunohistochemistry

IUR	Isotropic Uniform Random
L_p	Length-per-Point
m	Mean
M	Male
n	Number of subjects
N_A	Profile number per unit area
$N_{A\ cell}$	Cell profile number per unit area
$N_{A\ nucleus}$	Nuclear profile number per unit area
N_V	Cell number per unit volume (Numerical density)
N. A.	Not analysed
NS	Nonsignificant
OCV	Observed Coefficient of Variation
OV	Observed Variance
P	P-value
PAS	Periodic Acid Schiff
PBS	Phosphate Buffered Saline
PC_{20}	Provocative Concentration of a substance causing a 20% fall in FEV_1
PDGF	Platelet-Derived Growth Factor
pg	Page
r	Pearson's product-moment correlation coefficient
r^2	Coefficient of determination
r_s	Spearmann's rank order correlation coefficient
RBM	Reticular Basement Membrane
$s_{d\|m}$	Standard error of the regression estimates of *d* on *m* / Standard deviation of the residuals of the regression of *d* on *m*
SD / s	Standard Deviation
SE	Standard Error
SURS	Systematic Uniform Random Sampling
TBS	TRIS Buffered Saline
TGF	Transforming Growth Factor
TRIS	Trisaminomethane hydrochloride

UR	Uniform Random
W	Wilcoxon’s signed rank test statistic

1 Introduction

1.1 Chronic inflammatory airway disorders

Airway inflammation is a common characteristic feature of chronic airway diseases like asthma and chronic obstructive pulmonary disease (COPD). Both inflammatory conditions are associated with structural remodelling of the airways, which is inappropriate to the maintenance of normal lung function. Asthma and COPD are not very well defined disease entities but rather non-specific clinical terms describing two different patterns of obstructive airway disease with respect to reversibility, spontaneously or under therapy. The ERS and ATS guidelines (1985; 1995) define COPD as ‘a disorder characterized by reduced maximum expiratory flow and slow forced emptying of the lungs, features which do not change markedly over several months’, whereas ‘asthma is a clinical syndrome characterized by increased tracheobronchial responsiveness to a variety of stimuli, manifest as variable airway obstruction’. These definitions point out that both asthma and COPD are not disease entities *per se*, but rather each is a complex of conditions that contribute to airflow obstruction. In asthma the airflow limitation is usually variable over short periods of time and is reversible, albeit an underlying irreversible component may develop upon exposure to noxious agents, particularly cigarette smoke (Thomson et al. 2004), or when inflammation persists in association with repeated allergen or occupational exposure (Lange et al. 1998). In COPD, the limitation, particularly of the expiratory flow, is usually persistent and typically shows a more rapid advance with age than is normal. Although the underlying inflammation of these two diseases is very different in most cases, some patients with COPD may have features of asthma resulting in a mixed inflammatory pattern with increased eosinophils and partial reversibility of the airflow obstruction under anti-inflammatory therapy (Chanez et al. 1997). This evidence led to the conclusion that in reality asthma and COPD are not single entities; instead each seems to have a spectrum of reversibility and there is overlap, most likely associated with the varying extent and the mix of both structural and inflammatory changes and the predominant anatomic site within the lung at which these occur (Jeffery 2004).

In atopic and non-atopic asthma activated ($CD25^+$) T-helper ($CD4^+$) lymphocytes and activated ($EG2^+$) eosinophils are increased in the inflammatory infiltrate of the subepithelial layer of the airways (Azzawi et al. 1990; Bradley et al. 1991; Robinson et

al. 1992). Nevertheless, in non-atopic severe asthma a significant neutrophilia was noticed (Wenzel et al. 1999). In contrast, the chronic inflammation in smokers with COPD is characterized by increased numbers of total leucocytes ($CD45^+$), T-lymphocytes ($CD3^+$), the subset of suppressor/cytotoxic T-lymphocytes ($CD8^+$) and macrophages ($CD68^+$) (Lacoste et al. 1993; Saetta et al. 1993; Di Stefano et al. 2004). However, Saetta et al. (1994; 1996) found that the numbers of tissue eosinophils are markedly and significantly increased when there is an exacerbation of bronchitis, similar to those reported in stable asthma. Interestingly the increase of the $CD8^+$ T-cell subset correlates with the decline in lung function as quantified by FEV_1 (O'Shaughnessy et al. 1997; Saetta et al. 1998). These findings describing the inflammatory pattern are not only relevant for understanding the pathophysiology of the chronic disease but also in elucidating its aetiology. As only 15% of life-long smokers develop emphysema (Pauwels and Rabe 2004), constitutional factors are likely to be of importance besides cigarette smoke, air pollution resulting from burning of biomass fuels and cadmium exposure. O'Shaughnessy et al. (1997) suggested that the lung susceptibility to the effects of cigarette smoke would be greater in individuals with a genetically determined low $CD4^+/CD8^+$ T-cell ratio in the peripheral blood (Amadori et al. 1995).

The structural changes that accompany the chronic inflammation are collectively referred to as 'remodelling'. It may be appropriate, as in normal lung development *in utero* or during acute reaction to injury, or 'inappropriate' when it is chronic and results in abnormally altered tissue structure and function, as for example in asthma and COPD. The anatomic site at which the remodelling occurs differs between the two clinical forms of chronic airway inflammation. In COPD it is mainly destruction of (or failure to repair) the lung parenchyma with loss of alveolar attachments to the outer wall of small airways and permanent enlargement of the airspaces distal to the terminal bronchiolus – characteristic of emphysema. In chronic bronchitis, another clinical condition of COPD, there is hyperplasia and hypertrophy of the tracheobronchial submucosal glands with a disproportionate increase in mucous acini, goblet cell hyperplasia and mucus hypersecretion in the proximal bronchi. The small airways show a chronic obstructive bronchiolitis with mucous metaplasia and hyperplasia, increased intraluminal mucus, bronchiolar smooth muscle hypertrophy, bronchiolar fibrosis and stenosis (Saetta et al. 1998). In asthma, large and small airways are structurally altered

but there is no parenchymal destruction in the asthmatic non-smoker. The airway walls show a marked smooth muscle hypertrophy of all airway generations, especially in severe and fatal asthma (Saetta et al. 1991; Carroll et al. 1993). Marked thickening of the reticular basement membrane (RBM) represents subepithelial fibrosis of the asthmatic airway and is a key feature of asthma not noticed in COPD (Jeffery 1992). Hyperplasia and hypertrophy of the mucous bronchial glands, as well as mucous metaplasia and hyperplasia with consecutive mucus hypersecretion are similar to COPD, although in asthma the normal proportion between mucous and serous glandular acini appears to be retained (Glynn and Michales 1960). Epithelial fragility is also a controversial specific feature of asthma, although recent evidence puts more emphasis on the dysfunctionality of the respiratory epithelium as a key factor in the homeostasis of the airway wall (Fixman et al. 2007; Holgate 2008). Following injury, normal epithelium reacts by increased proliferation mediated through ligands acting on epidermal growth factor receptors (EGFR) or transactivation of the receptors (Holgate et al. 1999; Tang et al. 2006). The epithelial response to such stimulation appears to be impaired in asthma, despite upregulation of EGFR and CD44, which is capable of enhancing the presentation of EGF ligands to EGFR (Lackie et al. 1997; Puddicombe et al. 2000). Consequently the epithelium is held in a repair phenotype and becomes a continuous source of proinflammatory and growth factors. Both pathophysiological and morphopathological changes of asthma are thought to be dependent on these impaired inflammatory and humoral functions of the epithelial cells (Hackett and Knight 2007; Holgate 2008). For instance the RBM thickening was shown to be a consequence of increased collagen type III and V deposition by the myofibroblasts under the stimulatory influence of the epithelial cells, involving TGF-β2 and PDGF among other mediators (Brewster et al. 1990; Vignola et al. 1997; Puddicombe et al. 2000). The smooth muscle hypertrophy is also thought to be the result of an increased release of endothelins by epithelial cells and a phenotypic alteration of the myofibroblasts (Polito and Proud 1998; Fixman et al. 2007).

As none of the clinical variables used to diagnose chronic inflammatory airway diseases can give precise and specific information about the inflammatory and remodelling processes responsible for the pathophysiology, a more direct assessment involving histopathological examination of the airway wall and/or cytology of airway secretions is necessary.

1.2 Bronchial biopsies and airway inflammation

Studies aiming at unravelling the pathophysiological mechanisms of asthma and COPD, while being able to differentiate between or at least specifically recognize the two entities, and at the clinical evaluation of drugs with disease-modifying activity require the implementation of techniques for a reliable quantification of the inflammatory and/or inappropriate remodelling processes of the airways (Jeffery 2001; Jeffery et al. 2003; Jeffery 2004). For this purpose a variety of investigative methods were developed and employed in previous research on these topics: endobronchial biopsy, bronchoalveolar lavage (BAL), induced sputum, analyses of blood, urine and exhaled air. During the last decade there has been an increasing interest in the results obtained by examination of biopsies of the airway lining, which, whilst invasive, is safe provided it is performed by experienced staff adhering to the published recommendations (NHLBI/NIAID/AAAI/ACCP/ATS 1991). The sampled bronchial mucosa comprises the respiratory epithelium and its supportive subepithelial tissue, the lamina propria. The epithelial layer forms the barrier between the external and internal environments and is the site of first interaction between environmental pathogens or allergens and the host tissue, resulting in the response initiation. In clinical studies, endobronchial biopsies offer a suitable gateway to the assessment and quantification of such airway mucosa related processes. They have provided novel information about changes which persist in the stable phase of inflammatory airway disease, changes associated with exacerbations, alterations associated with the response to allergen or to occupational pollutant exposure and reversibility of the inflammatory process following therapy or removal of the triggering environmental or occupational agent. Studies in healthy volunteers provided an invaluable baseline for comparison with disease and for differentiating normal repair processes and technical artefactual changes from real pathology (Soderberg et al. 1990; Ordonez et al. 2000). Biopsies can also be prepared as explant cultures to enable epithelial outgrowths to be studied *in vitro* for their response to chemical, immunological and mechanical damage and for their capacity to produce cytokines and chemokines, lipid and peptide mediators, reactive oxygen species, enzymes and enzyme inhibitors (Wang et al. 1996).

Whilst bronchial biopsies were much used to research the basic cellular, immunological and molecular abnormalities of airway disease, their clinical application for more

accurate diagnosis and monitoring of more specific therapy in the management of airway inflammatory conditions like asthma, chronic bronchitis, COPD and cystic fibrosis remains a major goal (Jeffery 1996). It is also probable that distinct therapy forms are required to separately target the inflammatory and remodelling processes (Barnes et al. 2000; Jeffery 2004). Since the clinical parameters used to diagnose and monitor such conditions cannot give precise information about the disease-related inflammation and structural alterations, a more direct assessment is necessary. By measuring changes in selected specific markers associated with the long-term clinical outcome, the underlying disease process can be monitored. Such biopsy markers include the number and activation of T-lymphocytes, mast cells, eosinophils and neutrophils, the structure of the airway epithelium, the RBM thickness, the number and ultrastructure of contractile and exocrine cells (Jeffery 1998; Jeffery et al. 2000).

There are now sufficient data available for biopsies to act as the basis for the validation of less invasive techniques such as BAL, spontaneous or induced sputum and bronchial brush biopsies. Nevertheless, the inflammatory phenotype may differ between the lumen of the airways (sampled by BAL), the epithelium and the lamina propria (sampled by biopsy), so that the quantitative morphologic study of endobronchial biopsies provides valuable data that cannot be obtained from BAL, sputum analysis, or exhaled breath condensates, in spite of its limitation to the relatively large airways. For example, the high numbers of neutrophils and their product, myeloperoxidase, reported in BAL from COPD subjects (Thompson et al. 1989) are in contrast with the scarcity of this cell type in the lamina propria, the zone usually quantified in endobronchial biopsies (Lacoste et al. 1993; O'Shaughnessy et al. 1997). However, upon application of an antibody against neutrophil elastase an intense positivity was noticed within the surface epithelium, a biopsy site not often quantified (Jeffery 1996; O'Shaughnessy et al. 1997). Then again, in a clinical setting the disease-associated structural remodelling of the airway wall can only be studied by endobronchial biopsy.

To simplify interpretation of future biopsy studies and facilitate greater opportunities for meta-analyses, many attempts have been made to standardise all steps, including sampling of the airway tree, excision, processing and sampling of the specimen and analysing the histology (NHLBI/NIAID/AAAI/ACCP/ATS 1991; Bousquet 2000; Poulter et al. 2000; Jeffery et al. 2000; Jeffery et al. 2003). For the remodelling assessment most previous publications employed methods based on image analysis of

one or several arbitrarily chosen sections of the investigated biopsies. Similarly, the standard practice of counting the cut cell profiles of interest in a tissue section and normalising these counts to the submucosal area or the length of the epithelial RBM, i.e., a 2D design, continues to be a popular quantitative approach of the inflammatory infiltrate of the lamina propria. These approaches failed to fully comply with the recommendations for a rigorous study design, adequate sampling and unbiased quantification imposed by the large variability between and within patients. The distribution of the cells and the morphological changes may not be uniform and sampling only one region of the specimens will not deliver data representative of the whole biopsy (Sont et al. 1997; Sullivan et al. 1998; Laprise et al. 1999). On bidimensional tissue sections, 3D structures are recognizable as transects or boundaries. Direct measurement of lengths on sections of an arbitrary orientation and interpretation of these data in terms of surface area or mean height of 3D structures are prone to serious geometrical and statistical errors leading to invalidation of the data (Howard and Reed 1998). For similar theoretical reasons the probability of visible cells being counted in a 2D section is not only proportional to their density, the variable of interest, but also to the size and the orientation of the cells relative to the sectioning plane, as well as to the thickness of the tissue section (Abercrombie 1946), thus introducing a bias in favour of larger cells. However, design-based stereological tools are available in microscopy for morphometrical studies to count particles (i.e., cells or alveoli) or measure length, area and volume without the need for any bias-prone assumptions about the geometry, orientation and distribution of the structures, i.e., a 3D design (Ochs 2006). To the best of my knowledge only one other study compared data obtained by design-based stereologic and assumption-based ‘area profile’ counting techniques (Carroll et al. 2006). The correlation analysis employed in this study to test the agreement between the two approaches is insufficient, as it only demonstrates more or less linear variation of the data, but not their ‘equality’ (Altman and Bland 1983; Gallagher 1996). Another study proposed a stereological method based on orthogonal intercepts and correction for tangential cuts for measuring the RBM thickness in healthy and asthmatic subjects and compared the obtained values with previous reports, which employed uncorrected point-to-point measurements in arbitrary sections (Ferrando et al. 2003).

1.3 What is morphometry?

1.3.1 Classical geometry

The basic geometrical principles were first used by ancient Egyptians. About 6000 years ago they employed surface area measurements to calculate their land areas. They did this by marking the land boundaries with ropes, whose length, an indirect measure of the enclosed area, was measured. They were the first humans to use geometrical approaches to solve practical problems. A broader usage of geometry was promoted by the Greeks, who used geometrical principles in architecture, road, wagon and ship building and in gymnasiums. After Pythagoras (582 – 500 B.C.) and his well known theorem, Euclid (330 – 275 B.C.), another famous Greek mathematician, made important contributions to the use of geometry: his work *Elementa* deals with planar and spatial geometry and number theory. The classical Euclidean geometry enables the construction of regular geometric objects and the understanding of the mathematical relationships governing their shape. These approaches, however, are not valid for biological structures since they do not fit in the models of classically shaped objects and also show a large variation. Therefore, applying classical geometrical principles and formulae to biological elements will introduce a bias due to this variability.

1.3.2 Stochastic geometry and probability theory

Starting in the 15th century several contributions established the theoretical foundations of morphometry. The term *morphometry* is derived from the Greek and means ‘measurement of form’.

In the Habsburg Empire, today Italy, the mathematician Bonaventura Francesco Cavalieri (1598 – 1647), a student of Galileo Galilei in Florence during the height of the Italian Renaissance, became inspired by the works of Euclid and started applying classical geometrical principles to practical problems. In 1635 his discovery made him famous in morphometrical science. Cavalieri then showed that the volume of a randomly shaped object can be estimated in an unbiased manner from the sum of areas and the thickness of sections cut though the object. This deviation from classical geometry is today the most common stereological method for estimating the reference volume of biological structures from their areas on tissue sections.

The French mathematician Georges-Louis Leclerc, Comte de Buffon (1707 – 1788) studied probability, geometry, number theory and differential and integral calculations. His most famous mathematical experiment, the Needle Problem, presented in 1777 to the Royal Academy of Sciences in Paris, France is his most important contribution to morphometry. He noticed that a needle tossed at random onto a grid of lines intersects one of the lines with a probability directly proportional to the length of the needle. This experiment inaugurated a new mathematical domain, today known as *the theory of geometrical probability*. This theory supplies the basis for current approaches to estimate length and surface area of non-classically shaped objects in an unbiased manner.

Auguste Delesse (1817 – 1881), a French geologist and mining engineer, discovered a method to measure the amount of a particular mineral in a rock. He demonstrated that the profile area of a phase per unit area of a random section cut though the rock is proportional to the expected value for the volume of that phase per unit volume of the specimen. Delesse's unbiased principle was further refined by the geologist Thompson, who showed that for a randomly positioned point grid the number of points hitting the phase of interest divided by the number hitting the whole section gave an unbiased estimate of volume fraction. Today the Delesse principle provides the basis for accurately estimating the volume fraction of non-classically shaped objects from their profile area fraction on random sections.

S. D. Wicksell, a Swedish mathematician, demonstrated in the early 20th century (Wicksell 1925) what became known as the Corpuscle Problem: the number of profiles per unit area noted in 2D on histological sections does not equal the number of objects per unit volume in 3D. The Corpuscle Problem arises from the fact that not all arbitrary-shaped 3D objects have the same probability of being sampled by a 2D sampling probe (knife blade). Larger objects, objects with more complex shapes and objects with their long axis perpendicular to the plane of sectioning have a higher probability of being sampled / hit by the knife blade, mounted onto a glass slide, stained and counted, an aspect today referred to as 'size-bias'. Wicksell himself and many other scientists tried to develop assumption- and model-based correction factors, in an attempt to 'fit' biological objects into classical Euclidean formulae. These attempts have only added further systematic error (bias), since the models and assumptions used were not true for biological objects with random shapes. These approaches failed to overcome the

Corpuscle Problem and the conclusion was that accurate estimates of the number of biological objects with arbitrary sizes and shapes cannot be obtained from histological sections using assumption-based morphometry.

1.3.3 Unbiased stereology

By the early 1980s, the Corpuscle Problem remained a significant test for the credibility of the newly emerging field of unbiased stereology. *Stereology* literally translates from the Greek as 'the study of objects in 3D'. It is actually a science dealing with the geometrical relationships between three-dimensional objects and images or sections of these visualised in 2D (Howard and Reed 1998). Stereological approaches primarily developed for material sciences and geological sections are also valid for histological sections and even sections obtained non-invasively by computerized tomography, ultrasound, magnetic resonance imaging or confocal microscopy and their associated questions (e.g., how many cells are there in a volume unit? how many cells are there in an organ? how much connective / muscular tissue does an organ contain? what is the volume of an organ?). Thus stereology is concerned with making quantitative estimates of the 'amount' of a geometrical feature (e.g., number, length, area, volume) within an object of interest. If the feature is associated with a population, then the average per item can be estimated.

Mathematicians, also known as theoretical stereologists, recognized the fault in the traditional approaches to biological morphometry based on modelling biologic structures as classical shapes. They also rejected 'correction factors' based on non-verifiable assumptions intended to force biological objects into Euclidean models. Instead, they proposed that stochastic geometry and probability theory provided the correct foundation for quantification of arbitrary non-classically shaped biological objects. Furthermore they developed efficient unbiased sampling strategies for the analysis of biological tissue at different magnifications.

The solution to the Corpuscle Problem came in a *Journal of Microscopy* report in 1984 by D. C. Sterio, the one-time pseudonym of a well-known Danish stereologist (Sterio 1984). The solution, known as the disector principle, was the first truly unbiased method for the estimation of the number of particles in a specified tissue volume (N_V), without the need for further assumptions about the size, shape or orientation of the particles in

the given tissue region. The disector is a 3D probe that consists of two serial sections a known distance apart (disector height), with an unbiased counting frame (Gundersen 1978) of known area superimposed onto one section. This counting frame avoids the bias (i.e., double counts) arising from objects at the edges of the field of view (edge effects). The number of objects whose 'tops' fall within the disector volume provides an unbiased estimate of the numerical density. The invention of the disector principle was a breakthrough in quantitative morphometrical analysis. This approach could overcome the most severe forms of bias introduced by cutting three-dimensional objects into two-dimensional sections. By this point it became obvious that making an unbiased estimate of any stereological parameter required choosing the correct probe. This can be ensured when the total dimensions of the parameter of interest and the probe equal at least 3: $\text{parameter}_{\text{dim}} + \text{probe}_{\text{dim}} \geq 3$ (Howard and Reed 1998; Ochs 2006).
Today a number of unbiased stereological methods are available for estimating average or total quantities such as number, volume, particle volume, length, surface area.

1.4 Principles of unbiased stereology

1.4.1 Estimation and bias

Especially in microscopical analyses of macroscopical objects the amount of interest usually far exceeds the possibility to exhaustively examine and quantify a certain feature (i.e., *identity*), so that it is often necessary to take a *sample* of the material and make an *estimate* of the required quantity. Because an estimate must be valid for the entire object, although only parts of it were contained in the sample examined, the nature of the sampling is of crucial importance. Besides that, the *estimator* (i.e., the well specified numerical method describing how to calculate the estimate of a parameter from a sample) should not make any restrictive assumptions, approximations or modelling of the quantity to be measured and its spatial distribution. By repeating the sampling and performing the quantification on different samples, a series of estimates called *sampling distribution* is generated. If the mean of the sampling distribution is equal to the true number, then the estimator is *unbiased* (Stuart 1984). Otherwise the difference between the mean of the sampling distribution and the real value represents the *bias* (i.e., systematic error) of the employed sampling scheme and estimator. As the

true number is usually unknown, a potential bias and its magnitude are totally invisible at the end of an experiment so that they cannot be corrected or removed. Even obtaining very similar values upon repeating the measurement does not say anything about the bias – a narrow sampling distribution of an estimator implies high efficiency (precision) and must not be confused with unbiasedness (accuracy). Precision is therefore characterized by the spread of the sampling distribution, i.e., its standard deviation and/or variance. The standard deviation (SD) of the sampling distribution is generally referred to as *standard error* (SE) of the estimator. Dividing it by the mean of the distribution will yield a relative measure known as *coefficient of error* (CE). An overview of basic stereological terms is given in table 1.1.

Table 1.1 Stereological terms and their meaning

Terms	*Meaning*
Sample	Collection of individuals / units taken from a population
Parameter	Population distribution value estimated in a sample
Expected value	Value expected to be true for a parameter
Estimate	Numerical approximation of a parameter, calculated from a sample
Estimator	Well specified numerical method describing how to calculate an estimate in a sample
Sampling distribution	Series of estimates of a parameter from repeated sampling
Reference space	Anatomical region defined by natural borders, which contains the objects of interest

The bias encountered in microscopy can be stereological or non-stereological (Peterson 1999). Non-stereological bias is introduced by:

- incomplete / defective staining
- improper calibration of the instruments / observer bias
- incorrect mathematical computation of the results / ascertainment bias.

Stereological bias can be divided into:

- sampling bias

- methodological bias (faulty corrections, incorrect assumptions, unsuitable probes).

1.4.2 Random sampling

To avoid a *sampling bias* the collected sample has to be *uniform random* (UR) – i.e., every part of the original object must have the same probability of being selected (uniform selection) and it must be impossible in advance to predict which parts will be sampled (randomness). The uniform random sampling must be employed at every sampling level, e.g., tissue blocks, sections, fields of view. Under no circumstances should anything within the defined reference space be 'chosen'. Stereology is fundamentally *statistical* and its methods rely upon a careful sampling design and a robust sampling theory. The methods cannot be applied unless a uniform random sample has been taken throughout the reference space.

Genuinely uniform random spatial samples tend to cluster together, thereby unpredictably sampling some regions more heavily than others. As this can lead to some redundancy, a far more efficient approach is to use a *systematic uniform random sampling* (SURS) scheme. It consists of a uniform random component and a systematic component. First the spacing of the units to be collected has to be defined. The first unit to sample from an object or population has to be randomized in an interval equal to this spacing distance from one end of the object. All other units are collected at integer multiples of this interval from the first sampling unit. Although the sampled units will not be random with respect to each other (systematic component), if any *one* of them is uniformly randomized with respect to the object then *all* of them are (uniform random component). SURS is both easier to apply in practice and yields estimates with a lower variability, i.e., a lower SE of the estimator (Gundersen and Jensen 1987), which increases repeatability.

1.4.3 Geometrical probes and random geometry

The only way to avoid a methodological bias is to use a 'measurement tool' that is inherently imbued with unbiasedness. Accuracy cannot be adjusted during the experiment by increasing the work load, either when sampling or quantifying. In

stereology, accuracy is guaranteed by the application of a set of unbiased 'geometrical questions' in 3D which are called *probes*. The geometrical properties of features in 3D space can be quantified by randomizing a test system of various dimensions (e.g., points, lines, planes or volumes) and known properties in the space containing the specimen and counting the number of times the feature is intersected by the probes of the test system. There is a certain relationship between the feature being quantified and the dimensionality of the geometrical probes to be used – the total dimensions in the parameter of interest and the probe must equal at least 3: $parameter_{dim} + probe_{dim} \geq 3$ – Table 1.2 (Howard and Reed 1998; Ochs 2006; Hyde et al. 2006).

Table 1.2 Parameters and probes in stereological designs

Structure	*Parameter*	*Parameter dimensions*	*Probe*	*Probe dimensions*	*Sum of dimensions*
Volume	Volume	3	Point	0	3
Surface	Area	2	Line	1	3
Linear	Length	1	Plane	2	3
Cardinality	Number	0	Disector	3	3

Randomizing a geometrical probe with respect to a set of features is very similar to the SURS of an object as described above. Stereological application of geometrical probes in 3D is usually achieved in microscopy by physically cutting the object into thin sections and then using a 2D grid on the section. However, in order to stay consistent with 3D perceptions it is important to acknowledge a peculiar and marked problem caused by the act of sectioning: the dimensionality of the geometrical information that one obtains from a thin section through an object is not the same as in the real 3D environment (Hyde et al. 2006). Nevertheless, stereological designs (i.e., the combination of a sampling scheme and an unbiased estimator) are able to derive real 3D quantitative data for irregular objects from measurements made on 2D sections.

1.4.3.1 Points probe volume

For very small objects, like biopsies, or objects completely enclosed within another object or matrix, traditional volumetry by weighing or water immersion (Scherle 1970)

is not practicable. The most direct stereological approach for estimating volume is the Cavalieri method (Cavalieri 1635; Gundersen et al. 1999). This estimator requires a series of parallel sectioning planes a fixed distance, *T* units, apart to exhaustively cut the study object, giving rise to a series of slabs. For the volume estimator to be unbiased, it is necessary that the first sectioning plane be uniform random in an interval 0–*T* from one end of the object in the sectioning direction. The resulting slabs are to be laid the same way up and the cross-sectional area of each slab is measured or estimated. The object volume is estimated by summing the areas and multiplying by the slab thickness, *T*:

Formula 1.1

$$\hat{V} = T \times \sum_{i=1}^{m} A_i$$

$\hat{V}$ = estimated volume

T = slab thickness

A_i = cross-sectional area of the object transect seen on the *i*-th slab

The cross-sectional areas do not need to be precisely measured; for practical purposes they can be estimated with a suitable precision using a UR translated point grid with a known area (a_p) assigned to each point of the test system. Then an unbiased estimate of the cross-sectional area is given by:

Formula 1.2

$$\hat{A} = a_p \times P$$

$\hat{A}$ = estimated area

P = the number of points hitting the object transect

Then Formula 1.1 becomes

Formula 1.3

$$\hat{V} = T \times a_p \times \sum_{i=1}^{m} P_i$$

P_i = the number of points hitting the object transect on the *i*-th slab

At this point it should be noted that using a UR translated point grid on UR translated serial sections amounts to a UR translated 3D point test system, where each point is associated with a volume element of $a_p \times T$.

Sectioning a small object into 10-15 relatively thick slabs can be cumbersome and render further processing and analyses of the object impracticable. Since only the 'top side' of the slabs is taken into consideration, an alternative approach would be to exhaustively cut the object into thin microscopical sections and sample *all* sections situated a *T* distance apart, i.e., the 'tops of the slabs', with a random start between 0 and *T* from one end of the object.

1.4.3.2 Lines probe surface

An appropriate probe for the estimation of total surface area or area fractions is a line (Howard and Reed 1998; Hyde et al. 2006). In analogy with SURS, it is more efficient to employ a systematic uniform random grid of lines, instead of simply randomizing each line probe. Since a line has a certain spatial orientation, both translational and *directional* randomness are required in order to randomize a systematic test grid of lines with respect to an object. Translational randomness is achieved by randomizing any one line in an interval equal to the spacing distance of the grid and perpendicular to it. The direction of the line grid is described by the direction the lines of the grid have with respect to an arbitrary but fixed direction in space. The directional equivalent of uniform randomness is known as *isotropy* – therefore a random direction is called isotropic direction. A grid of lines that is both isotropic in direction and uniform random in position is known as an isotropic uniform random (IUR) line grid. If an IUR line grid is placed over an object, the number of intersections between the grid and the surface of the object will be proportional to the surface area. The estimators of surface area will only be unbiased if either the analysed surface is isotropic, the line grid is isotropic or both are isotropic in 3D.

1.4.3.3 Volumes probe number

1.4.3.3.1 The unbiased counting frame

In microscopy, the number of cell transects to be counted often far exceeds the ability to enumerate them exhaustively. Thus it becomes necessary to be able to relate any particular count to a given sampling area, in the 2D case. An obvious problem is represented by the objects that cut the edges of the given sampling area, e.g., the microscopical field of view. The solution in general use in microscopy was proposed by Gundersen (1978) and addresses the 'edge effect'. It consists of an unbiased counting frame of known area with an acceptance line and infinite exclusion line (for an example see Figure 2.4, pg. 38). Any transect that is cut *anywhere*, i.e., even outside the area of the frame, by the infinite exclusion line is not counted. Cell transects falling fully inside the counting frame or those that cut the acceptance line without also cutting the exclusion line are counted. To implement this rule it is necessary to leave a 'guard area' around the counting frame. Therefore, it cannot be applied to a complete microscopical field of view. The application of the unbiased counting rule associates a definite count with the area of the counting frame, leading to an unbiased estimate of the number of cell transects per unit area.

If a SURS scheme is applied, then in practice it is found that some fields of view and the contained unbiased counting frames actually cross the edge of the object. The simplest solution is to allocate a point to each counting frame, e.g., the upper right frame corner. For each position of the counting frame, the allocated point is judged to be either 'inside' or 'outside' of the reference space. A cumulative count is recorded for the number of counting frame points that hit the reference space, for each section. This count, multiplied by the area of a single counting frame, is an unbiased estimate of the total sampled tissue area. Independently of whether a frames-associated point is counted or not, profile counts must be performed on *all parts of counting frames hitting the reference compartment*.

1.4.3.3.2 The physical disector

For 3D counting, the physical disector (Sterio 1984; Howard and Reed 1998) is the ultimate minimalist approach to a 3D probe. It consists of a pair of serial sections a known distance apart. The method relies upon the principle that, if the transect of a

particle is seen in one section (reference section) and not the next (look-up section), it is counted. Thus the disector counts the ‘tops’ of the particles, ensuring that each particle is counted only once. The disector is in effect an approximation to the continuous scan through a volume (Howard et al. 1985). It is not known for sure what happens between the two disector planes, but if the planes are closely spaced, i.e., about 30% of the average height in the cutting direction of the smallest cell to be counted, a reasonable deduction can be made.

For 3D counting it is necessary to extend the unbiased 2D counting rule to a directional unbiased 3D cell counting rule. This is done by superimposing an unbiased counting frame onto the reference section of a physical disector. For each transect correctly sampled by the unbiased counting frame, i.e., associated with its area, in the reference section, a corresponding transect is sought in the look-up section. If no corresponding transect is found anywhere in the look-up section, then this cell is counted in 3D (see Figure 2.4, pg. 38 for an applied example). The count is associated with a volume of tissue equal to the area of the unbiased counting frame multiplied by the disector height, i.e., the distance between the two sections. This counting rule is an unbiased estimator of numerical density, i.e., number of cells per unit volume. The combination of the disector principle and the 2D unbiased counting frame is the disector (Sterio 1984).

As the disector is a directional counting rule, its efficiency can be nearly doubled by making separate counts in both directions, that is, by going up and down between the two sections. This is achieved for a pair of sections by first using one as the reference section and the other as the look-up section and then interchanging the roles played by the two sections.

A field sampling regime must be adopted, in which each part of each section pair has the same chance of appearing in the fields of view. To calculate the volume, which the disector count must be related to, the volume of the disector must be multiplied by the number of disectors that ‘hit’ the reference space. The same point-allocation solution is applied, as for counting frames in the 2D approach. This count, multiplied by the area of a single counting frame and the disector height, is an unbiased estimate of the total sampled tissue volume. Independently of whether a frames-associated point is counted or not, disector counts of cells must be performed on *all parts of counting frames hitting the reference space*.

1.5 Aim of the study

The aim of this study was to propound several stereological designs for the quantitative histopathological analysis of human endobronchial biopsies with respect to reliable markers of the inflammation and remodelling occurring in chronic inflammatory airway diseases.

The present study was designed to empirically address the issue of agreement between the data delivered by the simultaneous application of a stereological numerical density estimator – the physical disector – and the classical approach of area profile counting. For this, the extent and the variation of a potential size-bias had to be assessed by examining macrophages and T-lymphocytes, two cell populations with clearly different mean sizes and of great interest to the research on chronic airway diseases. To address the question of dependency of the agreement between the two methods on the study sample, two groups of human subjects, i.e. non-smokers and smokers, were separately analysed.

A stereological estimator was also proposed for the assessment of the epithelial integrity in the bronchial biopsies of the same groups – the first stereological attempt at this matter – and the outcome was related to already available data obtained by image analysis of bronchial biopsies or BAL examination from healthy volunteers and asthmatics. In addition, the association between the integrity of the epithelium and the biopsy volume was investigated.

For the appraisal of the airway wall remodelling a stereological estimator of membrane mean thickness was adapted for the bronchial RBM in the groups of healthy non-smokers and non-asthmatic smokers and the results were compared with previously published data of another stereological method and non-stereological approaches.

2 Material and methods

2.1 Material

All chemicals in highest available purity and quality, unless otherwise stated, were provided by: Merck AG (Darmstadt, Germany), Sigma (Deisenhofen, Germany), Fluka/Sigma-Aldrich Chemie GmbH (Steinheim, Germany), Carl Roth GmbH (Karlsruhe, Germany), Riedel de Haën (Seelze, Germany), Chroma (Münster, Germany), B Braun Melsungen (Melsungen, Germany), PAA Laboratories GmbH (Pasching, Austria) and Vogel Medizinische Technik und Elektronik (Gießen, Germany).

2.1.1 Subjects and bioptic material

In this study endobronchial biopsies from 7 healthy non-smokers and 7 smokers were examined. All subjects were volunteers who gave their written consent after being fully informed about the purpose and nature of the study, which was approved by the ethics committee of Hannover Medical School (Hannover, Germany). None of the included subjects suffered from acute respiratory illness within 4 weeks before the bronchoscopic investigations.

The subjects' demographic and clinical data are shown in Table 2.1. In the non-smoker group 6 subjects were never-smokers, whereas 1 was an ex-smoker with a history of 0.9 pack years, who had quit more than 1 year before the onset of the study. The smokers had a significantly longer smoking history (23.4 - 54.4 pack years) and were actively smoking at the time of enrolment.

All non-smokers had normal relative FEV_1 (i.e., larger than 70% of the FVC), no signs of obstructive pulmonary disease and were therefore designated as 'healthy'. In the smoker group, 3 subjects (2 males, 1 female) had normal relative FEV_1; the other 4 subjects (2 males, 2 females) had relative FEV_1 below 70% (58.1% – 66.8%) and were diagnosed with COPD stage 1 according to the GOLD criteria (Global Initiative for Chronic Obstructive Lung Disease ; Pauwels et al. 2001).

Table 2.1 Subject demographics

Group	Non-smokers	Smokers
No. of subjects	7	7
Sex (M/F)	4/3	4/3
Age (years)		
Mean ± SD	30.9 ± 6.96	46.7 ± 7.91
Range	25-42	40-61
FEV_1 (L)		
Mean ± SD	4.6 ± 0.59	3.4 ± 0.96
Range	3.80-5.43	2.35-4.69
FEV_1/FVC (%)		
Mean ± SD	81.7 ± 2.61	68.5 ± 9.2
Range	78.8-86.3	58.1-80.2
Healthy / Obstruction	7/0	3/4
Packyears		
Median	0	33
Range	0.0-0.9	23.4-54.4

2.1.2 Equipment and software

AKITA® inhalation system (Activaero GmbH, Gemünden/Wohra, Germany)

Fenestrated cup Radial Jaw® biopsy forceps (Boston Scientific Medizintechnik GmbH, Ratingen, Germany)

Automated embedder Tissue-Tek VIP (Sakura Finetek BV, Zoeterwoude, Netherlands)

Tissue embedding console system Tissue-Tek TEC (Sakura Finetek BV, Netherlands)

Motorized rotary microtome HM355S with Cool Cut and STS (Microm International GmbH, Walldorf, Germany)

Computer linked Olympus BX 51 light microscope (Olympus, Ballerup, Denmark) with a motorized stage (Prior Scientific Instruments Ltd., Cambridge, UK)

CAST-Grid 2.01 (Olympus, Ballerup, Denmark)

SigmaStat 3.1 (Jandel Scientific, Erkrath, Germany)

SigmaPlot 9.0 (Jandel Scientific, Erkrath, Germany)

2.1.3 Specimen collection

10% (v/v) formalin:

100 ml formaldehyde solution min. 37% stabilised with approx. 10% methanol (Merck)

90 ml PBS (Dulbecco's Phosphate Buffered Saline 10x, PAA Laboratories)

810 ml Ampuwa (Aqua ad iniectabilia, Braun)

Alcoholic eosin solution (Sigma)

2% (w/w) Agar-Agar:

2 g Agar-Agar granulate (Merck)

100 ml tap water

Boil in the microwave at 450 W

2.1.4 Paraffin embedding, deparaffination, hydration, dehydration and mounting

Embedding medium / paraffin wax (Vogel)

Xylene (Merck)

100% (v/v) alcohol: ethanol absolute (Riedel de Haën)

96% (v/v) alcohol:

96 ml ethanol absolute (Riedel de Haën)

4 ml aqua dest.

70% (v/v) alcohol:

70 ml ethanol absolute (Riedel de Haën)

30 ml aqua dest.

10% (v/v) neutral buffered formalin (Sigma-Aldrich)

Entellan rapid embedding agent (Merck)

2.1.5 Histochemical staining procedures

PAS (periodic acid Schiff)

1% (w/w) periodic acid:

1g periodic acid (Merck)

100 ml aqua dest.

Schiff reagent (Merck)

Mayer's haematoxylin:

50 ml Mayer's haemalum solution (Merck)

250 ml aqua dest.

2.1.6 Immunohistochemical staining procedures (ABC-Method)

2.1.6.1 Solutions and buffers

PBS 0.15M (2 l stock solution 10x):

160 g NaCl (Merck)

4 g KCl (Roth)

23.3 g Na_2HPO_4 * $2H_2O$ (Merck)

4 g KH_2PO_4 (Merck)

ad 2 l aqua dest.; pH 7.4 with 1N HCl (Merck)

TBS (TRIS Buffered Saline) (1 l stock solution 10x):

53 g NaCl (Merck)

12 g TRIS (Roth)

ad 1 l aqua dest.; pH 7.4 with 1N HCl (Merck)

Citrate buffer 0.01M (1 l stock solution 10x):

29.41 g Tri-Sodium citrate dihydrate (Roth)

ad 1 l aqua dest.; pH 6.0 with 1N HCl (Merck)

TRIS-HCl-Buffer 0.05M (1.5 l stock solution 10x):

60.57 g TRIS (Roth)

ad 1.5 l aqua dest.; pH 7.4 with 1N HCl (Merck)

Blocking solution for the endogenous peroxidase:

6 ml H_2O_2 30% (Merck)

200 ml methanol (Merck)

2% skim milk powder solution:

4 g skim milk powder (Merck)

200 ml PBS

DAB solution:

0.4 g DAB (Sigma)

400 ml TRIS-HCl-Buffer

2.1.6.2 Primary antibodies

Polyclonal rabbit anti-human CD3 antibody (DakoCytomation, Golstrup, Denmark)

Diluted in skim milk solution 1:100

Monoclonal mouse anti-human CD68 antibody, clone PG-M1 (DakoCytomation)

Diluted in skim milk solution 1:100

2.1.6.3 Secondary antibodies

Biotinylated anti-rabbit IgG (H+L), made in goat (Vector BA-1000)

Diluted in skim milk solution 1:100

(against anti-CD3-antibody)

Biotinylated anti-mouse IgG (H+L), made in horse (Vector BA-2000)

Diluted in skim milk solution 1:100

(against anti-CD68-antibody)

2.1.6.4 Immunohistochemical kits

Vectastain Elite ABC Kit (Vector Laboratories, Burlingame CA, USA)

2 ml reagent A (avidin DH)

2 ml reagent B (horseradish peroxidase H)

AB-complex preparation:

60 µl reagent A and 60 µl reagent B added to 3 ml PBS, mixed and incubated for 30 min at room temperature

2.1.6.5 Normal serum

Normal goat serum (Vector S-1000)

Diluted in skim milk solution 1:10

(for secondary antibodies anti-rabbit)

Normal horse serum (Vector S-2000)

Diluted in skim milk solution 1:10

(for secondary antibodies anti-mouse)

2.1.6.6 Counterstaining

Mayer's haematoxylin:

50 ml Mayer's haemalum solution (Merck)

250 ml aqua dest.

2.2 Methods

2.2.1 Flexible bronchoscopy and biopsy

Bronchoscopy and biopsy were performed by staff members of the Department of Clinical Airway Research of Fraunhofer ITEM (Hannover, Germany) under the supervision of Prof. Dr. N. Krug and Prof. Dr. J. Hohlfeld.

The subjects received premedication according to the routine protocols: 0.2 mg aerosolized salbutamol and fractionated intravenous midazolam (0.05 mg/kg). In addition, smokers received 3 ml nasal nebulized lidocaine 4%, whereas healthy non-smokers underwent inhalative anaesthesia with 2.5 ml lidocaine 4% by electronically controlled and regulated inhalation using the AKITA® inhalation system. This device enables controlled mechanical ventilation with a predefined breathing rate, inspiratory flow and tidal volume. Subsequently, local anaesthesia of the bronchial mucosa was performed during bronchoscopy using lidocaine 2% up to a maximal dose of 6 mg/kg, as previously described (Erpenbeck et al. 2004). The subjects were continuously monitored by pulsoxymetry and one channel ECG. Oxygen was continuously applied through a nasal canula.

Per subject, two or three biopsies from the segmental branches of the right lower pulmonary lobe were collected during flexible bronchoscopy performed according to the international guidelines (American Thoracic Society 1987; NHLBI/NIAID/AAAI/ACCP/ATS 1991). Using the fenestrated cup Radial Jaw® biopsy forceps in total 24 endobronchial biopsies, 12 per group, were obtained from the two subject groups. The collected biopsies underwent overnight fixation in 10% phosphate-buffered formalin to preserve tissue architecture and cell morphology. They were shipped by overnight express mail to Marburg where further processing and analysis of the tissue was carried out in the Clinical Research Group “Chronic Airway Diseases” of Philipps University (Marburg, Germany) as described below.

2.2.2 Paraffin-embedding of the biopsies

Prior to paraffin embedding the biopsies were embedded in agar. For this the biopsies were aspirated with a plastic Pasteur pipette and deposited on a small sieve. To ease macroscopical identification of the small specimens, they were reversibly stained with

one drop of alcoholic eosin solution and rinsed in PBS. After placing the sieves on a flat surface, melted 2% aqueous agar-agar at 60 °C was poured onto each sieve until it covered the specimen. After a hardening time of 20 min the biopsies, surrounded by agar, were cut out, wrapped in filter paper and laid in embedding cassettes (Engelbrecht Medizin und Labortechnik GmbH, Edermünde, Germany). The embedding cassettes were deposited in 10% formalin until further processing.

Paraffin embedding took place in the automated embedder Tissue-Tek VIP in the Institute of Pathology of University Hospital Marburg and Gießen (Marburg, Germany). First, the specimens were incubated for 1 hour in 10% neutral buffered formalin at 40 °C. Then they were incubated three times for each 1 hour in 96% alcohol, four times for each 1 hour in 100% alcohol and two times for each 1 hour in xylene at 40 °C. After this, the actual paraffin embedding began by transferring the probes into melted paraffin for 45 min at 60 °C. This step was repeated three times for each 1 hour, until the tissue was saturated with paraffin.

Further processing was performed at the tissue embedding console system Tissue-Tek TEC. Thereto, melted paraffin at 60 °C was filled in a base mould (Engelbrecht) and the paraffin saturated sample in the embedding cassette was inverted over it. The base mould was placed on a cold plate, for the paraffin to cool off and harden, which allows for the paraffin block comprising the biopsy to be removed from the mould.

2.2.3 Sectioning and sampling of the paraffin blocks

The paraffin tissue blocks were exhaustively sectioned using the motorized rotary microtome HM355S equipped with a 4 °C cooled object clamp (Cool Cut), a section transfer system and a 42 °C heated water bath (STS). The sections were obtained with a 2 µm average block advance (BA), calibrated by means of a digital calliper measuring the block height before and after cutting 500 sections at a given microtome setting. Beginning with the first section, every three consecutive sections were collected on numbered StarFrost adhesion glass slides (76 x 26 mm, Engelbrecht). They were allowed to air dry for 30 min and were baked in a 37-40 ºC oven over night.

According to the SURS principles (Gundersen and Jensen 1987; Howard and Reed 1998) every 9^{th} or 20^{th} slide, depending on the size of the biopsy, was sampled in a slide series with a random outset between the 1^{st} and the 9^{th} or the 20^{th} slide of a biopsy,

respectively (Figure 2.1). This resulted in a section-sampling fraction (i.e., the fraction of the total number of sections sampled by SURS in a series) of 1/9 or 1/20, respectively. By this algorithm nine samples of 5-11 glass slides per biopsy were collected for histology and indirect immunohistochemistry. Each slide sample was randomly assigned a different histochemical or immunohistochemical (IHC) staining.

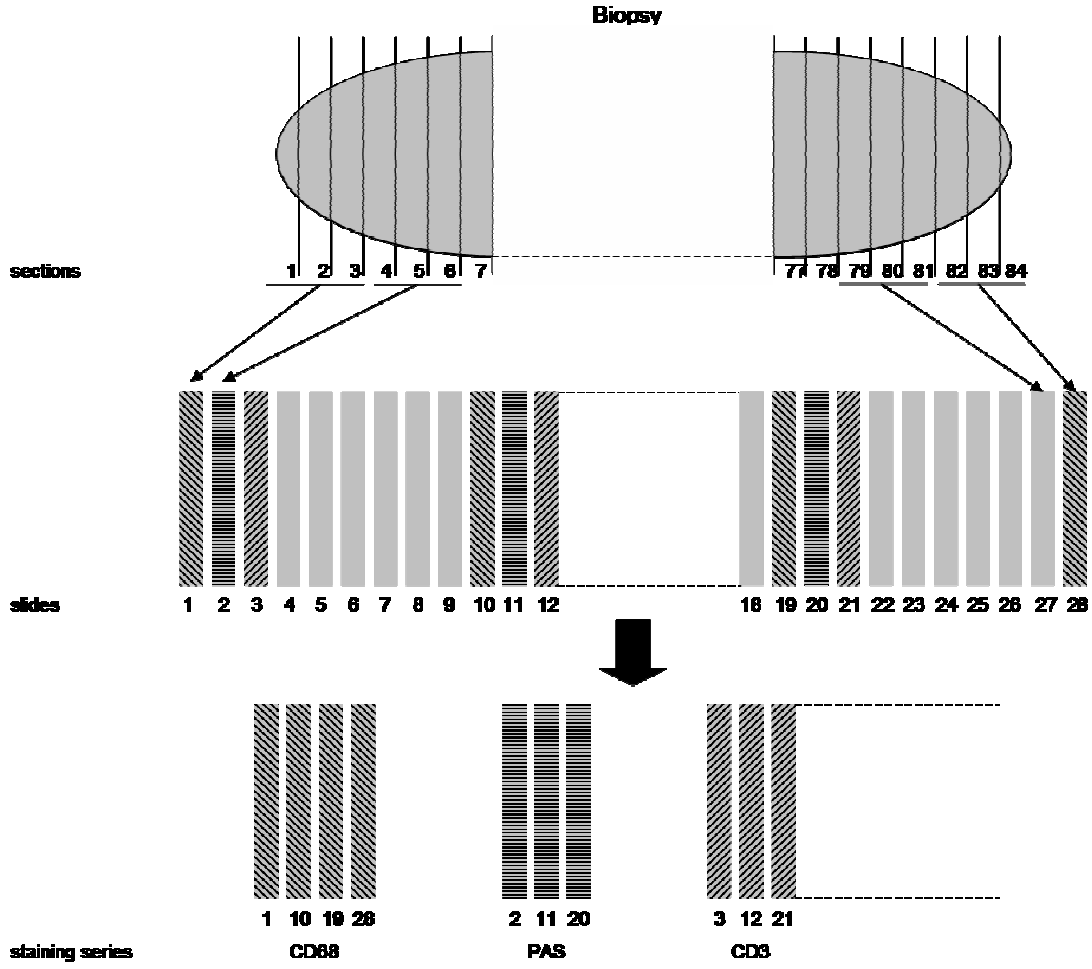

Figure 2.1 Schematic SURS of the sections of a biopsy
After exhaustive sectioning every three sections were mounted on numbered glass slides (1 to 28 in this example). With a random outset between the 1st and the 9th slide, nine slide samples, each consisting of every 9th glass slide, were collected and stained.

2.2.4 Histochemical staining

2.2.4.1 Deparaffination and hydration

Before the actual staining, the sections were deparaffinated 30 min in xylene. Subsequently they were hydrated in graded alcohol solutions beginning with 10 min in 100% alcohol, 5 min in 96% alcohol and 10 min in 70% alcohol, as the employed stains are only water-soluble. Finally the slides were thoroughly rinsed in tap water.

2.2.4.2 PAS staining

By this staining the glycol groups of carbohydrates are selectively oxidised with periodic acid to aldehyde groups. The aldehydes are subsequently condensed with the Schiff reagent (fuchsin-sulfurous acid) to produce a purple-magenta colour. The basal laminae, mucin, glycogen and fungi will be stained purple.

After deparaffination and hydration the sections were oxidised 10 min in 1% periodic acid and rinsed in tap water. Subsequently, they were placed in Schiff reagent for 15 min and washed under running tap water for another 15 min. Counterstaining of the nuclei was achieved in Mayer’s haematoxylin for 5 min. Finally, the sections were washed in lukewarm running tap water for 5 min (blueing), dehydrated and mounted (see below).

2.2.4.3 Dehydration and mounting

The dehydration of histochemically (or immunohistochemically) stained sections took place in graded alcohol solutions. The glass slides were first placed in 70% alcohol for 10 min, then transferred into 96% alcohol for 5 min and into 100% alcohol for another 10 min. Finally, they were cleared in xylene for 15 min before being mounted with Entellan rapid embedding agent and a coverslip (Engelbrecht). The mounting medium was allowed to dry for 20 min at room temperature.

2.2.5 Immunohistochemical staining by the indirect Avidin-Biotin-Complex method

The indirect ABC-method is an immunohistochemical detection assay involving incubation of the tissue sections with a specific unlabeled primary antibody against the antigen of interest. In the next step, a secondary antibody is added to the antigen-antibody complex. The secondary antibody must be labeled with biotin and directed against the IgG of the animal species in which the primary antibody has been raised. These biotinylated antibodies can be bound by a preformed avidin-biotinylated-peroxidase-complex. Avidin is a glycoprotein with 4 binding sites for biotin. Because avidin has such an extraordinarily high affinity for biotin (over one million times higher than antibody for most antigens), the binding of avidin to biotin is essentially irreversible. Most proteins, including enzymes, can be conjugated with several molecules of biotin. These properties allow macromolecular complexes (ABC's) to be formed between avidin and biotinylated enzymes. In the preformed ABC only three binding sites of avidin are occupied by biotin, so that the fourth binding site can affix to the biotinylated secondary antibody. Finally, the horseradish peroxidase in this complex can be histochemically identified with DAB, a chromogen which in the presence of a peroxidase enzyme produces a brown precipitate that is insoluble in alcohol. This method is more sensitive than direct IHC, due to the signal amplification through several secondary antibody reactions with different antigenic sites on the primary antibody and avidin cross-linking of several biotinylated enzyme molecules, all of which increase the peroxidase concentration attached to an antigen.

2.2.5.1 Deparaffination

To dewax, the sections were placed for 30 min in xylene and for 10 min in 100% alcohol.

2.2.5.2 Endogenous peroxidase blocking

The endogenous peroxidase activity was blocked with 200 ml H_2O_2 1% in methanol. After incubating 30 min at room temperature, the slides were rinsed several times in tap water.

2.2.5.3 Heat-induced epitope retrieval

Although aldehyde-based fixatives are excellent for preserving cellular morphology, they also cause protein cross-linking, thereby masking the antigenic sites, resulting in the inability of some protein epitopes to bind complementary antibodies. The demonstration of many antigens can be significantly improved by a pretreatment procedure, in this case the exposure of slide-mounted specimen material to a heated buffer solution that breaks the protein cross-links formed by formalin fixation and thereby uncovers hidden antigenic sites.

The glass slides were placed in plastic cuvettes (Sigma), which were filled to the brim with sodium citrate buffer (pH 6.0). The cuvettes were heated three times for each 5 min at 450 Watt in a microwave oven. Each time citrate buffer was refilled. In the end, the cuvettes were removed to room temperature and the slides were allowed to cool for 15 min. The citrate buffer was poured away and the slides were rinsed in TBS for 5 min.

2.2.5.4 Staining by the indirect ABC-method using the ABC kit

For this staining, the Vectastain Elite ABC kit and a special system of Coverplates™ (Thermo Shandon, Waltham MA, USA) and Sequenza® slide racks (Thermo Shandon) were used. The glass slides and a negative control were laid on Coverplates™, with the tissue sections inwards and avoiding the entrapment of air bubbles. The Coverplates™ were placed in slide racks where the following steps were carried out.

The Coverplates™ were filled with PBS to rinse the sections for 5 min. To block non-specific protein binding reactions, the sections were incubated for 20 min with normal serum diluted 1:10 in skim milk solution. The normal serum originated form the same species as the secondary antibody. In each Coverplate™, including the negative control, 100 µl normal serum solution was added. Subsequently 100 µl of the preliminarily diluted primary antibody were pipetted in each Coverplate™, except for the negative control; instead 100 µl skim milk solution were added to this Coverplate™. All slides were incubated for 1 hour at 37 °C. Thereupon, the sections were rinsed for 5 min in skim milk solution. Then 100 µl diluted biotinylated secondary antibody were added. The slides were incubated again for 30 min at room temperature. After that, the sections were rinsed in PBS for 5 min. Subsequently, 100 µl ABC-peroxidase were pipetted in each Coverplate™ and they were incubated for another 30 min at room temperature.

The sections were rinsed again in PBS for 5 min before removing the slides from the Coverplates™. They were placed in cuvettes with 200 ml DAB solution. 100 µl H_2O_2 30% were pipetted into the cuvettes, thoroughly mixed and allowed to develop a reaction for 10 min. Finally, the sections were thoroughly rinsed in running tap water, counterstained, dehydrated and mounted (see below).

2.2.5.5 Counterstaining

After IHC all sections were counterstained to identify the rest of the tissue. Thereto the slides were quickly immersed into a cuvette with Mayer's haematoxylin six times in a row and then washed in lukewarm tap water (blueing). Mayer's haematoxylin stains the nuclei dark blue and the rest of the tissue light blue.

2.2.5.6 Dehydration and mounting

The dehydration of immunohistochemically stained sections took place in graded alcohol solutions. The glass slides were first placed in 70% alcohol for 10 min, then transferred into 96% alcohol for 5 min and into 100% alcohol for another 10 min. Finally, they were cleared in xylene for 15 min before being mounted with Entellan rapid embedding agent and a coverslip (Engelbrecht). The mounting medium was allowed to dry for 20 min at room temperature.

2.2.6 Microscopical analyses

All quantitative analyses were conducted on a computer linked Olympus BX 51 light microscope equipped with a motorized stage and the CAST-Grid 2.01 software.

2.2.6.1 Biopsy volume

The Cavalieri method (Cavalieri 1635; Gundersen et al. 1999) was employed to directly estimate the biopsy volume. For each biopsy, one of the nine slide series resulted at 2.2.3 was randomly chosen for the assessment. From the three sections mounted on each slide the middle section was analysed. The sections were examined using dry lenses with a magnification of 10x and a numerical aperture of 0.4, at a final magnification of 425x. In order to depict the whole biopsy transect contained in a section, the area

sampling fraction, i.e., the fraction of the area of interest to be sampled by SUR positioned fields of view, was set to 100%. A test system consisting of 16, 25 or 36 points, depending on the biopsy size, with an area-per-point (a_p) of 18724, 11983 or 8322 µm^2 respectively was superimposed onto the fields of view. The size of the point grid was chosen so that 100 - 200 points were counted per biopsy (Gundersen and Jensen 1987; Gundersen et al. 1999). A cumulative count of the number of points landing within the biopsy transect was recorded for each section. The distance between the sections (*T*) was dictated by the block advance of 2 µm and therefore *T* = 54 or 120 µm, depending on the biopsy size and the sampling scheme adopted at 2.2.3. The volume of each biopsy was calculated using Formula 1.3.

2.2.6.2 Epithelial integrity

Endobronchial biopsy tissue tends to curl after collection because of inherent tissue elasticity, which leads to an isotropic orientation of the contained tissue structures (Jeffery et al. 2003). The biopsies floating in fixative solution were deposited on sieves and embedded in agar without being touched and thereby potentially preferentially orientated. Thus the isotropy was preserved during subsequent embedding and sectioning. This rendered the randomization of the line probes unnecessary, so that a test system of arbitrarily oriented lines could be used.

This analysis was performed on the PAS stained sections, which allow an easy identification of the RBM as a purple-magenta band between the respiratory epithelium and the lamina propria of the airway mucosa. The sections were examined using dry lenses with a magnification of 20x and a numerical aperture of 0.7, at a final magnification of 850x. As there are no data available about the contribution of the different sampling levels to the overall between–subject variability, the results of all available biopsies for each subject were averaged to yield a mean value.

For each biopsy, all slides of the PAS stained series were used for quantification. From the three sections mounted on each slide the middle section was analysed. On each section, the fields of view were selected by a SURS scheme. Thereto, the microscope objective was randomly positioned outside the tissue section at its upper left corner. This way a starting point was set, which was located independently of the features to be analysed (Howard and Reed 1998; Fehrenbach and Ochs 1998). Then the motorised

stage of the microscope was systematically shifted in the *x* and/or *y* direction by the preset sampling distance of 350 µm. The sampling distance was chosen so that roughly 100 - 200 counting events were obtained for each examined feature (Gundersen and Jensen 1987; Gundersen et al. 1999). To comply with the requirement of uniform sampling probability, a constant *x* / *y* sampling distance was used throughout all sections of the same biopsy. This regular pattern led to a SURS of the fields of view. All specimen parts that appeared in the field of view were accepted for analysis.

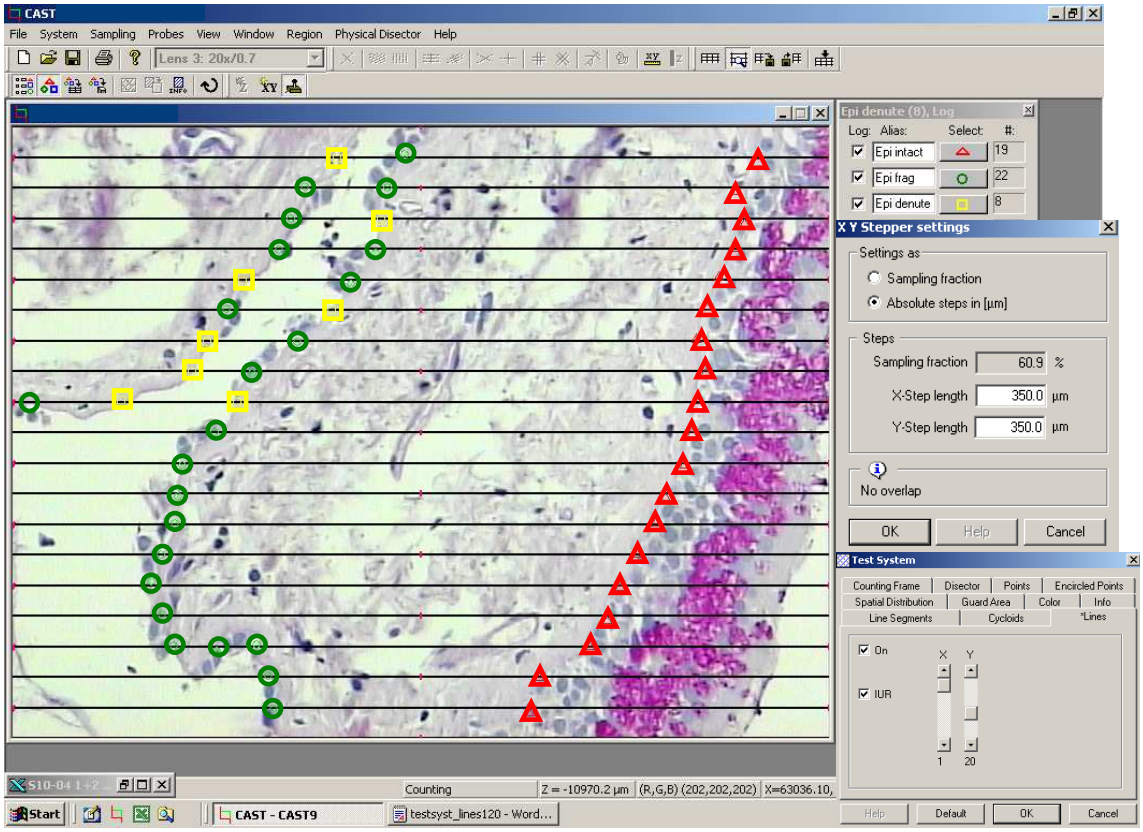

Figure 2.2 Assessment of the epithelial integrity by fraction of the RBM area
Red triangles mark RBM covered by intact respiratory epithelium; green circles mark RBM covered by a single layer of epithelial basal cells; yellow squares mark RBM denuded of the epithelial layer.

To quantify the proportion of RBM surface denuded or covered by intact or fragmented epithelium, a test system consisting of 20 parallel horizontal lines of 316.14 µm length (total grid length = 6322.81 µm) was superimposed onto the fields of view. As already discussed, further steps to achieve 3D isotropy of the test system were not necessary in this case. Each intersection of the line probes with the RBM was assessed as being

covered by intact or fragmented epithelium or denuded of the epithelial layer. This assessment was based upon the height of the epithelium along the perpendicular to the tangent to the RBM at the intersection point. RBM covered by goblet cells or several layers of ciliated epithelial cells (the cilia not necessarily always visible in light microscopy, partly because of tangential sectioning) represented the category of intact epithelium. RBM covered by a single layer of basal cells with no intact ciliated or goblet cells was classified as fragmented respiratory epithelium. RBM with a complete loss of epithelial cells, including basal cells, was classified as denuded (Figure2.2).

A cumulative count of the number of intersections between the RBM and the linear probes was recorded for each category (i.e., denuded, covered by intact or fragmented epithelium) and section. Each area fraction of the RBM was calculated according to the equation:

Formula 2.1

$$\hat{S}_S = \frac{\sum I_{\text{intact / fragmented / denuded}}}{\sum I_{\text{intact}} + \sum I_{\text{fragmented}} + \sum I_{\text{denuded}}}$$

$\hat{S}_S$ = estimated surface area fraction of the RBM

I_{intact} = number of intersections between the line grid and RBM covered by intact epithelium

$I_{\text{fragmented}}$ = number of intersections between the line grid and RBM covered by fragmented epithelium

I_{denuded} = number of intersections between the line grid and denuded RBM

2.2.6.3 Mean thickness of the reticular basement membrane

As already discussed, the tissue elasticity and the consequent curling of the biopsy specimens after their collection result in an isotropy of the contained structures, including the RBM (Jeffery et al. 2003). Therefore, arbitrarily cut serial sections will display RBM transects at all angles from 0° to 90° between the section plane and the RBM. Intuitively, transects at angles lower than 90° will have a higher thickness than the real thickness measurable in a section perpendicular to the RBM at that point.

Measuring the thickness of these transects perpendicularly to their boundaries and averaging it over several fields and sections will clearly overestimate the mean RBM thickness.

The arithmetic mean thickness can be assimilated to the mean height of the RBM. This can be defined as the ratio of the volume to the area of the RBM. Since the RBM is continuously covering the lamina propria of the airways, it is not possible to calculate either its total volume or surface area from biopsy samples. However, the volume and surface density (i.e., the volume or surface area of the phase of interest per unit volume of the reference space) of the RBM can be easily determined for a biopsy specimen. If related to the same reference space, e.g., the biopsy itself, then the mean arithmetic thickness of the RBM can be rewritten as the ratio of the volume density to the surface density (Weibel and Knight 1964; Weibel 1990). These can be estimated simultaneously using a coherent test system of points and disconnected line segments on SURS sampled fields of view. A coherent test system is a set of test points (P_T) and test lines (L_T) designed in such a way that the number of points and the length of the lines are in a precisely defined relation to each other (Weibel 1990; Weibel et al. 2007).

The assessment was performed on the PAS stained sections that allow an easy recognition of the RBM. The sections were examined using oil immersion lenses with a magnification of 100x and a numerical aperture of 1.4, at a final magnification of 4270x. As previous data revealed a high intra-subject between-biopsy variability (Ferrando et al. 2003), the results of all available biopsies for each subject were averaged to yield a mean value.

For each biopsy, all slides of the PAS stained series were used for quantification. From the three sections mounted on each slide the middle section was analysed. On each section, the fields of view were selected by a SURS scheme, as already described above. The sampling distance in the *x* and *y* direction was chosen between 100 and 130 µm, depending on the size of the biopsy. The aim was to obtain between 100 and 200 counting events for each examined feature (Gundersen and Jensen 1987; Gundersen et al. 1999). All specimen parts that appeared in the fields of view were accepted for analysis.

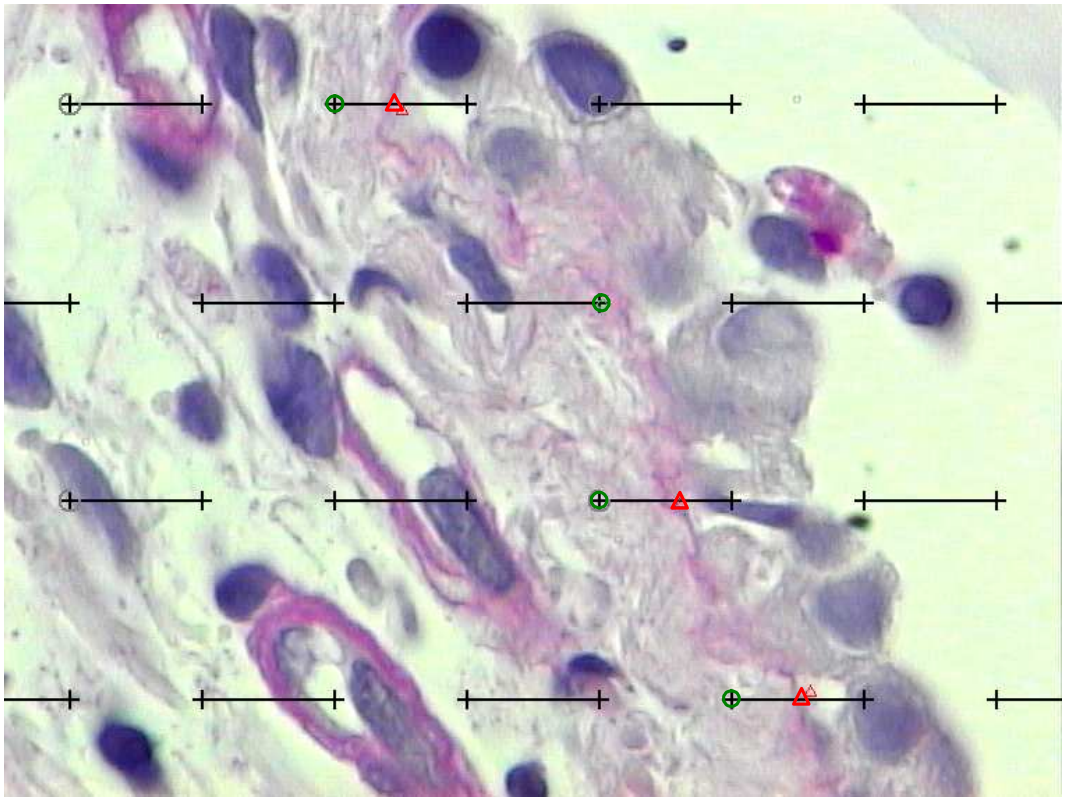

Figure 2.3 Coherent test system for the estimation of the arithmetic mean thickness of the RBM
Red triangles mark the intersections of the line segments with the apical RBM border; green circles mark the points falling onto the RBM.

The coherent test system used for quantification was made up of 16 disconnected line segments of 7.85 µm length (total length = 125.62 µm) and their end points as test points, resulting in 32 test points with a length-per-point (L_p) of 3.93 µm. For the estimation of the surface density, each intersection of the line segments with the apical surface of the RBM was counted. The volume density was estimated by counting the test points that hit the RBM (Figure 2.3). A cumulative count of the number of intersections and points was recorded for each section. The arithmetic mean thickness of the RBM was calculated according to the following equation adapted from Weibel (1990):

Formula 2.2

$$est\bar{\tau} = \frac{\sum P \times L_p}{2 \times \sum I_{ap}} \text{ [µm]}$$

$\bar{\tau}$ = arithmetic mean thickness

P = number of points hitting the RBM

I_{ap} = number of intersections of the segments with the apical surface of the RBM

L_p = length-per-point

2.2.6.4 Cell counting and cell density estimation

Due to the very low contribution of the within-airway between-biopsy variation to the total inter-subject variability of inflammatory cell counts (Gamble et al. 2006), only the biopsy yielding the most sections / slides was selected for cell counting from each subject. The IHC stained sections were analysed using oil immersion lenses with a magnification of 40x (CD68 series) and 60x (CD3 series). The final magnifications were 1400x (CD68) and 2100x (CD3), with a numerical aperture setting of 1.00 and 1.40 respectively, in order to minimize the depth of field.

The reference compartment for cell counting was confined to the lamina propria of the airway mucosa for both cell types. The stained T-lymphocytes and macrophages were quantified over the entire IHC staining series by performing the 2D and 3D counting simultaneously.

2.2.6.4.1 2D Counting – The 'Area Profile' Approach

The 2D profile counting was performed on one of the two sections and its same fields of view sampled for 3D counting (see below). The counting criterion used for the small T-lymphocytes with poorly developed cytoplasm was the stained transect itself. For quantifying macrophages two 2D approaches were used, by counting: 1) all stained cell transects (with or without nucleus) and 2) only stained transects containing a nuclear profile – in order to reduce the influence of differing cell size, while assuming that nuclear size varies less (Jeffery et al. 2003). The results were recorded as cumulative counts for each section. The number of profiles per unit area (N_A) was estimated for each biopsy and cell type according to:

Formula 2.3

$$\hat{N}_A = \frac{\sum profile\ counts}{\sum frames \times frame\ area} \times 10^6\ [\text{mm}^{-2}]$$

$\hat{N}_A$ = estimated number of cell profiles per unit area

2.2.6.4.2 3D Counting – The Physical Disector

Two consecutive sections were selected for the physical disector on each slide. The choice of the disector pair from the three sections mounted on each microscope slide was based on the technical quality of the specimens. Due to the high numerical apertures of the objectives allowing a sufficiently low depth of field, the image was focused on the top side of each section. Thereby the disector height was equal to the mean section thickness represented by the BA of the microtome of 2 µm. Although the final mean section thickness is likely to differ from the BA, the physical disector is insensitive to any form of tissue shrinkage – differential, non-uniform or anisotropic (Dorph-Petersen et al. 2001). By focusing only on the upper side of the sections the rest of the section thickness serves as a guard area. Registration of the sections was achieved semi-automatically with the CAST-Grid 2.01 software, after outlining the specimens and identifying and marking the same anatomical features, e.g., several larger glands or blood vessels, in both sections. The fields of view were determined by a meander SURS scheme with a random start within the outlined specimen, as defined by the software. The sampling distance to step in *x* and *y* was automatically chosen by CAST-Grid 2.01 after manually pre-setting a certain area sampling fraction, i.e., the fraction of the area of interest to be sampled by SUR positioned unbiased counting frames. All sections of a given biopsy were analysed using the same area sampling fraction in order to ensure a uniform sampling probability within the biopsy.

The registered pairs of SUR fields were sequentially presented on the high-resolution monitor and positively stained cell transects within a single focal plane were sampled by an unbiased counting frame (Gundersen 1978; Howard and Reed 1998) with an area of 30% of the displayed field of view. The cell counting was performed according to the directional unbiased counting rule of the physical disector (Figure 2.4).

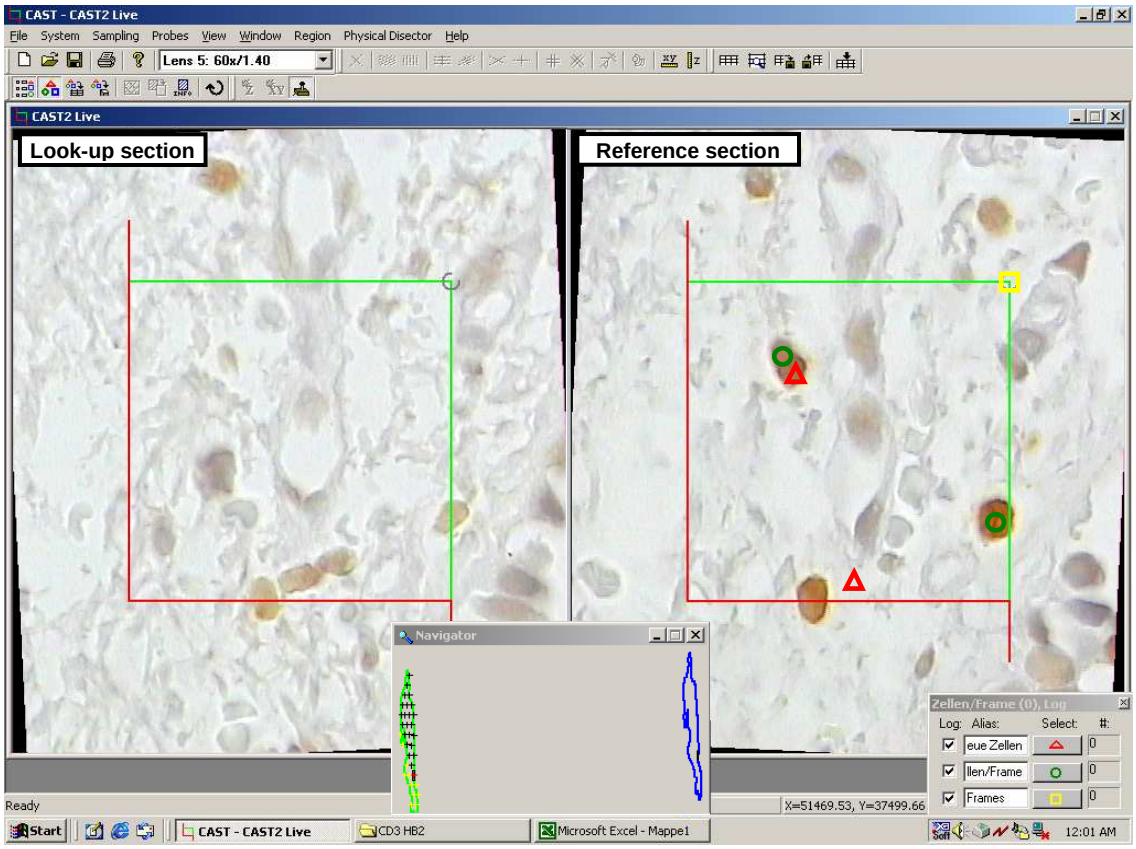

Figure 2.4 Physical disector (3D) and profile counting (2D) within a consecutive reference and look-up section

Red triangles mark cell profiles seen in the reference section which are not present in the look-up section (bidirectional counting); green circles mark all cell profiles seen in the right section; yellow squares mark each assessed counting frame/field of view. The cell profile cutting the lower exclusion (red) line is not counted either in 3D or 2D.

In order to increase efficiency, the counting was performed bidirectionally by interchanging the reference and the look-up sections once the fields were registered, as generally recommended (Howard and Reed 1998). The results were recorded as cumulative counts for each section. Area-sampling fractions ranging 4-16% for the CD3 and 9-25% for the CD68 stained sections yielded sufficiently high counts per biopsy to achieve appropriate CE (Gundersen and Jensen 1987; Gundersen et al. 1999). The numerical density (N_V) was estimated for each biopsy and cell type according to:

Formula 2.4

$$\hat{N}_V = \frac{\sum disector\ counts}{\sum frames \times frame\ area \times BA} \times 10^9\ [mm^{-3}]$$

$\hat{N}_V$ = estimated number of cells per unit volume

2.2.7 Statistical analyses

2.2.7.1 Descriptive statistics

The biopsy volume was reported as median and value range in each group. For each subject and epithelial desquamation pattern, the results of the 1-3 analysed biopsies were averaged to yield the data on the integrity of the epithelial layer. Each group was characterized by the mean value, SD and coefficient of variation (CV) for every morphological category of the epithelium. Similarly, the arithmetic mean thickness of the RBM for each subject was calculated as the average value of 1-3 analysed biopsies. In each group the mean, median, SD and range of values were reported.

For each subject and selected biopsy, N_V [mm^{-3}] and N_A [mm^{-2}] were calculated as discrete values accompanied by the CE calculated with the quadratic approximation formula, which takes into account the nugget effect due to complete random distribution of the cells {Gundersen, 1999 92 /id;West, 1991 122 /id;West, 1996 121 /id}. Mean values are accompanied by the mean CE calculated as the quadratic mean of the individual CEs.

The observed coefficients of variation (OCV) of the study samples were obtained by dividing the observed standard deviations by the sample means. The observed variance (OV) of the estimates, calculated as the mean square deviation of the 7 individual values characterising each subject, has two contributions: (i) the inherent variation between specimens (biological variability) and (ii) the variation introduced by the employed sampling scheme, which is depicted by the mean CE. To ensure that OV mainly depends on the biological variability, the design has to be tuned so that the variation introduced by the sampling is smaller than the biological variability. Taking into account the following relationship:

Formula 2.5

$$OCV^2 = CV^2 + \overline{CE}^2$$

OCV = observed coefficient of variation

CV = true biological coefficient of variation

$\overline{CE}$ = mean coefficient of error of the estimator

and that the true biological variance is not directly available in an estimation design, the previous requirement is fulfilled if the variance due to the sampling is less than half of OV, or rewritten $\overline{CE}^2 < OCV^2/2$ {Miller, 1997 11 /id;West, 1991 122 /id}.

The two cell counting methods deliver results with different dimensions and very different magnitudes. To enable a direct comparison of the 3D and 2D approaches, zero-dimensional ratios between the macrophages and the T-lymphocytes were calculated for N_V, as well as for N_A. The mean ratio values are reported for each group. The CEs of the ratios were calculated as the square root of the sum of squared CEs of the ratio terms. Mean ratios are accompanied by mean CEs, calculated as the quadratic mean of the ratio CEs.

2.2.7.2 Inferential statistics and exploratory data analysis

All statistical analyses were performed using SigmaStat 3.1, charts were created with SigmaPlot 9.0.

The Kolmogorov-Smirnov test was used to test sample data for normality of the underlying populations. The equality of population variances was tested by the variance ratio test (F-test). Parametric testing was then applied to data drawn from normally distributed populations with equal variances. Otherwise non-parametric tests were employed.

Mann-Whitney's non-parametric rank sum test was used to test the biopsy volumes and the extent of epithelial desquamation for significant differences between the smoker and the non-smoker group. The association between biopsy volume or arithmetic mean RBM thickness and the extent of the different patterns of epithelial disruption was investigated by Spearmann's rank correlation coefficient. The arithmetic mean thickness of the RBM was tested for a significant difference between the two groups by Student's unpaired two-tailed t-test.

Pearson's correlation coefficient (r) was used to test the relationship between 3D and 2D density estimates. For each group of subjects, each of the 2D approaches and the physical disector design were tested for differences of the mean $CD68^+/CD3^+$ ratios using Wilcoxon's signed rank test. The mean $CD68^+/CD3^+$ ratios obtained by 2D cell profile counting were tested for differences between the two groups by Mann-Whitney's

non-parametric rank sum test, after standardisation by dividing them by the corresponding 3D mean ratio. P values <0.05 were considered to be significant.

The method agreement was tested for interchangeability of the results using the Bland-Altman analysis (Gallagher 1996; Bland and Altman 1999). Usually both established and alternative methods include substantial error. Comparisons under such circumstances evaluate the agreement between the techniques, not the absolute errors associated with each measurement method. Besides the inherent random measurement error of each method (a gauge of precision), a systematic error, i.e. bias, of one or both methods (a gauge of accuracy) can lead to discrepancies in the results. The bias can be either constant (on offset) or proportional to magnitude of the measurement. The Bland-Altman analysis quantifies these two types of measurement error of the tested method relative to another method, usually a standard. This facilitates a comparison of the so calculated bias and variation of the random error with a priori defined acceptable ranges. The definition of these acceptance intervals depends on the use to which the result is put and is a matter of biological and medical judgement – statistics alone cannot answer such a question.

For each pair of measurements, the difference between the alternative and the standard method (d_i) has to be calculated. The mean of these differences ($\bar{d}$) is an estimate of the relative bias between the two methods; the standard deviation of the differences (s_d) measures random fluctuations around this mean and approximates the variation of the random measurement error. If the differences are normally distributed, 95% of the differences are expected to lie between $\bar{d} - 1.96 s_d$ and $\bar{d} + 1.96 s_d$, which are called 95% limits of agreement – the approximation $\bar{d} \pm 2 s_d$ can be used with minimal loss of accuracy. Such differences are actually likely to follow a normal distribution because most of the variation between subjects (the biological variability) has been removed and only the random measurement errors are left, which are likely to be normal. The estimates of bias and random error are meaningful only if the mean difference and the standard deviation are reasonably uniform throughout the range of measurement, in other words independent of the magnitude of the measurements. These assumptions can be checked graphically. Ideally, the differences between the two methods would have to be plotted against the true value. As this is usually unknown, the best estimate available

is the mean measurement magnitude (m_i), i.e., the mean of the values delivered by the two methods for the same subject. Plotting the differences against the values of either the standard or the alternative method is prone to a statistical artefact, which will eventually lead to entirely false conclusions about the agreement of these methods (Bland and Altman 1995). Any possible relationship between the discrepancies of the methods and the true values can be investigated visually, when a relationship is obvious, or formally by calculating the rank correlation. If there is an association between the differences and the size of the measurements, then the mean difference will tend to rise or fall with increasing magnitude. In this case the analysis will still give limits of agreement which will include most differences, but they will be wider apart than necessary for small magnitudes and rather narrower than they should be for large magnitudes. Such deviations from the assumptions of uniformity of the mean and standard deviation of the differences can be dealt with by a suitable transformation of the raw data, e.g., logarithmic (Bland and Altman 1986; Bland and Altman 1996), or, if this fails, by modelling these parameters as a function of the magnitude of the measurement, using a linear regression approach. The limits of agreement are then obtained by combining the two regression equations in a manner similar to the definition of the 95% limits of agreement mentioned above (Altman 1993; Bland and Altman 1999).

Based on theoretical reasons, the physical disector was regarded as the standard method and the area profile approach as the alternative method. To be acceptable, the 95% limits of agreement had to lie within $\pm\, 2\,\overline{CE}$ of the mean ratios for each group. This takes into account the precision of the ratio estimators, as quantified by the mean CE, and follows the definition of the 95% coefficient of repeatability proposed by the British Standards Institution (1979) - it cannot be reasonably expected for the agreement between two methods to be better than the precision of each estimator. Spearmann's rank correlation coefficient was used to assess the relation between the ratio differences of the two designs and their mean values. Routinely recommended logarithmic transformations of the data usually cannot solve the problem when the differences tend to be in one direction (e.g., negative) for low magnitudes and in the other direction (e.g., positive) for high values. Therefore, model fitting of the relation between the relative bias of the 2D design and the magnitude was performed by linear regression:

Formula 2.6

$$\hat{d}_i = a + bm_i$$

$\hat{d}_i$ = regression estimate of the difference for the *i*-th pair (describes a proportional bias)

a = intercept

b = slope / regression coefficient

m_i = mean magnitude for the *i*-th pair.

The model fitting was quantified by the coefficient of determination (r^2), which for a simple linear regression is equal to the squared Pearson's correlation coefficient and designates the proportion of the total variation of the differences that is explained by the variation of the magnitudes. The Kolmogorov-Smirnov test was used to test the data for normality of the underlying population about the regression line. The Breusch-Pagan test was used to test the regression residuals ($d_i - \hat{d}_i$) for homoscedasticity. Assuming normality about the regression line, a critical assumption for the simple linear regression, the 95% regression based limits of agreement were calculated as $\hat{d}_i \pm 2s_{d|m}$, or using formula 2.6 rewritten as:

Formula 2.7

$$a + bm_i \pm 2s_{d|m}$$

$s_{d|m}$ = standard error of the regression estimates = standard deviation of the residuals, which is given by:

Formula 2.8

$$s_{d|m} = \sqrt{\frac{\sum_{i=1}^{n}(d_i - \hat{d}_i)^2}{n-2}}$$

The regression coefficients and the intercepts of the two groups were tested for differences by Student's t test.

P values <0.05 were considered to be significant. For this threshold of type I error, the desired statistical power was > 80%.

3 Results

3.1 Biopsy volume

The median biopsy volumes were 0.125 (0.059 – 0.530) ml in the non-smoker group and 0.197 (0.058 – 0.491) ml in the smoker group (Figure 3.1).

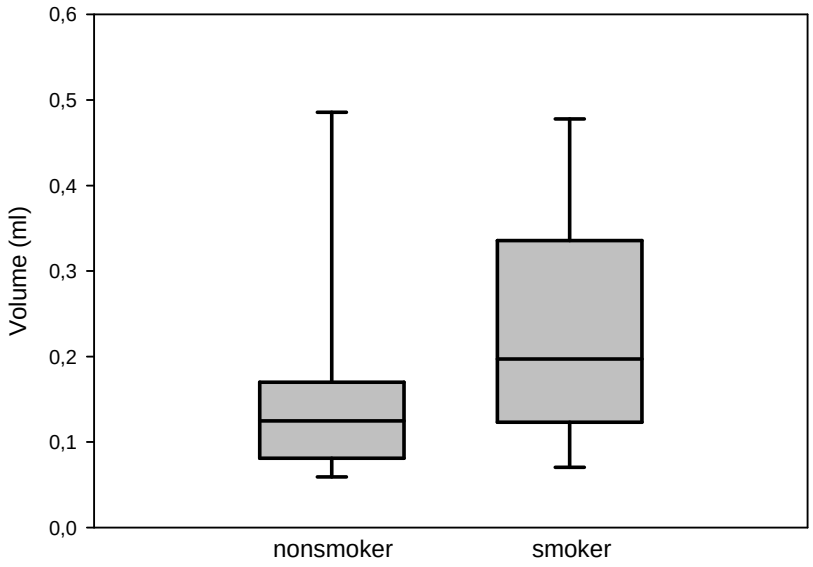

Figure 3.1 Biopsy volumes of the two subject groups
The boundary of the box closest to zero indicates the 25th percentile, the line within the box marks the median and the boundary of the box farthest from zero indicates the 75th percentile. Whiskers (error bars) above and below the box indicate the 95th and 5th percentiles.

Although the value ranges were similar and Mann-Whitney's rank sum test did not detect a significant difference between the medians of the non-smoker and smoker group, there was a clear trend for most non-smoker specimens to cluster around smaller volumes, as shown by the much lower 75th percentile of the non-smoker group: 0.168 ml *versus* 0.317 ml in the smoker group.

3.2 Epithelial integrity

The epithelial lining of the bronchial mucosa displayed a heterogeneous morphology. This ranged from a normal histological appearance of the respiratory epithelium to areas completely lacking this layer, although the RBM was fully preserved (Figure 3.2).

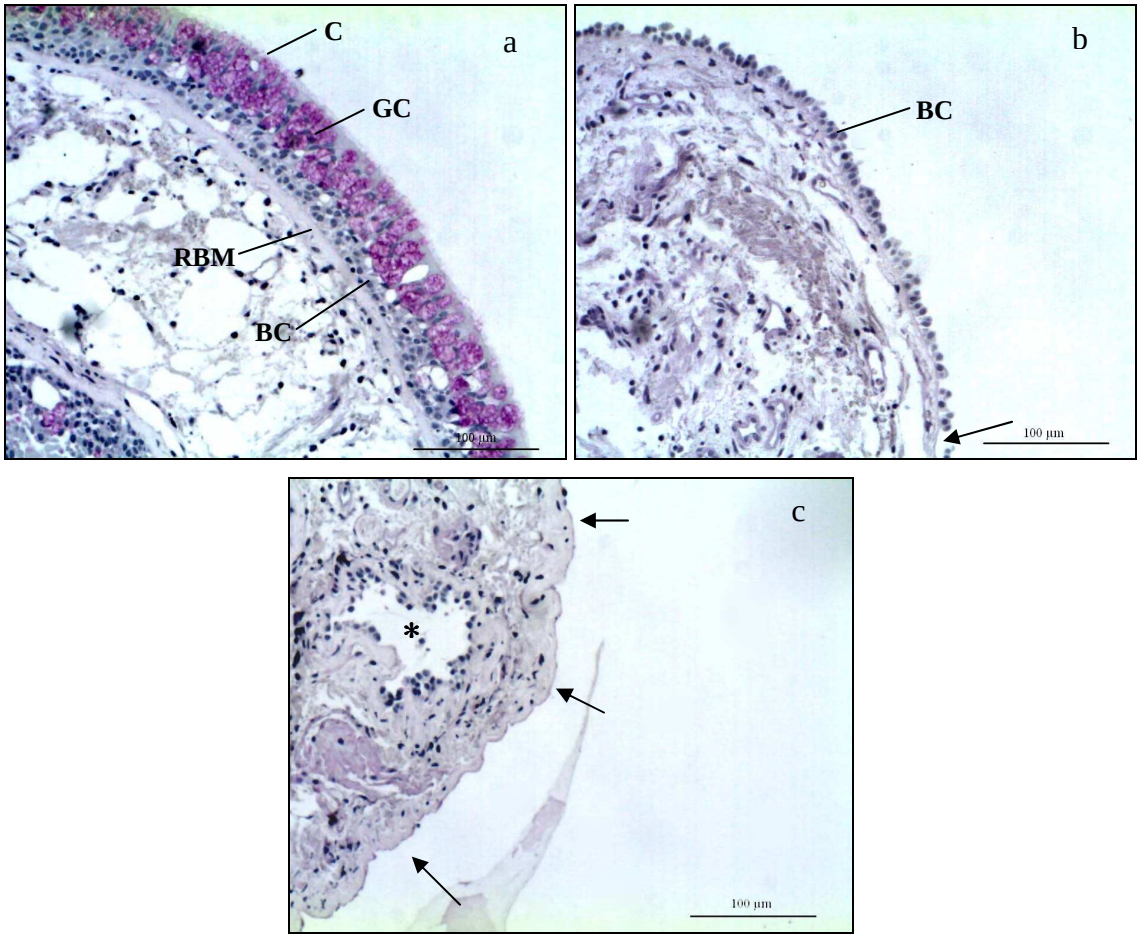

Figure 3.2 Heterogeneous morphology of the respiratory epithelium (20x)
(a) Intact epithelial layer with basal cells (BC), several nuclear rows and visible cilia (C) at the luminal border of the cells. Interspersed goblet cells (GC) with PAS positive (magenta) mucin-filled secretory granules. **(b)** Continuous monolayer of basal cells (BC) with no cilia, no columnar or goblet cells. Completely disrupted epithelium with no cells covering the RBM (←) at the lower image border. **(c)** Intact RBM not covered by epithelial cells (←) following total desquamation of the epithelium. A further closed RBM boundary (∗) displays mostly a monolayer of basal cells.

In both groups only a small fraction of the epithelium was intact, i.e., more than only one layer of basal cells preserved. Two patterns of epithelial damage were noted. The most frequent one was the RBM being covered by a single layer of basal cells with no intact ciliated or goblet cells. Less commonly observed was the complete denudation of all epithelial cells with a bare RBM. The percentage of RBM covered by a single layer of basal cells or no epithelial cells was similar in the endobronchial biopsies of both groups (Table 3.1 and Figure 3.3).

Table 3.1 Epithelial morphology by pattern and subject group

RBM area	non-smoker (n=7)			smoker (n=7)		
	mean	**SD**	**CV**	**mean**	**SD**	**CV**
Intact epithelium	17.5%	9.7%	0.55	20.0%	12.3%	0.61
Fragmented epithelium	47.8%	10.4%	0.22	56.3%	12.9%	0.23
Denuded	34.7%	6.3%	0.18	23.7%	15.5%	0.65
Total disrupted epithelium	82.5%	9.7%	0.12	80.0%	12.3%	0.15

Definition of abbreviations: SD = standard deviation of the sample, CV = coefficient of variation of the sample

The spread of the individual values about the mean was large, especially for the RBM covered by intact epithelium.

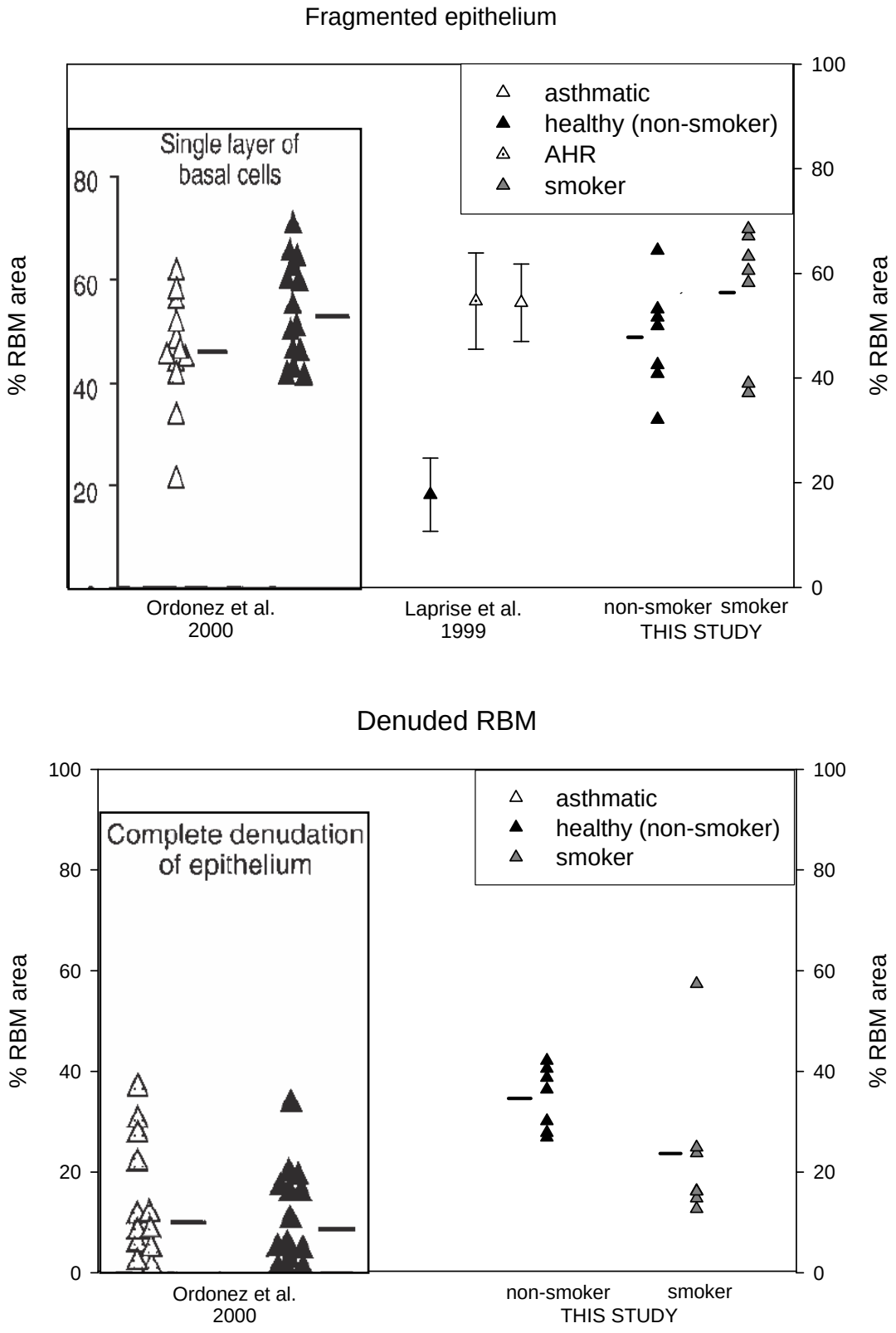

Figure 3.3 Epithelial integrity by pattern and subject group – comparison with published data

Horizontal bars represent sample mean values, *error bars* represent 2 SD.

When examining the relation between the epithelial integrity of each biopsy and its volume, there was a trend for the largest areas of denuded RBM and smallest areas of intact epithelium to be encountered in small biopsies with a volume up to 0.1 ml. The largest areas of intact epithelium in the smoker group were noticed in the largest biopsies, with a volume over 0.4 ml, though a similar behaviour could not be identified in the non-smoker group (Figure 3.4).

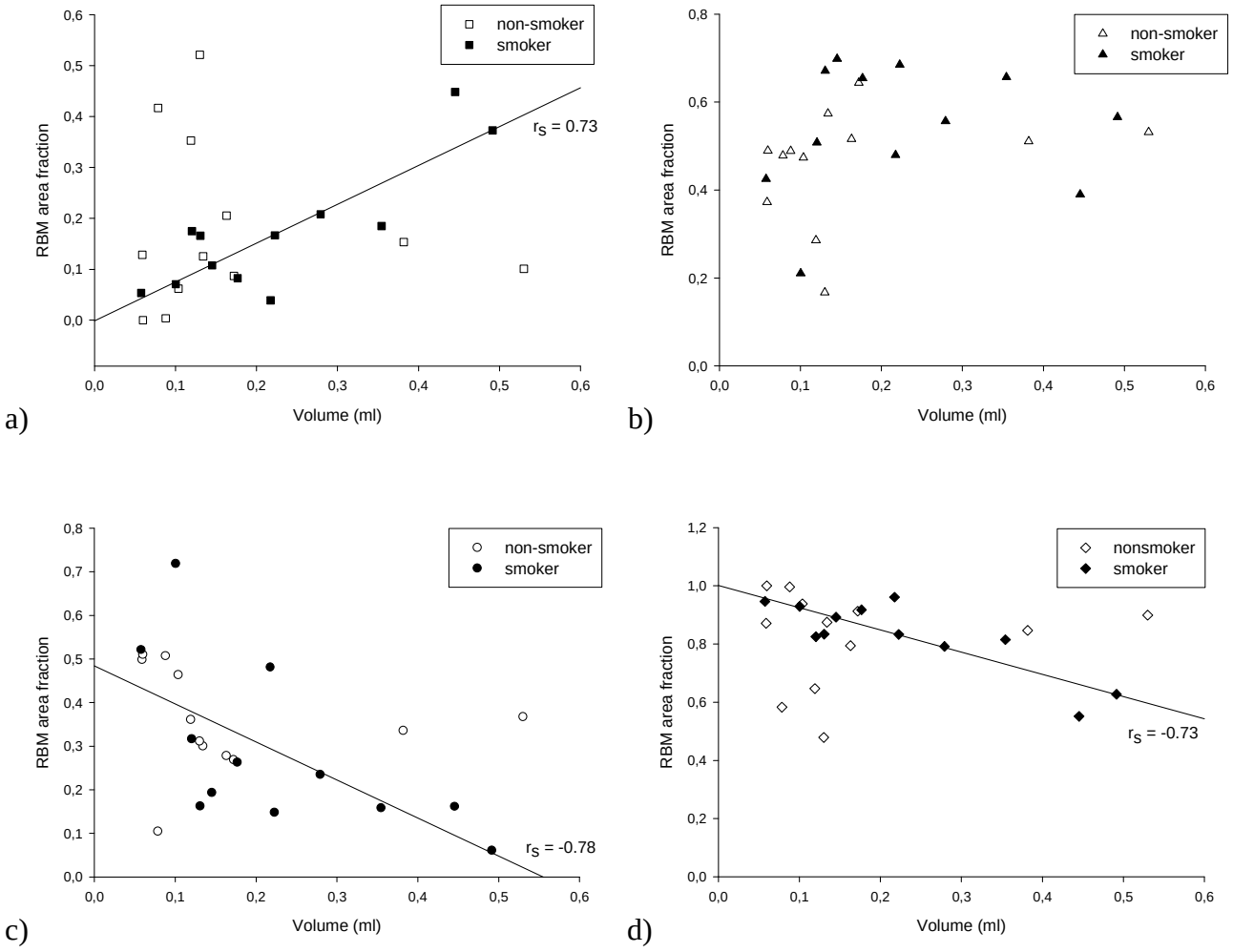

Figure 3.4 Correlation of the epithelial morphology with the biopsy volume
(a) intact respiratory epithelium, **(b)** fragmented epithelium, **(c)** epithelium denuded RBM and **(d)** total disrupted epithelium (fragmented *and* absent). Regression lines depict very strong correlations between RBM area fraction and biopsy volume in the smoker group. No significant correlations were found in non-smokers.

A very strong and significant correlation between the biopsy volume and the epithelial morphology could be noticed for intact epithelium ($r_s = 0.73$, $P_r = 0.005$), denuded RBM ($r_s = -0.78$, $P_r = 0.001$) and total disrupted epithelium ($r_s = -0.73$, $P_r = 0.005$) only in the

smoker group. The RBM area covered by fragmented respiratory epithelium mostly ranged between approx. 40% and 70%, without a noticeable dependence on the biopsy volume in any group.

Mann-Whitney's rank sum test did not detect any significant differences between the non-smoker and the smoker group with regard to the RBM area fractions covered by fragmented epithelium or completely denuded of respiratory epithelium, respectively. Furthermore no significant difference could be detected for the total RBM area fraction of disrupted epithelium (fragmented *and* absent) between the two groups.

3.3 Thickness of the reticular basement membrane

The reticular basement membrane appeared as a homogenous PAS positive band of various width between the lamina propria and the epithelium, where preserved (Figure 3.2).

The arithmetic mean thickness of RBM showed a high within-group variability but no significant difference between the non-smoker and the smoker group, as assessed by Student's unpaired t-test: 3.28 ± 0.97 µm *versus* 4.36 ± 1.20 µm respectively, P = 0.1 (Figure 3.5). Median values and ranges were 2.97 (2.33 – 5.13) µm and 3.73 (3.54 – 6.83) µm.

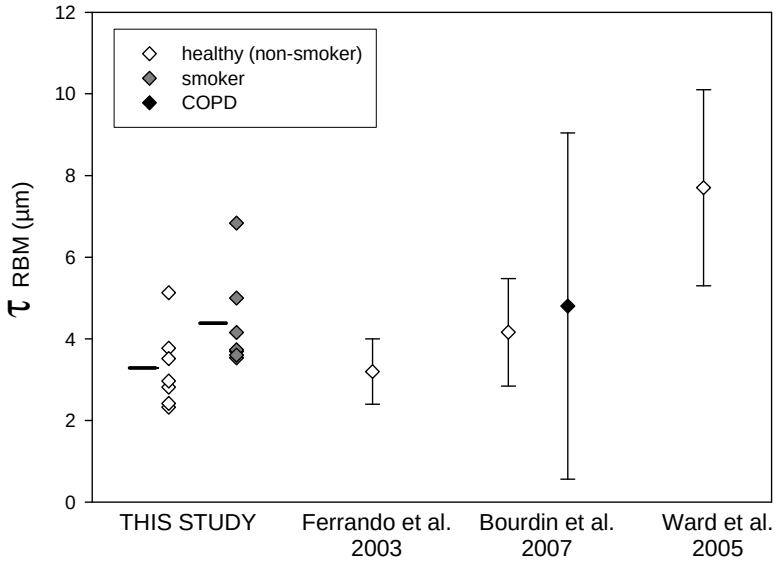

Figure 3.5 Arithmetic mean thickness of the RBM
Horizontal bars represent average values, *errors bars* represent 2 SD.

As there were no significant differences between the two groups either in the RBM area fractions of epithelial damage or in the arithmetic mean thickness of the RBM, the results of all 24 biopsies were pooled for a correlation analysis between the arithmetic mean thickness of the RBM and the amount of epithelial disruption. No significant correlation between the arithmetic mean thickness of the RBM and the extent of the different patterns of epithelial damage (i.e., fragmented or completely absent) could be found using Spearmann's rank order correlation coefficient. Similarly, no significant correlation could be found between the arithmetic mean thickness of the RBM and the total extent of the epithelial disruption (fragmented *and* absent).

3.4 2D and 3D inflammatory cell counts

On the IHC sections, the cells of interest appeared dark brown stained against the pale blue background. The nuclei of all cells, IHC-positively stained or not, appeared dark blue (Figure 3.6 and 3.7). Low levels of non-specific positive staining were displayed by the nuclei of epithelial cells on anti-CD3 stained sections; however, this compartment was not subject to the quantitative analyses of inflammatory cells, so that false positive results were avoided. The anti-CD68 stained sections did not display any non-specific positive reaction.

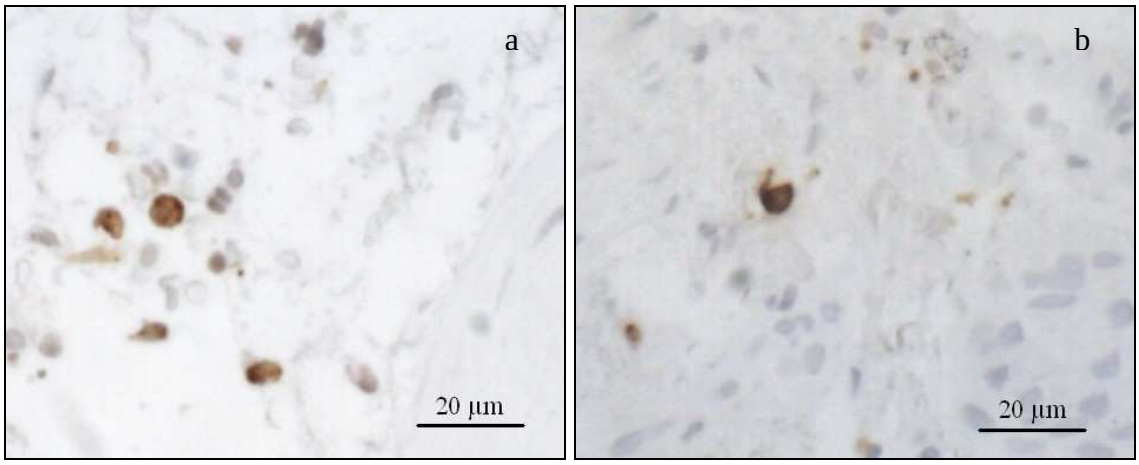

Figure 3.6 Anti-CD68 stained sections of endobronchial biopsies (40x)
Macrophage profiles stained brown in a **non-smoker (a)** and a **smoker (b)** subject. Pale blue counterstaining of the background. Nuclei stained blue.

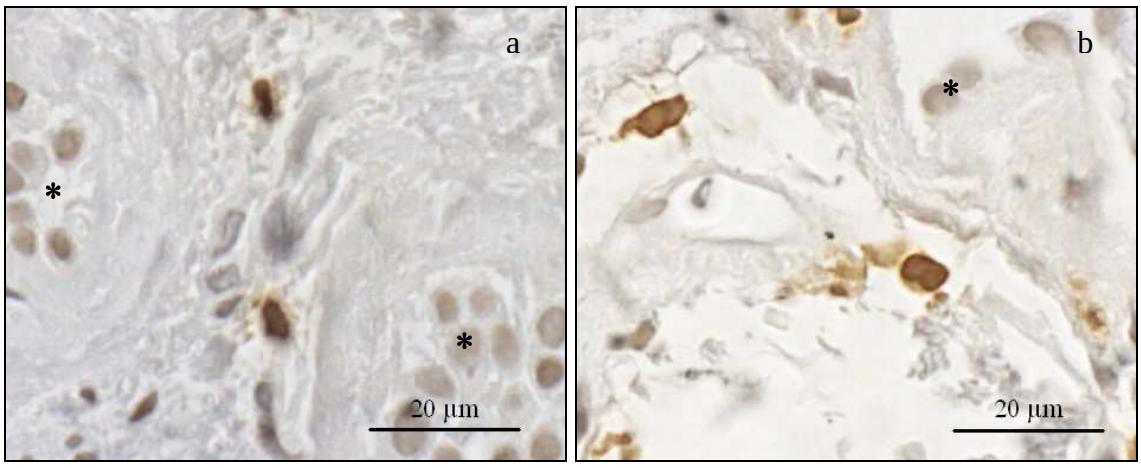

Figure 3.7 Anti-CD3 stained sections of endobronchial biopsies (60x)
T-lymphocyte profiles stained brown in a **non-smoker (a)** and a **smoker (b)** subject. Non-specific positive staining of epithelial nuclei (∗).

Table 3.2 summarises the mean counts per unit for each group, cell population and counting method.

Table 3.2 Quantitative morphological data by group and cell type

Group	Cell Type	N_V (mm^{-3})		$N_{A\ nucleus}$ (mm^{-2})		$N_{A\ cell}$ (mm^{-2})	
		mean	**CE**	**mean**	**CE**	**mean**	**CE**
non-smokers	$CD68^+$	85987	9.7%	350	10.1%	569	7.6%
	$CD3^+$	228612	9.3%	N. A.	N. A.	931	9.3%
smokers	$CD68^+$	46025	11.5%	163	12.4%	534	6.6%
	$CD3^+$	91870	10.4%	N. A.	N. A.	322	11.2%

Definition of abbreviations: N_V = numerical density, $N_{A\ nucleus}$ = nuclear profile per unit area, $N_{A\ cell}$ = cell profile per unit area, CE = coefficient of error of the mean estimate, N. A. = not analysed

The area profile number was considerably higher when counting all cell profiles instead of only nuclear profiles in both groups. Because in the 2D approach the data were recorded as cell or nuclear profile counts per unit area (N_A), whereas in the 3D approach cell numbers per unit volume (N_V) were obtained, the completely different scale units precluded a direct statistical testing for differences or agreement between these methods. The OCV of the 2D and 3D densities ranged from 29% to 51%. Although counting was performed on the same sampled fields of view, the variation between subjects tended to be lower in the 3D as compared with the 2D approach, reflected in lower OCVs (Figure 3.8). The mean CEs were fairly constant: 7.6 to 12.4 %, regardless of the approach used, the cell population under investigation or the study group. They represented 1.7 - 10.9% of the OV, in accordance with the recommendation for the sampling variance (i.e., counting noise) to be less than half of the OV {Miller, 1997 11 /id;West, 1991 122 /id}.

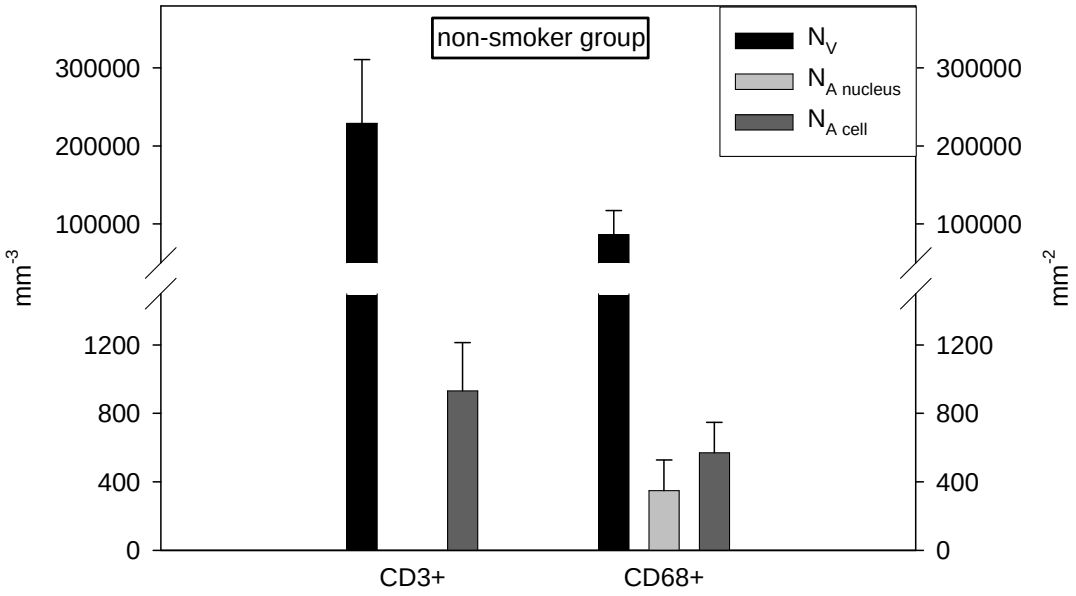

a)

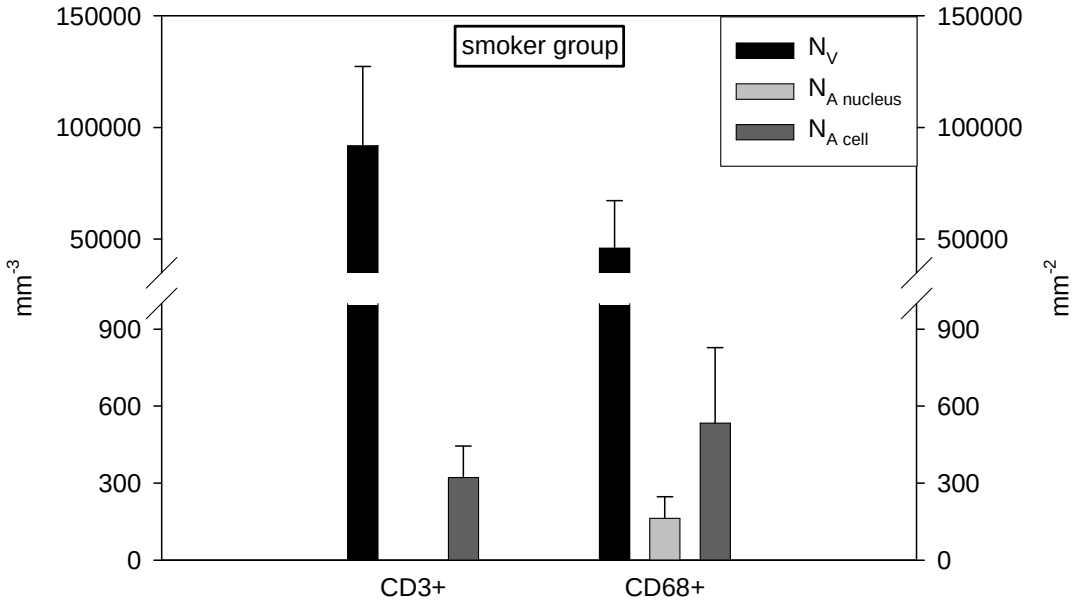

b)

Figure 3.8 Mean counts per unit volume and area (mean + SD) by group and cell population

In both groups, N_A and N_V were very strongly (Kühnel and Krebs 2004) and significantly correlated, as shown by Pearson's product-moment correlation coefficient for both T-lymphocytes (Figures 3.9 a and b) and macrophages (Figures 3.9 c and d). However, the calculated slopes of the regression lines ranged 0.0029 to 0.0123.

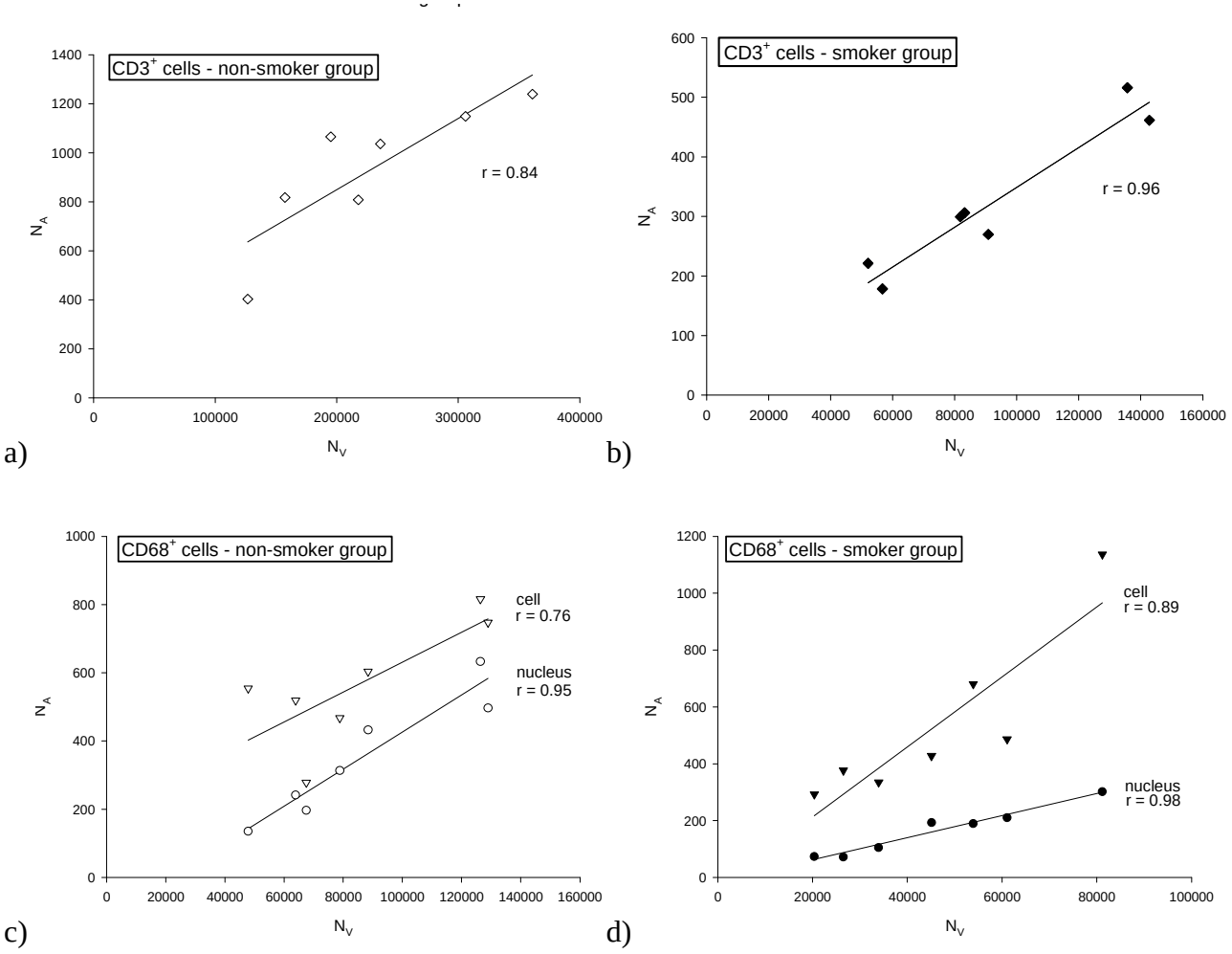

Figure 3.9 2D profiles per unit area *versus* 3D numerical density
(a) T-lymphocytes, non-smokers, r = 0.84, $p < 0.05$; **(b) T-lymphocytes, smokers**, r = 0.96, $p < 0.001$; **(c) macrophages, non-smokers**, $r_{nucleus} = 0.95$, $p < 0.005$; $r_{cell} = 0.76$, $p < 0.05$; **(d) macrophages, smokers**, $r_{nucleus} = 0.98$, $p < 0.0005$; $r_{cell} = 0.89$, $p < 0.01$

In order to enable direct statistical comparisons of the two methods, the dimensionless ratio between $CD68^+$ and $CD3^+$ counts was calculated. The trend for the OCV to be higher in the 2D than the 3D approach was also present and even more pronounced for the $CD68^+/CD3^+$ cell ratios. The CE of the mean ratios ranged from 12 to 16.7% (Table 3.3).

Table 3.3 $CD68^+/CD3^+$ cell ratios by group and counting design

Group	$CD68^+/CD3^+$ 3D		$CD68^+/CD3^+$ 2D nucleus		$CD68^+/CD3^+$ 2D cell	
	Mean	**CE**	**Mean**	**CE**	**Mean**	**CE**
non-smokers	0.39	13.4%	0.43	13.7%	0.68	12.0%
smokers	0.49	15.5%	0.50	16.7%	1.68	12.9%

Definition of abbreviations: 3D = physical disector, 2D nucleus = counts of nuclear profiles, 2D cell = counts of cell profiles (with and without nucleus), CE = coefficient of error of the mean ratio estimate

In each study group, the mean $CD68^+/CD3^+$ ratios obtained from 3D and 2D cell profile counts showed statistically significant differences ($P < 0.05$), with the 2D values being on average 1.7 (non-smokers) to 3.4 (smokers) times higher. This difference in the relative amplitude of the 2D estimator across the two subject groups was also statistically significant (Mann-Whitney's non-parametric rank sum test, $P < 0.005$). When counting only $CD68^+$ cell profiles containing a nucleus, the mean results of the 3D and 2D nuclear profile approaches were almost identical and the hypothesis of the difference being due to chance could not be rejected (Table 3.4 and Figure 3.10).

Table 3.4 Hypothesis testing and correlation of the $CD68^+/CD3^+$ cell ratios between the 3D and 2D counting designs

Group	Counting designs		W	P_W	r	P_r
non-smokers	3D	2D nucleus	2	NS	0.970	< 0.0005
	3D	2D cell	28	< 0.05	0.955	< 0.001
smokers	3D	2D nucleus	6	NS	0.772	< 0.05
	3D	2D cell	28	< 0.05	0.665	NS

Definition of abbreviations: W = Wilcoxon's test statistic, r = Pearson's correlation coefficient, 3D = physical disector, 2D nucleus = counts of nuclear profiles, 2D cell = counts of cell profiles (with and without nucleus), NS = nonsignificant

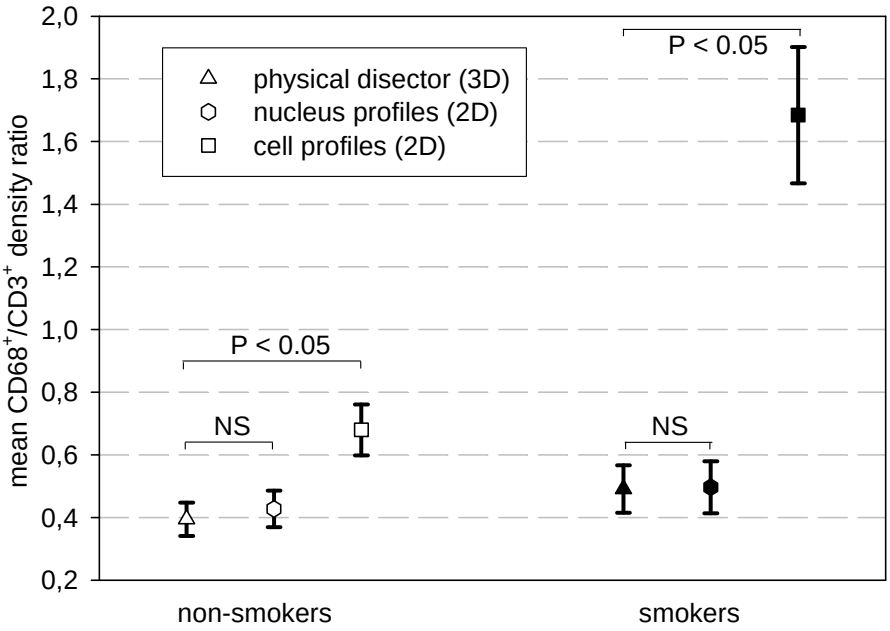

Figure 3.10 Mean $CD68^+/CD3^+$ cell density ratios (mean ± SE) for each design and study group

Nevertheless, after plotting the ratios calculated from the 2D nucleus and 3D design against each other it was fairly obvious that most measurement pairs were not in good agreement, i.e. they were widely scattered around the line of equality y = x (Figure 3.11).

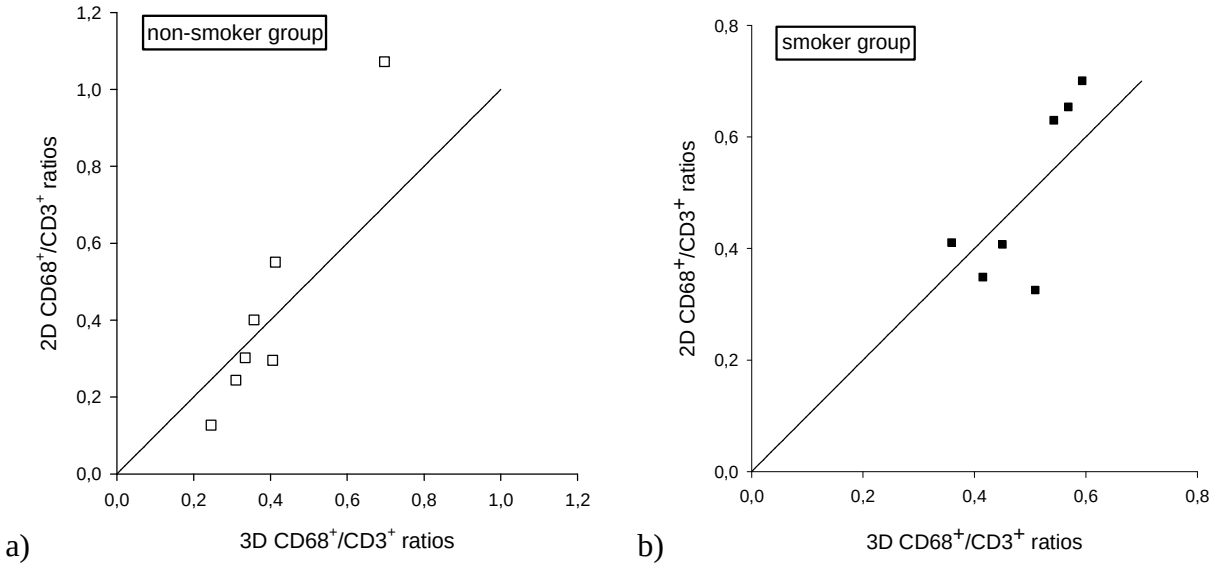

Figure 3.11 $CD68^+/CD3^+$ cell density ratios by the 2D (nucleus) and 3D design (a) non-smoker and **(b) smoker** group with the line of equality (y = x)

In order to quantitatively assess the agreement, the difference between the ratios by the two methods was plotted against their mean, for each subject (Figure 3.12).

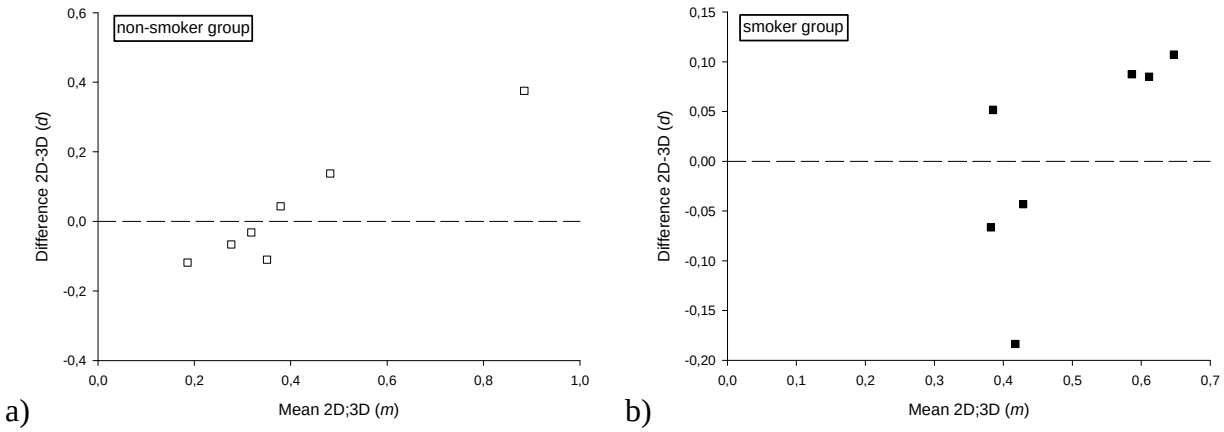

Figure 3.12 Bland-Altman plots of the CD68$^+$/CD3$^+$ cell density ratios by both designs (2D;3D)
Dashed line y = 0 represents the line of equality, which stands for perfect agreement.

A striking relation between the differences and the magnitude (mean of ratios) could be noticed and formally examined by assessing the rank order correlation: Spearmann's correlation coefficient r_s was 0.89 for the non-smoker group and 0.79 for the smoker group, both statistically significant ($P_r < 0.05$).

In the non-smoker group, the ratio means reflected 91% of the variability in the ratio differences, as measured by the coefficient of determination r^2. The regression of the differences (d_i) on the means (m_i) according to formula 2.6 gave:

Formula 3.1

$$\hat{d}_{i_1} = -0.273 + 0.744 \times m_{i_1}$$

which represents the proportional bias of the 2D ratios compared to the 3D approach (Figure 3.13a). The constant variance test was passed, indicating homoscedasticity of the differences. Therefore, instead of regressing the residuals on the means, the standard deviation of the residuals (0.053) was used to calculate the regression based 95% limits of agreement, as given by formula 2.7:

$$-0.273 + 0.744 \times m_{i_1} \pm 2 \times 0.053 = -0.273 + 0.744 \times m_{i_1} \pm 0.106$$

This fell under the criteria of acceptance for the 95% limits of agreement set to ± 2SE, respectively ± 0.12 less bias. When constructing such a parametric reference range for the predicted variable, the assumption of normality for the distribution of the source population about the regression line is critical (Altman 1993; Zar 1999). The normality test of the residuals was passed. Finally, the power of the performed regression was 97.6% indicating a high appropriateness in describing the relationship between the differences and the magnitude.

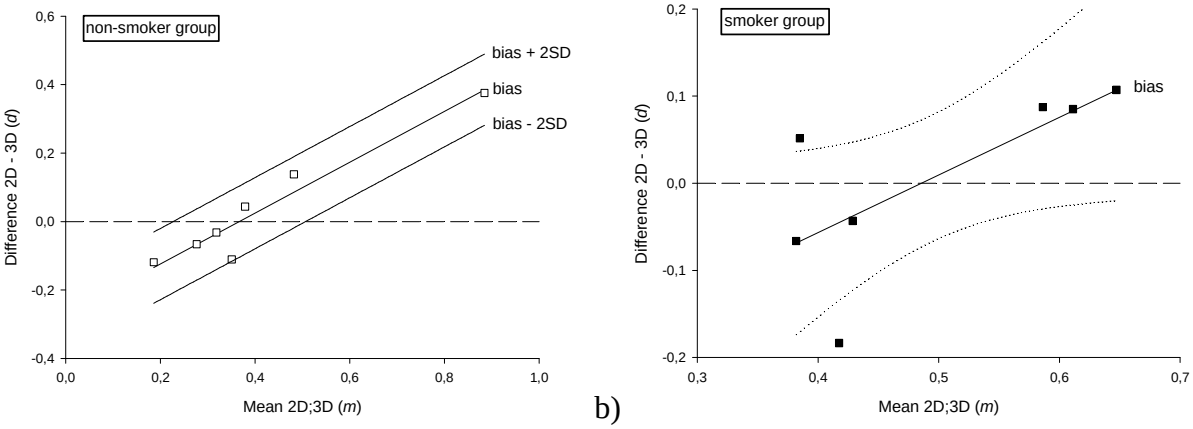

a) b)

Figure 3.13 Regression based Bland-Altman plots of the CD68$^+$/CD3$^+$ density ratios

(a) Regression based mean difference (bias) and 95% limits of agreement for the differences of the CD68$^+$/CD3$^+$ cell density ratios as determined by the 2D nucleus and 3D approaches in the **non-smoker group**. All values lie within the interval between the calculated 95% limits of agreement; **(b)** Regression based mean difference (bias) with 95% C.I. of the regression line (dotted) for the differences of the CD68$^+$/CD3$^+$ cell density ratios in the **smoker group**. The 95 % C.I. includes several horizontal lines (slope = 0) so that the fitted linear model does not achieve the desired statistical significance.

In the smoker group fitting a linear regression model showed that the ratio means account for only 41.4% of the variability of the ratio differences, as measured by the coefficient of determination r^2. The regression equation of d_i on m_i (Formula 2.6) gave:

Formula 3.2

$$\hat{d}_{i_2} = -0.321 + 0.662 \times m_{i_2}$$

which represents the proportional bias of the 2D ratios compared to the 3D approach. The chosen level of significance was not reached for either the slope (regression coefficient) or the F-statistic (P = 0.07) (Figure 3.13b). The statistical power of the performed regression for the sample size n = 7 and α = 0.05 was 43.4%. A subsequent polynomial regression showed no fitting improvement for higher order equations, so the linear model was further elaborated. By examining the plot of the ratio differences against the means, two large outliers could be easily identified (Figure 3.12b). As these two subjects appeared to have very low $CD68^+$ and $CD3^+$ N_V (the lowest in the sample), the counting results were very low and therefore the CE quite high for both $CD68^+$ and $CD3^+$ cells in both designs. This also led to high CE (up to 25%) of the calculated ratios. Because this very high measurement error was likely to be a strong confounder in a sample of n = 7, these two subjects were excluded and then the regression analysis of the differences on the means was repeated. This led to a remarkable improvement, with the mean ratios reflecting 98.3% of the variability in the ratio differences. The regression equation of d_i on m_i became:

Formula 3.3

$$\hat{d}_{i_3} = -0.332 + 0.690 \times m_{i_3}$$

which represents the proportional bias of the 2D ratios compared to the 3D approach (Figure 3.14). The constant variance test was passed, indicating homoscedasticity of the differences. Therefore, instead of regressing the residuals on the means, the standard deviation of the residuals (0.011) was used to calculate the regression based 95% limits of agreement, as given by formula 2.7:

$$-0.332 + 0.690 \times m_{i_3} \pm 2 \times 0.011 = -0.332 + 0.690 \times m_{i_3} \pm 0.022$$

Because of the decrease in the mean relative error of the ratio estimator (mean CE) to approx. 11%, acceptable agreement had to be redefined as ± 0.11 less bias. The recalculated regression based limits of agreement fully complied with this new definition. The statistical power of the regression increased considerably to 98.1% (for α = 0.05).

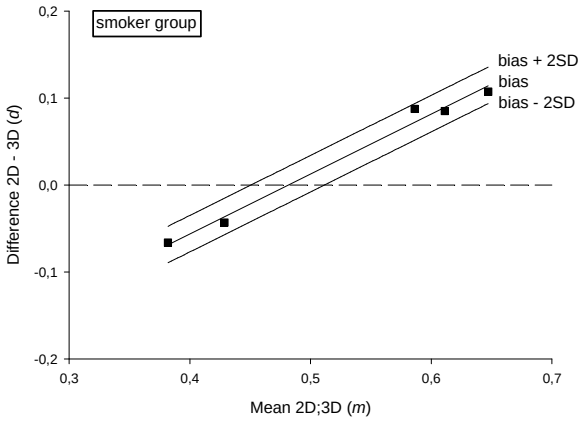

Figure 3.14 Regression based Bland-Altman plot for smokers without outliers
Regression based mean difference (bias) and 95% limits of agreement for the differences of the $CD68^+/CD3^+$ cell density ratios as determined by the 2D nucleus and 3D approaches in the **smoker group** after removing the two large outliers.

The regression coefficients of formula 3.1 and 3.3 were tested for a significant difference using Student's t test (Zar 1999). This yielded a value smaller than the critical one at $\alpha = 0.05$, which led to the conclusion that the difference of the two slopes was not statistically significant. Its 95% confidence interval (-0.396; 0.504) included the 0 value. Therefore, an estimate of the population regression coefficient (β) underlying the regression coefficients of both samples, which is called the common (or weighted) regression coefficient, could be computed: $b_c = 0.736$. A Student's t test, which compared the two intercepts of formula 3.1 and 3.3, yielded a value larger than the critical one, indicating a statistically significant difference ($P < 0.01$). Thus the regression equations 3.1 and 3.3 became:

Formula 3.4

$$\hat{d}_{i_1} = -0.273 + 0.736 \times m_{i_1}$$

Formula 3.5

$$\hat{d}_{i_3} = -0.332 + 0.736 \times m_{i_3}$$

Summarizing, even though the differences between the mean ratios of N_V and those of $N_{A\ nucleus}$ were not statistically significant and they showed a consistent correlation (Table 3.4), the Bland-Altman analysis identified a non-uniform bias of the 2D profile number estimator (Figure 3.13 and 3.14). Nevertheless, the random error about the bias

was low enough for the regression based 95% limits of agreement to be acceptable in both groups.

4 Discussion

4.1 Epithelial integrity

Recent publications increasingly stress the putative central pathophysiological role of the respiratory epithelium in the initiation of the chronic inflammation, its maintenance and the inappropriate remodelling of the airways in asthma (Holgate et al. 1999; Holgate et al. 2003; Hackett and Knight 2007; Holgate 2008; Folli et al. 2008). The function of the epithelium as a physical barrier between the environmental air in the lumen of the airways and the organism was amended by its humoral autocrine and paracrine functions (Davies and Devalia 1992; Polito and Proud 1998; Puddicombe et al. 2000). Both the structural and humoral properties contribute to the homeostasis of the airways and are intuitively thought to be at least in part dependent on the morphological integrity of the epithelial layer. Consequently and following some early reports of epithelial damage in mild to fatal asthma (Dunnill 1960; Naylor 1962; Cutz et al. 1978; Laitinen et al. 1985) the morphology of the airway lining became an appealing topic in pulmonary research. During the past two decades many studies examined the integrity of the respiratory epithelium by different approaches and the results were somehow equivocal. The post-mortem findings of shed epithelial cells in the asthmatic airway lumen (Dunnill 1960) could not be confirmed as significantly increased by a later comparative necroptic study (Carroll et al. 1993). Similarly, discrepant results were obtained in induced sputum analyses. Fahy et al. (1995) could not confirm the increased shedding of epithelial cells previously noticed in asthmatic sputa (Naylor 1962). BAL examinations claiming more extensive epithelium damage and sloughing in asthma (Beasley et al. 1989; Montefort et al. 1992; Chanez et al. 1999) were not supported by others (Kirby et al. 1987; Foresi et al. 1990; Redington et al. 1995). Whereas some bioptic studies sustain the hypothesis of increased epithelial desquamation being a pathologic feature of asthma (Laitinen et al. 1985; Jeffery et al. 1989; Montefort et al. 1993b; Laprise et al. 1999), later publications based on larger numbers of subjects and homogenous clinical characteristics of the study groups failed to detect a significant difference (Lozewicz et al. 1990; Boulet et al. 1997; Ordonez et al. 2000; Fahy 2001). Similarly, findings of a correlation between epithelial disruption and airway hyperresponsiveness (AHR) in asthmatics (Jeffery et al. 1989; Beasley et al. 1989; Laprise et al. 1999) were not confirmed by other studies (Laitinen et al. 1985; Boulet et

al. 1997; Ordonez et al. 2000). In addition, extensive epithelial damage was documented in endobronchial biopsies of healthy volunteers (Soderberg et al. 1990), highlighting the potential for artefactual damage during biopsy sampling and processing, which should be considered before attributing all epithelial alterations to pulmonary disease. This hypothesis is supported by the findings of Aleva et al. (1998) that biopsy morphology and size largely vary with the size and shape of the biopsy forceps. Therefore, the potentially artefactual nature of the specimen morphology due to bronchoscopist skills, forceps type and sharpness, tissue properties and further processing has to be acknowledged.

Another interesting *in vitro* observation argues against the complete denudation of RBM seen in endobronchial biopsies being a true morphopathological feature. The remaining basal cells in adjacent regions of experimentally denuded areas were seen to flatten and spread to cover the denuded RBM within 20 minutes (Erjefalt et al. 1997; Polito and Proud 1998). If asthma were to cause complete denudation of the epithelial lining of the RBM, this alteration would be repaired by the remaining neighbouring basal cells very quickly, so that epithelium denuded areas of the RBM should barely be distinguishable in biopsy specimens.

In spite of the high variability of the available data on the epithelial integrity in endobronchial biopsies, a common finding of all reports is the most frequent pattern of disruption in both healthy and asthmatic subjects being the RBM covered by a single layer of basal cells with no intact ciliated or goblet cells. In the present study this was also true for both groups (Figure 3.3). This pattern represented approx. 50% (35-65%) of the RBM area in both non-smokers and smokers and is in excellent agreement with the results of Ordoñez et al. (2000), who also found it to be approx. 50% (35-60%) in both healthy and asthmatic subjects. Similar results were reported by Boulet et al. (1997) for healthy controls: approx. 30% (20-60%), with an even higher variability in chronic bronchitics: approx. 60% (5-80%). Notably, Laprise et al. (1999) studying a group of mild asthmatic patients and a group of asymptomatic subjects with AHR found mean values of 54.4 ± 3.7% and 54.7 ± 4.6%, respectively (Figure 3.3). This points out that the extent of the desquamation appears to be independent of the presence or the type of an airway disorder.

Less commonly observed was a completely denuded RBM, in this study amounting to an area fraction of approx. 30% (15-55%). This is more extensive than in the observations of Ordoñez et al. (2000), but with a similar spread: approx. 15 % (0-40%). The large spread of the values around the mean, noticed for all categories, is in accordance with some previous reports (Lozewicz et al. 1990; Montefort et al. 1993b; Ordonez et al. 2000).

These findings further support the theory that the plane of cleavage of the respiratory epithelium is usually located between the suprabasal and the basal cell layers (Montefort et al. 1992) and strengthen the belief that the bronchial epithelium is a truly stratified structure with the ciliated columnar cells entirely depending on the underlying basal cells for anchorage to the RBM (Evans and Plopper 1988; Roche et al. 1993; Montefort et al. 1993a). When considering the total extent of epithelial disruption, this amounted to approx. 80% (55-95%) in both groups of the present study and appeared to be higher than previous data (Ordonez et al. 2000). Conversely, the amount of RBM covered by intact ciliated epithelium was approx. 20% (5-45%), very similar to the data previously reported by Montefort et al. (1993b) for asthmatics: 15% (3-36%). This high variability of the results of the present and previous studies makes the reliability of the epithelial desquamation in endobronchial biopsies, as an indicator and quantifier of airway pathology, questionable.

As expected, there were no significant differences in the extent and the patterns of epithelial disruption between the non-smoker and the smoker groups. Moreover, the quantitative results were in accordance with those of previous studies, which found no significant differences between an asthmatic and a healthy control group (Boulet et al. 1997; Ordonez et al. 2000). This confirms and reinforces the validity of these data and the conclusion that the morphological changes noticed in endobronchial biopsies are largely an artefact of tissue sampling and not associated with airway disease. Interestingly, the value ranges were similar although different histological techniques (i.e., fixation, embedding, staining) and quantitative approaches (i.e., stereology in the present study and image analysis in previous work) were employed. This argues against a significant influence of the biopsy processing and analysis on the epithelial integrity in endobronchial biopsies and underlines the robustness of the data.

The influence of bronchoscopy and biopsy procedures on the epithelial morphology of endobronchial biopsies was already postulated (Jeffery 1996; Jeffery 2001). The size

and type of biopsy forceps was shown to have an influence on specimen size and the preservation of tissue architecture (Aleva et al. 1998). The stereologic design of this study allowed implementing the Cavalieri method for direct estimation of the biopsy volume. Subsequently, the hypothesis that the epithelial integrity depends on the biopsy size, i.e., volume, was examined. In accordance with the findings that suggested a significant procedural influence on the biopsy morphology, the largest areas of denuded RBM and total areas of disrupted epithelium, hence the least preserved epithelium, were encountered in the smallest biopsies, whereas the largest biopsies predominantly exhibited fully preserved epithelium and little disruption. The area fraction of RBM covered by intact ciliated epithelium displayed a very strong positive correlation with the biopsy volume in the smoker group. In the same group the area fraction of completely denuded RBM and that of total disrupted epithelium showed a very strong negative correlation with the volume of the biopsies (Figure 3.4). This leaves room to speculate that smaller biopsies encounter a higher mechanical force per area unit during extraction, which leads to a higher proportion of complete desquamation of the epithelial layer from the RBM. Conversely, with larger biopsy volume and therefore lower mechanical force per area unit more intact epithelium is preserved. No similar correlations could be identified in the non-smoker group. This might be explained by the tight clustering of most biopsy volumes in the non-smoker group around lower values, as shown by the much lower 75th percentile (Figure 3.1). It can be further speculated that in this volume range the mechanical forces acting on the unit area of RBM were probably so high that a threshold-effect, ‘overriding’ a gradual synchronous variation of the two variables, might have been encountered. A higher tissue consistency of the non-smokers, as reported by the bronchoscopist, could have also led to higher mechanical forces being applied during biopsy collection. A similar explanation could be imagined for the lack of a significant correlation between the RBM area covered by fragmented epithelium and the biopsy volume in both study groups. As already stated, the preferential cleavage plane of the epithelial layer is situated suprabasally. This was attributed to the weaker resistance of the desmosomes between the ciliated and the basal cells, as compared to the hemidesmosomes attaching the basal cells to the RBM (Montefort et al. 1992; Montefort et al. 1993b). Possibly, strong mechanical forces above a certain threshold, as during the biopsy extraction, exert further damage rather

by an increasing disruption of the more stable hemidesmosomes after most desmosomal attachments have already been split.

The present findings do not rule out the possibility of weaker than normal intercellular adhesion in the asthmatic epithelium. This possible alteration of the *epithelial fragility* rather than integrity could explain the higher epithelial cell numbers in BAL fluid from asthmatics by an increased susceptibility to the trauma of the lavage procedure in asthma patients. However, since biopsy extraction is far more traumatic than BAL this increased fragility and susceptibility to disruption of the asthmatic epithelium probably dwindles within the far larger artefactual damage, which apparently affects both normal and asthmatic epithelium equally (Ordonez et al. 2000).

The present evidence together with the lack of epithelial desquamation in murine models of allergic asthma (Blyth et al. 1996; Trifilieff et al. 2000) are likely to weaken the hypothesis that the epithelial desquamation and loss of the physical barrier lead to the functional abnormalities of asthma like AHR and consecutive airway narrowing. Newer concepts about asthma pathogenesis focusing on the inflammatory and immunological properties of a dysfunctional epithelium in airway remodelling are gaining more support (Holgate et al. 2000; Holgate et al. 2003; Hackett and Knight 2007; Holgate 2008).

4.2 Thickness of the reticular basement membrane

Conditions such as asthma, cystic fibrosis and chronic bronchitis are associated with chronic endobronchial inflammation and structural airway remodelling inappropriate to the maintenance of normal lung function. Although for a long time the structural remodelling was thought to be a direct consequence of chronic inflammation (Bousquet et al. 2000), recently emerged evidence sustains different mechanisms and distinct pathways for the inflammatory process and the structural alterations as responses to chronic injury (Jeffery 2001; Fixman et al. 2007). This would have very important implications for the identification of disease-modifying drugs: effective anti-inflammatory treatment may not necessarily prevent, attenuate or reverse the structural alterations.

Thickening of the RBM was clearly identified as a remodelling feature highly characteristic and usually pathognomonic of asthma (Roche et al. 1989; Jeffery 1999), distinguishing it from the other chronic inflammatory airway disorders (Jeffery 2001; Fabbri et al. 2003; Bourdin et al. 2007). In some studies, this thickening was shown to correlate with the AHR, as quantified by metacholine PC_{20} (Jeffery et al. 1989; Boulet et al. 1997), whereas others could not confirm this association (Kim et al. 2007). While most reports did not find a relation between the RBM thickness and age, disease duration and severity (Chu et al. 1998; Payne et al. 2003; Payne et al. 2004; Kim et al. 2007), a recent study proved the RBM thickness to be suitable to differentiate between severe asthma, mild asthma, COPD and healthy controls (Bourdin et al. 2007). Although the correlations between the RBM thickness and the inflammation extent, clinical disease severity and respiratory physiology are somehow controversial, the thickness of the RBM is the most favoured variable for the assessment of the airway remodelling in asthma and has even been propounded as surrogate marker for other changes of the cartilaginous airway wall, like smooth muscle and submucosal mucous gland volume fraction (Jeffery et al. 2000; James et al. 2002). This is understandable since the RBM thickening was shown to occur even at very young ages and early in the course or even before the onset of the disease (Payne et al. 2003; Payne et al. 2004; Pohunek et al. 2005), being present even in atopic individuals with asymptomatic AHR prior to the development of asthma (Jeffery et al. 1989; Sohn et al. 2008). The increase of the RBM thickness persisted even in mild and therapeutically controlled asthma (Jeffery et al. 1992; O'Shaughnessy et al. 1996), which supports the hypothesis of a different pathophysiology underlying the inflammatory and remodelling processes. In contrast, a recent study showed a significant decrease of the RBM thickness of 1.9 µm after 12 months in an asthmatic group receiving inhaled fluticasone propionate, as compared to a placebo treated asthmatic group (Ward et al. 2002).

Despite the constant finding of significantly thickened RBM in asthma as compared to healthy subjects, many quantitative investigations of airway remodelling reported very different ranges for the two populations, sometimes even overlapping (Lundgren et al. 1988; Jeffery et al. 1989; Roche et al. 1989; Soderberg et al. 1990; Brewster et al. 1990; Jeffery et al. 1992; Wilson and Li 1997; Sullivan et al. 1998; Ferrando et al. 2003; Ward et al. 2005; Kim et al. 2007). Since all but one of these studies used direct point-to-point measurements or image analysis to estimate the RBM thickness, a bias due to the

orientation of the RBM and tangential cutting is inherent. Stereology provides methods emphasizing sampling and sources of bias and is therefore particularly valuable for measurements of length and surface area. A stereological approach for the measurement of the RBM thickness in endobronchial biopsies was already proposed (Ferrando et al. 2003). The results for both asthmatic and healthy subjects were substantially lower than previously reported, supporting the hypothesis of an orientation bias in earlier data.

This study presents another stereological method for estimating the RBM thickness, which was originally developed for measuring the thickness of the pulmonary air-blood barrier (Weibel and Knight 1964; Weibel 1990). Appropriate sampling is of paramount importance to the unbiased stereological approaches. This was also stressed by former investigations revealing considerable between and within biopsy variability for measurements of the RBM thickness in both stereologic and non-stereologic designs (Sullivan et al. 1998; Ferrando et al. 2003). Therefore, 1-3 biopsies per subject were evaluated and a SUR sampling design was adopted at biopsy and section level.

The unpaired two-tailed t-test did not detect a significant difference between the average values of the arithmetic mean thickness of the RBM in the non-smoker and smoker group, which is consistent with earlier findings (O'Shaughnessy et al. 1996; Chanez et al. 1997; Jeffery 2001). The noted trend for the RBM thickness to be higher in the smoker group, without reaching the level of significance, is also supported by other reports (O'Shaughnessy et al. 1996; Boulet et al. 1997). However, a recent study comprising larger subject groups found a significant RBM thickening in COPD patients in comparison with healthy controls and similar to mild asthmatics (Bourdin et al. 2007), although this is in contrast with the prevalent concepts (Jeffery 1999; Jeffery 2004).

The mean values for each group were considerably lower than some former reports for healthy subjects, which found a mean RBM thickness of approx. 8 µm, as shown in figure 3.5 (Roche et al. 1989; Soderberg et al. 1990; Ward et al. 2005). A study employing image analysis based on the principle of Weibel (1990) applied on 2D sections cut perpendicular to the epithelial layer, i.e., area by length ratio, reported a much lower mean value: 3.19 ± 0.55 µm (Wilson and Li 1997), which is very similar to my results of the same principle in a stereological design. They are further supported by the findings of Bourdin et al. (2007) using the image analysis method of Wilson and Li: 4.16 ± 0.66 µm for healthy subjects and 4.8 ± 2.12 µm for COPD patients (Figure 3.5).

However, because of the isotropy of the RBM in endobronchial biopsies (Jeffery et al. 2003), the stereologic approach can be applied to any sections, without the need for cumbersome sectioning perpendicular to the RBM.

As shown in figure 3.5, the mean value for non-smokers in the present study was also very similar to that of Ferrando et al. (2003): 3.2 ± 0.4 µm, supporting the validity of the stereologic data. Even with lower medians, the ranges of values resembled those of Lundgren et al. (1988): 4.8 (2.9 – 6.7) µm, and Payne et al. (2003): 4.4 (3.2 – 6.3) µm, emphasizing once again the high within-group data variability reported by Ward et al. (2002; 2005) and Bourdin et al. (2007) – Figure 3.5. Therefore, further attempts to quantify the RBM thickness in a stereologic approach should use multiple biopsies per subject and larger subject samples in order to obtain stable average data. This will also lead to an increase in statistical power, facilitating the substantiation of a possible slight thickening of the RBM in COPD patients as compared to healthy controls. Ultimately, the proposed stereologic design involving point counting is quick and easy to apply, without the need to outline the RBM or to orientate the specimen for strictly perpendicular sectioning, nonetheless avoiding the bias of tangential sectioning.

Since a pronounced epithelial desquamation was noticed in the biopsies of the (non-asthmatic) non-smokers and smokers, the correlation between the RBM thickness and the extent of the epithelial disruption was examined. The lack of a significant association is in contradiction with the results of Boulet et al. (1997), who found a medium correlation between RBM thickness and the percent desquamation of the bronchial epithelium in a group of patients with chronic bronchitis, allergic rhinitis and healthy controls with airway normoresponsiveness. The heterogeneity of that normoresponsive group probably led to an increase in parameter variances, which strengthened correlation.

4.3 Comparison of 2D and 3D inflammatory cell counts

Endobronchial biopsies have been widely used for quantitative assessments of inflammation and the related structural changes in chronic inflammatory airway diseases (Silva et al. 1989; Bradley et al. 1991; Holgate et al. 1992; Keatings et al. 1996; ten Hacken et al. 1998; Jeffery 1998; Faul et al. 1999; Bousquet 2000; Poulter et al. 2000; Barnes et al. 2000; Jeffery et al. 2000; Gamble et al. 2006; Carroll et al. 2006).

Up to the present day, most studies rely on 2D counting of inflammatory cells (Jeffery et al. 2003), although 3D approaches have been readily available for more than 20 years (DC Sterio, 1984). Design-based stereology represents *the state of the art* in other biomedical research areas, such as neurosciences and nephrology (Saper 1996; Madsen 1999), whereas its implementation in pulmonary research as a standard quantitative technique has been approached only recently (Hsia et al. 2008). The present study addressed the issue of agreement between the data supplied by the widely used 2D cell or nuclear profile counting and those relying on 3D cell counts. The main focus was on the size-bias and its variation, as an answer to previously formulated concerns on this subject {Jeffery, 2003 16594 /id;Fehrenbach, 2006 16568 /id}. For this purpose, two cell populations with clearly different mean sizes (‘small’ T-lymphocytes and ‘large’ macrophages) were quantified in human endobronchial biopsies using both approaches in parallel on two study groups comprising seven subjects each. It has to be emphasized once again that the study was not designed to pursue any comparison between the two subject groups. The rationale for including a group of smokers and a group of non-smokers was to gather some information on the robustness of the results and the behaviour of the theoretically expected differences between the two designs, when applied on samples from various source populations.

This thesis is, for a large part, based on stereology, which requires the observation of the naturally bounded reference space and the report of total quantities related to this reference space (Howard and Reed 1998). However, the usage of biopsy specimens from living subjects, who wish to remain so, precludes relating the estimated variables to a reference space, usually the whole organ or organism, in terms of total quantities (Hunziker and Cruz-Orive 1986). Therfore in this study, as in virtually all studies carried out on living subjects, the usage of stereological ratios and densities is the only available method (Cruz-Orive and Weibel 1981; Wulfsohn et al. 2004).

Prior to establishing the accuracy of a measurement method, quantified by the systematic error or bias, one should demonstrate adequate precision, quantified by the random measurement error. The estimated CE (inherent counting noise) for the 2D and 3D densities were acceptable with regard to the biological variability of the samples, i.e., the sampling variance represented less than half of the OV {Miller, 1997 11 /id;West, 1991 122 /id}. They were also very similar to previously published results on

the precision of 2D counting for different cell populations, which quoted CV of repeated counts in the range of 2-11% (Bradley et al. 1991; Bentley et al. 1992; O'Shaughnessy et al. 1997). However, the interpretation of results from bronchial biopsies poses challenges and their advantages are offset by the large variability between and within patients, which may reduce the reliability of the estimates. The large observed coefficients of variation in this study were consistent with the rather scarce previous findings in 2D counting designs (Jeffery et al. 2003; Gamble et al. 2006; Carroll et al. 2006). This variability can be addressed through a rigorous study and sampling design (Bousquet 2000). The adopted SUR sampling, which included 5-11 section pairs per biopsy and many fields per section, efficiently controls the within biopsy variability, adhering to the recommendations of previous 2D counting studies (Sont et al. 1997; Sullivan et al. 1998).

The two designs delivered results with very different orders of magnitude (mostly 10^2 for 2D and 10^4-10^5 for 3D counts) and expressed in different scale units: mm^{-2} and mm^{-3}, respectively. Moreover, the investigated entities were bidimensional cell transects in the first case and tridimensional cells in the second case. Therefore, it is obvious that the two data sets cannot substitute each other, although paired 2D and 3D data sets displayed very strong positive correlations (Figure 3.9), similar to previously published biopsy data for other inflammatory cells of the airways (Carroll et al. 2006). This is not surprising, as scale units do not affect correlation and it would be quite amazing if two methods designed to measure the same underlying quantity were not related. In this case, the relationship between N_A and N_V is described by the mean cell height perpendicular to the section plane (Hedreen 1998a; Kalisnik et al. 2001; Mouton 2002; Carroll et al. 2006). Another factor facilitating high correlation yields was the low measurement error (i.e., high precision) compared to the biological variation between individuals ($\overline{CE}^2 < 10\% OCV^2$). Nonetheless, this does not imply good agreement, as correlation lacks sensitivity to bias {Altman, 1983 16588 /id;LaMantia, 1990 16587 /id}. Besides that, the agreement of two methods would require the slope of the regression line as plotted in figure 3.9 to be approximately 1, taking into account the random measurement error of both methods (Bland and Altman 2003). Although all four graphs demonstrated good to very good correlation, the slopes were 0.0029 to 0.0123, which was far from a line of equality (slope = 1). In an attempt to prevent further usage

of this approach in method comparison studies biostatisticians repeatedly emphasized the pitfall of correlation analysis (Altman and Bland 1983; Bland and Altman 1986; Gallagher 1996).

Although regression was proposed as a tool for the evaluation of agreement when two methods of measurement have different units (Bland and Altman 2003), it is more a calibration approach, i.e., one would try to predict the value of the standard method (N_V) from the value obtained by the alternative method (N_A). While regression analysis allows calculating a 95% prediction interval, something akin to the limits of agreement of the Bland-Altman analysis, it is still 'blind' to a systematic error i.e., bias (Altman and Bland 1983). Moreover, a regression asymmetrically depicts the relationship between a dependent and an independent variable. In this case, N_V would have to be assumed being dependent on N_A, which is not true: N_A is indeed a function of N_V and the cell height, but N_V cannot be *logically* regarded as a function of N_A, although they are clearly correlated (Figure 3.9).

Thus, there is no way that would allow directly comparing the outcomes of the two designs for a single cell population.

4.3.1 Counts of all cell profiles

Because the two approaches deliver data with different dimensions, the measuring units had to be eliminated by calculating a relative variable, which would be zero-dimensional and allow a direct comparison of both methods. This was represented by the ratio of $CD68^+$ to $CD3^+$ counts for each approach. As the counting was performed simultaneously, i.e., on the same fields of view for both designs, one would expect the zero-dimensional index of macrophages to T-lymphocytes to be similar (accounting for the inherent random measurement error), no matter which approach was used, if no bias were present. This would be regarded as the null hypothesis of a statistical analysis based on hypothesis testing. However, a great measurement error of one or both methods would be an important confounder reducing the chance of a significant difference, without being a proof of 'equality' of the results. Although this approach, much like correlation analysis, is inappropriate to method comparison studies (Altman and Bland 1983; Bland and Altman 1999), it was performed for demonstrative purposes. The null hypothesis was tested by Wilcoxon's non-parametric signed rank test, which

was chosen because of the non-uniformity of variance that will be discussed in more detail below. The ratios showed statistically significant differences between the 2D and the 3D design when counting all stained cell profiles, with the 2D approach overestimating larger cells ($CD68^+$ macrophages) by the factor 1.7 to 3.4 in the two study groups, as compared to the 3D design (Figure 3.10 and Table 3.3). Apart from being very pronounced, the discrepancy of the two designs was also subject to a large (in this example twofold) and significant variation (Mann-Whitney's non-parametric rank sum test, $P < 0.005$) between the different study groups. This precludes any approach to define a general conversion factor or correlation formula to transform the results of a 2D approach into a real 3D quantity.

At this point, it has to be noted that for the non-smoker group there was even a very strong correlation between the $CD68^+/CD3^+$ ratios calculated from the two counting designs (Table 3.4) in spite of the large difference between them, as an additional argument that the correlation coefficient cannot be regarded as a measure of equality of two measurement methods.

4.3.2 Counts of nuclear profiles

Assuming that nuclear size varies less than overall cell size, opting to count only cells whose nucleus appears in the plane of the tissue section theoretically reduces the size-bias (Jeffery et al. 2003). When counting only macrophage profiles showing a nucleus, i.e., counting nuclear profiles, the differences of the ratios were not large enough in either group to achieve statistical significance (Wilcoxon's non-parametric signed rank test). However, the inability to reject the null hypothesis does *not* imply equality of results – it merely says that the difference is not large enough for significance to be reached, based on the size of the investigated samples. Thus it could not be concluded that the individual ratios of the cases by each design were 'equal' (within tolerance for the measurement error).

A simple and robust solution for the comparison of different methods was proposed by D.G. Altman and J.M. Bland more than two decades ago (Altman and Bland 1983; Bland and Altman 1986); subsequently, the Bland-Altman analysis was amended for the instances of non-uniformity or/and heteroscedasticity of the differences (Bland and Altman 1999). The data collected using both methods were plotted against each other;

one could then easily notice that they were widely scattered around the line of equality y = x (Figure 3.11). Although it could be already concluded that, based on the relatively small samples, agreement of the methods was not very good, it is necessary to look at this in more detail: how large are the random differences and how acceptable is that for our purpose? Is there a systematic difference (i.e., bias) when counting nuclear profiles compared to the 3D counting using the physical disector? And if any bias is present, is it constant or proportional to the magnitude of the measurement? If no systematic error were present, the results should be alike, within the achieved precision of the measurements. In contrast to hypothesis testing, agreement is not something, which is present or absent (i.e., true or false), but something, which must be quantified – the decision about what is acceptable agreement is a biological one, statistics alone cannot answer such a question. For that, it is necessary to define satisfactory agreement in advance and then verify whether most differences are smaller than the a priori set limits. In this case, the acceptance limits for the agreement were already set at approx. $\pm 2\,\overline{CE}$, i.e. 30%, of the mean ratios: ± 0.12 for the non-smoker group and ± 0.15 for the smoker group.

Plotting the difference of the ratios by the two methods against their mean (Altman and Bland 1983; Bland and Altman 1995), as shown in figure 3.12, revealed a striking correlation between the differences and the magnitude: Spearmann's correlation coefficient was $r_s = 0.89$ for the non-smoker group and $r_s = 0.79$ for the smoker group, both with a significance $P_r < 0.05$. This is equivalent to a test of equality of the observed variances of the ratios obtained by two methods: equal variances would yield a very low correlation (Bland and Altman 1995). Inequality of variances was already noted when a non-parametric test was chosen for hypothesis testing earlier on; indeed the OV for the disector measurements was half of that of the 2D approach in both groups, which explains the high correlation between the differences and the magnitude.

As already mentioned, I opted for fitting a linear model to the data in the Bland-Altmann analysis. For the non-smoker group, the regression of the differences (d_i) on the means (m_i) gave formula 3.1, which represents the proportional bias of the 2D ratios compared to the 3D ratios. The slope was significantly different from zero, confirming the contribution of the independent variable m_i to predicting the dependent variable d_i. This conclusion was also supported by the analysis of variance, which

yielded a high F-statistic (regression variation much higher than the residual variation about the regression line). The high statistic power of the performed regression indicated a high appropriateness in describing the relationship between the differences and the magnitude.

In the smoker group, the fitted linear regression model did not reach the chosen level of significance of $\alpha = 0.05$ for either the slope or the F-statistic ($P = 0.07$). For this reason one should decide not to reject the null hypothesis; hence it could not be concluded that the ratio differences of the smoker sample follow the linear distribution described by formula 3.2. This could also be visualized by drawing the 95% confidence interval of the regression line – between the two curves several horizontal lines could also be fitted, which would contradict a relation between the dependent variable d_i and the independent one m_i. The statistical power of the performed regression for the sample size $n = 7$ and $\alpha = 0.05$ was 43.4%, less than the desired level of 80%. Thus it is more likely to decide that formula 3.2 does not fit the data, when the relationship described by it actually exists, than to accept it. Therefore, the fitted model could be neither relied upon, nor rejected without doubt. In order to achieve a power of at least 80% with $\alpha = 0.05$ and $r = 0.715$, I suggest to increase the sample size to $n = 13$ in any future study. This is necessary because of the weaker correlation between the ratio differences and the ratio means in the smoker group. In turn, this correlation is conditional on the correlation between the two methods and the difference in their variances (Bland and Altman 1995). In the smoker group, the OV of the ratios was much smaller for both approaches, hence a smaller difference of the variances. A lower variability means the range of values is narrower, which will produce a weaker correlation. Since the OV was smaller, the CE (i.e., measurement error) was larger relative to the biological variability, which also weakens correlation. A further reduction of the CE would have required more counting events, which would have led to an enormous increase in the sampling and workload due to the much lower N_V of both cell types in this group. Increasing the sample size instead of improving the precision of the estimates per subject would also be in accordance with the already famous dogma of stereology ‘do more less well!’ (Gundersen and Osterby 1981).

The lack of statistical significance and power can also be entailed by outliers. Especially in small groups with a low variance it is advisable to assess the impact of such outliers

by eliminating them and repeating the statistical analysis (Bland and Altman 1999). The removal of the two large outliers visible in figure 3.12b led to a remarkable improvement: the slope became significantly different from zero, confirming the contribution of the independent variable m_i to predicting the dependent variable d_i. This conclusion was also supported by the analysis of variance, which yielded a very high F-statistic. Even though acceptable agreement had to be redefined and the range became narrower, the recalculated regression based limits of agreement fully complied with this new definition.

In an eye-gauge attempt to assess the behaviour of the 2D bias in different source populations, it could be noticed that the coefficients of formulae 3.1 and 3.3 appear to be somehow similar. Then, it may be asked whether the slopes of the two regression lines are significantly different or merely estimating the same population value of the regression coefficient (β). Student's t test did not reach statistical significance for the difference of the slopes (Zar 1999) and its calculated 95% confidence interval included the 0 value. Therefore, an estimate of the population regression coefficient (β) underlying the regression coefficients of both samples, which is called the common (or weighted) regression coefficient, could be computed: $b_c = 0.736$. A Student's t test to compare the two intercepts of formulae 3.1 and 3.3 yielded a value larger than the critical one thus indicating statistically significant difference ($P < 0.01$). This means that the two regression lines in figures 3.13a and 3.14 are parallel but not identical. The regression equations 3.1 and 3.3 can be re-written using the newly calculated common regression coefficient b_c, as already shown.

By looking at the absolute N_V data, it could be noticed that those cases displaying negative differences of the ratios had lower $CD68^+$ N_V than those showing positive differences. The latter also had lower CE than the former ones. With respect to the $CD3^+$ N_V such a trend could not be identified. Even for the same 3D ratio value, the difference of the ratios was negative for the case with lower N_V and positive for the case with higher N_V of both cell populations. In conclusion, the 2D approach showed a bias, which seemed to overestimate the macrophage density at high N_V while underestimating it at low N_V – amongst other reasons probably due to higher counting noise (CE) in specimens with lower N_V, which automatically yielded lower counts in the sampling process. Since such counting events follow a Poisson distribution, their

relative error, i.e. CE, will be inversely proportional to the square root of the counts (West et al. 1996). Another possible cause might be the 'lost caps' effect (Hedreen 1998a; Hedreen 1998b). The lost caps are small pieces of cells that are barely within or have fallen out of the section surface, which are not recognised and counted. This leads to a number underestimation in a method prone to the 'lost caps' bias. 2D counting in a histological section is inherently prone to this kind of bias – physically lost or unrecognisable cell fragments are omitted from the count and there is no practical method to compensate for this, since the lost caps are invisible and their number is unknown. Changes in cell number are likely to vary the amount of lost caps, especially by affecting recognisability of small fragments at the edge of the section. 3D counting is more robust to the problem of lost caps. The physical disector is insensitive to the fallen out cell fragments. Since it counts cell 'tops' without any influence of cell size, shape and orientation, a truly lost cap will solely 'shift' the top of that cell into the next section; in a rigorous sampling design this will have no effect on the counting result. Although barely contained and unrecognised cell caps have been shown to introduce a bias in physical disector counting, there are some ways to overcome this problem (Hedreen 1998b). When counting in adjacent sections, the bias arises from the asymmetry of the reference section serving as a guard space for the look-up section, without a guard space of its own. This will affect the recognisability of small caps in the reference and look-up section to a different extent. Counting bidirectionally is expected to partially reduce this effect by at least counting 'the other top' of a missed cell. The best solution would be having a similar guard space for the reference section as well. The high numerical aperture of the oil immersion objectives used in this study ensured a very shallow depth of field, which allowed focusing only on the top of the sections. Thereby, the rest of the section thickness could serve as a guard space for the analysed optical plane of the reference section. This and the bidirectional counting are thought to have rendered the 3D counting free from the 'lost caps' bias. In conclusion, it is possible that lost caps overrode the size-bias in the 2D approach in biopsies with a low $CD68^+$ N_V, whereas the 3D design was not affected; this resulted in negative differences of the $CD68^+/CD3^+$ ratios between the two methods.

For agreement between two methods to be sufficient, one should be able to use measurements by these two methods interchangeably, i.e., the method by which the measurement was made can be ignored. This is clearly not the case when using 2D or

3D approaches, since the 2D estimator shows a bias, which varies with the magnitude of the true cell density value. This emphasises once again the inappropriateness of hypothesis testing, which did not show a significant difference, for the investigation of method agreement. Presumably, the ‘positive’ and ‘negative’ deviations, i.e., bias, of the 2D design cancelled each other out to a large extent when calculating the mean value, *in this example*. Whether the bias really follows a different model in various subject populations and/or cell types should be addressed in future studies.

In summary, it can be concluded that 2D counting designs are not appropriate for quantifying inflammatory cells in the airway mucosa. Counting of all cell profiles clearly overestimates larger cells, thereby distorting the differential inflammatory profile of various conditions to a variable extent in different populations and/or clinical states. 2D counting of nuclear profiles failed to be reliable as well. The bias introduced by this approach is not constant throughout the measurement range and a ‘general correction’ cannot be applied. The direction of variation appears to depend on the density of the cells assessed. Therefore, we recommend using a 3D counting design in studies that aim at determining numerical densities or absolute cell numbers.

Summary / Zusammenfassung

Summary

Endobronchial biopsies collected by fiberoptic bronchoscopy have been increasingly used in biomedical research on disease mechanisms and clinical therapy studies of chronic inflammatory airway disorders. Although less invasive techniques are available for the investigation of the inflammatory infiltrate of the bronchial tree, a standardization of their results with respect to the extent or level of the sampled airway proved impracticable. Moreover in a clinical setting the structural alterations of the airway mucosa can only be assessed by histopathological biopsy analysis, which makes this approach indispensable to airway research.

More and more quantitative approaches in biopsy studies have been reported. The high variability of their results points out the need for reliable and robust quantitative methods and sampling designs in order to allow for an easier interpretation and corroboration of the outcomes of different studies. It is unclear whether classical 2D approaches and unbiased stereological 3D designs for counting inflammatory cells, measuring area fraction or layer thickness on histological sections are equally well-suited for these purposes. The aim of this study was to characterise the agreement between 2D and 3D approaches for inflammatory cell counting by simultaneously applying them on bioptic material. Furthermore, stereological designs were proposed for quantifying the extent of epithelial desquamation and the mean thickness of the reticular basement membrane, and the results were related to previously published data gained by 2D tissue analyses. The hypotheses that the epithelial integrity depends on biopsy size or mean basement membrane thickness were also verified.

Biopsies from the segmental bronchi were collected by fiberoptic bronchoscopy in a group of smokers (n=7) and a group of healthy non-smokers (n=7), embedded in paraffin and exhaustively sectioned. Systematic uniform random samples of sections were stained histochemically (PAS) or immunohistochemically for macrophages (CD68) and T-lymphocytes (CD3), respectively. On the same systematic uniform random samples of fields of view, cell numbers per unit volume were assessed using the physical disector and cell and nuclear profiles were counted and related to the subepithelial layer area. To obtain a zero-dimensional index allowing for a direct comparison of the two methods, the $CD68^+/CD3^+$ ratio was calculated for each

approach. The extent of epithelial desquamation was assessed as area fraction of the basement membrane by counting the intersections of a line grid with the basement membrane on PAS stained sections. On the same sections the arithmetic mean thickness of the reticular basement membrane was estimated using a coherent test system of points and line segments.

Counting cell profiles per unit area severely overestimated the number of larger cells (macrophages) relative to smaller cells (T-lymphocytes). Counting of nuclear profiles delivered average values similar to the physical disector but a bias proportional to the magnitude of the $CD68^+/CD3^+$ ratios was identified.

The extent of epithelial desquamation was similar between the two groups and in accordance with previous studies in healthy volunteers and asthmatics. The lack of a difference between the (non-asthmatic) subjects of this study and published data on asthma patients confirms earlier similar findings. This strengthens the doubt about the morphopathological significance of the epithelial disruption, suggesting an artefactual cause.

The arithmetic mean thickness of the reticular basement membrane, an important marker of airway remodelling in biopsy studies of asthma, showed no significant difference between healthy non-smokers and smokers in the small studied groups. The average values were very similar to the results of another published stereological design and to those obtained by image analysis of perpendicular sections. At the same time they were conspicuously lower than the data reported by studies employing direct point-to-point measurements on sections. This underlines the overestimation of the mean thickness introduced by tangential cutting of the basement membrane when relying on 2D measurements of this three-dimensional structure.

Zusammenfassung

In klinisch-therapeutischen Studien chronisch-entzündlicher Atemwegserkrankungen und in der biomedizinischen Erforschung ihrer Pathomechanismen werden fiberoptisch-bronchoskopisch entnommene endobronchiale Biopsien zunehmend häufig verwendet. Obgleich auch weniger invasive Untersuchungsmethoden der entzündlichen Veränderungen des Bronchialsystems zur Verfügung stehen, hat sich eine Standardisierung dieser alternativen Methoden bezüglich Ausmaß und Generation der untersuchten Atemwege bislang als undurchführbar erwiesen. Darüberhinaus können die strukturellen Veränderungen der Atemwegsmukosa in einem klinischen Kontext lediglich durch histopathologische Analysen von Biopsien beurteilt werden. Aus diesen Gründen erscheint die Analyse endobronchialer Biopsien für die Atemwegsforschung unabdingbar zu sein.

Immer häufiger wird auch über quantitative Ansätze in Biopsiestudien berichtet. Die hohe Variabilität ihrer Ergebnisse betont die Notwendigkeit verlässlicher und robuster quantitativer Methoden und Designs der Stichprobenerhebung, um eine einfachere Interpretation und Untermauerung der Ergebnisse unterschiedlicher Studien zu ermöglichen. Es ist unklar, ob konventionelle 2D Ansätze und bias-freie stereologische 3D Designs zum Zählen der Entzündungszellen, Messen der Flächenanteile oder der Schichtdicke auf histologischen Schnitten dafür gleich gut geeignet sind. Das Ziel dieser Arbeit war, die Übereinstimmung der 2D und 3D Zellzählansätze durch ihre gleichzeitige Anwendung zur Zählung der Entzündungszellen in bioptischem Material zu überprüfen. Darüber hinaus wurden stereologische Methoden zur Quantifizierung der Epitheldesquamation und der mittleren arithmetischen Dicke der Basalmembran vorgestellt und ihre Ergebnisse mit bereits veröffentlichten, durch 2D histologische Untersuchungen gewonnenen Daten verglichen. Die Hypothesen, dass die Epithelintegrität von dem Biopsievolumen oder der mittleren arithmetischen Dicke der Basalmembran abhängig ist, wurden ebenfalls überprüft.

Biopsien aus den Segmentbronchien wurden in einer Gruppe von Rauchern (n=7) und einer Gruppe von gesunden Nichtrauchern (n=7) durch fiberoptische Bronchoskopie entnommen, anschließend in Paraffin eingebettet und erschöpfend geschnitten. Systematische, proportional geschichtete Zufallsstichproben von histologischen Schnitten wurden histochemisch (PAS) oder immunohistochemisch für Makrophagen

(CD68) bzw. T-Lymphozyten (CD3) gefärbt. In denselben systematischen, proportional geschichteten Zufallsstichproben von mikroskopischen Sichtfeldern wurden die Zellzahlen per Volumeneinheit mit dem physical Disector ermittelt und die Zell- und Kernprofile gezählt und auf die Fläche der Lamina propria bezogen. Um eine nulldimensionale Größe für den direkten Vergleich der zwei Methoden zu erhalten, wurde der $CD68^+/CD3^+$ Quotient für jeden Ansatz berechnet. Das Ausmaß der Epitheldesquamation wurde als Flächenanteil der Basalmembran bewertet. Dies geschah durch das Zählen der Schnittpunkte eines Linienrasters mit der Basalmembran auf den PAS gefärbten Schnitten. Auf denselben Schnitten wurde die mittlere arithmetische Dicke der Basalmembran mittels eines kohärenten Testsystems aus Punkten und Segmenten ermittelt.

Im Ergebnis überschätzte das Zählen der Zellprofile pro Flächeneinheit die Zahl der größeren Zellen (Makrophagen) relativ zu kleineren Zellen (T-Lymphozyten). Das Zählen der Kernprofile ergab ähnliche Gruppenmittelwerte zum Physical Disector, aber ein systematischer Fehler proportional zum Wert des $CD68^+/CD3^+$ Quotientes wurde identifiziert.

Das Ausmaß der Epitheldesquamation war in beiden Gruppen ähnlich und stimmte mit früheren Studien mit gesunden Freiwilligen und Asthmatikern überein. Der fehlende Unterschied zwischen den (nicht-asthmatischen) Probanden dieser Studie und veröffentlichten Ergebnissen von Asthma-Patienten bestätigt vorherige ähnliche Erkenntnisse, bekräftigt den Zweifel an der pathologischen Bedeutung der Epithelabschilferung und deutet auf eine artifizielle Ursache hin.

Die arithmetische mittlere Dicke der Basalmembran, eine wichtige Kenngröße des strukturellen Umbaus der Atemwege in Asthmabiopsiestudien, zeigte keinen signifikanten Unterschied zwischen gesunden Nichtrauchern und Rauchern. Die Mittelwerte waren den Ergebnissen eines anderen publizierten stereologischen Designs und den durch Bildanalyse von Perpendikularschnitten gemessenen Werten sehr ähnlich. Zugleich waren sie deutlich niedriger als die Werte, die von Punkt-zu-Punkt Messungen an histologischen Schnitten berichtet wurden. Dies weist auf eine Überschätzung der mittleren Dicke durch Tangentialanschnitte der Basalmembran hin, wenn diese dreidimensionale Struktur mittels 2D Ansätze quantifiziert wird.

Sumar (Romanian)

Biopsiile endobronhiale colectate prin fibrobronhoscopie au fost utilizate din ce în ce mai frecvent în cercetarea biomedicală a mecanismelor fiziopatologice şi în studiile clinice terapeutice ale bolilor inflamatorii cronice ale căilor respiratorii. Deşi tehnici mai puțin invazive sunt disponibile pentru investigațiile infiltratului inflamator al arborelui bronşic, standardizarea rezultatelor acestora referitor la întinderea şi nivelul căilor respiratorii sondate s-a dovedit impracticabilă. De altfel, într-un scenariu clinic, alterările structurale ale mucoasei bronşice pot fi evaluate doar printr-o analiză histopatologică bioptică, ceea ce face aceasta abordare indispensabilă pentru cercetarea în domeniul căilor respiratorii.

Din ce în ce mai multe abordări cantitative au fost raportate în studiile bioptice. Variabilitatea mare a rezultatelor lor evidențiază necesitatea unor metode cantitative şi a unor designuri de sondaj sigure şi robuste, pentru a facilita interpretarea şi coroborarea consecințelor diferitelor studii. Momentan nu este clar, dacă abordările clasice 2D şi designurile stereologice imparțiale pentru numărarea celulelor, măsurarea fracțiilor de arie sau a grosimii unui strat pe secțiuni histologice sunt la fel de adecvate pentru aceste scopuri. Țelul acestui studiu a fost caracterizarea acordului dintre abordările 2D şi 3D pentru numărarea celulelor inflamatorii prin aplicarea lor simultană pe un material bioptic. Totodată au fost propuse designuri stereologice pentru cuantificarea descuamării epiteliale şi a grosimii medii a membranei bazale, iar rezultatele au fost relaționate cu date publicate anterior, obținute prin analize histologice 2D. Ipotezele conform cărora integritatea epiteliului depinde de volumul biopsiei sau de grosimea medie a membranei bazale au fost de asemenea verificate.

Într-un grup de fumători (n=7) şi unul de nefumători clinic sănătoşi (n=7) au fost colectate biopsii din bronhiile segmentale prin fibrobronhoscopie. Acestea au fost incluzionate în parafină şi secționate exhaustiv. Eşantioane aleatorii sistematic-proporțional stratificate au fost colorate histochimic (PAS) sau imunohistochimic pentru macrofage (CD68), respectiv limfocite T (CD3). Pe eşantioane identice de câmpuri microscopice, aleatorii şi sistematic-propoțional stratificate, numărul de celule pe unitatea de volum a fost determinat folosind disectorul fizic, iar profilurile celulare şi nucleare au fost numărate şi relaționate la suprafața corionului. Pentru a obține un index zero-dimensional, care permite compararea directă a celor două metode, raportul

$CD68^+/CD3^+$ a fost calculat prin fiecare metodă în parte. Amploarea descuamării epiteliului a fost evaluată ca fracție din aria membranei bazale prin numărarea intersecțiilor unui raster de linii cu membrana bazală pe secțiunile colorate PAS. Pe aceleaşi secțiuni, grosimea medie aritmetică a membranei bazale a fost estimată folosind un sistem coerent de puncte si segmente.

Numărarea profilurilor celulare pe unitatea de suprafață a supraestimat sever numărul celulelor mari (macrofage) relativ la celulele mici (limfocite T). Numărarea profilurilor nucleare a furnizat valori medii similare celor obținute prin disectorul fizic, însă o deplasare proporțională cu magnitudinea raporturilor $CD68^+/CD3^+$ a fost identificată.

Amploarea descuamării epiteliale a fost similară în cele două grupe şi în concordanță cu rezultatele unor studii anterioare pe voluntari sănătoşi şi pe astmatici. Lipsa unei diferențe între subiecții non-astmatici ai acestui studiu şi datele publicate despre pacienți asmatici confirmă constatările precedente similare şi consolidează dubiile asupra semnificației morfopatologice a dezagregării epiteliale, sugerând o cauză artefactuală.

În cazul grosimii medii aritmetice a membranei bazale, un marker important al remodelării căilor respiratorii în studiile bioptice despre astm, nu au fost identificate diferențe semnificative între nefumătorii sănătoşi şi fumători, pe baza grupurilor mici examinate. Valorile medii obținute au fost foarte similare cu rezultatele unui alt design stereologic publicat şi cu cele obținute prin analiza de imagine pe secțiuni perpendiculare. Totodată, ele au fost remarcabil mai mici decât datele raportate în studii ce au efectuat măsurători directe point-to-point pe secțiuni. Acest lucru subliniază supraestimarea grosimii medii introdusă prin secționarea tangențială a membranei bazale în cazul efectuării de măsurători 2D ale acestei structuri tridimensionale.

References

Summary and recommendations of a workshop on the investigative use of fiberoptic bronchoscopy and bronchoalveolar lavage in asthmatics 1985, *Am.Rev.Respir.Dis.,* 132: 180-182.

Standards for the diagnosis and care of patients with chronic obstructive pulmonary disease 1995, *Am J Respir Crit Care Med,* 152: S77-121.

Abercrombie M 1946, Estimation of nuclear population from microtome sections, *Anat Rec,* 94: 239-247.

Aleva RM, Kraan J, Smith M, ten Hacken NH, Postma DS and Timens W 1998, Techniques in human airway inflammation: quantity and morphology of bronchial biopsy specimens taken by forceps of three sizes, *Chest,* 113: 182-185.

Altman DG and Bland JM 1983, Measurement in Medicine: The Analysis of Method Comparison Studies, *Statistician,* 32: 307-317.

Altman DG 1993, Construction of age-related reference centiles using absolute residuals, *Stat Med,* 12: 917-924.

Amadori A, Zamarchi R, De SG, Forza G, Cavatton G, Danieli GA, Clementi M and Chieco-Bianchi L 1995, Genetic control of the CD4/CD8 T-cell ratio in humans, *Nat Med,* 1: 1279-1283.

American Thoracic Society 1987, Guidelines for fiberoptic bronchoscopy in adults. American Thoracic Society. Medical Section of the American Lung Association, *Am Rev Respir Dis,* 136: 1066.

Azzawi M, Bradley B, Jeffery PK, Frew AJ, Wardlaw AJ, Knowles G, Assoufi B, Collins JV, Durham S and Kay AB 1990, Identification of activated T lymphocytes and eosinophils in bronchial biopsies in stable atopic asthma, *Am Rev Respir Dis,* 142: 1407-1413.

Barnes NC, Burke CM, Poulter LW and Schleimer RP 2000, The anti-inflammatory profile of inhaled corticosteroids: biopsy studies in asthmatic patients, *Respir Med*, 94 Suppl F: S16-21.

Beasley R, Roche WR, Roberts JA and Holgate ST 1989, Cellular events in the bronchi in mild asthma and after bronchial provocation, *Am Rev Respir Dis*, 139: 806-817.

Bentley AM, Menz G, Storz C, Robinson DS, Bradley B, Jeffery PK, Durham SR and Kay AB 1992, Identification of T lymphocytes, macrophages, and activated eosinophils in the bronchial mucosa in intrinsic asthma. Relationship to symptoms and bronchial responsiveness, *Am Rev Respir Dis*, 146: 500-506.

Bland JM and Altman DG 1986, Statistical methods for assessing agreement between two methods of clinical measurement, *Lancet*, 327: 307-310.

Bland JM and Altman DG 1995, Comparing methods of measurement: why plotting difference against standard method is misleading, *Lancet*, 346: 1085-1087.

Bland JM and Altman DG 1996, Statistics Notes: Transforming data, *BMJ*, 312: 770.

Bland JM and Altman DG 1999, Measuring agreement in method comparison studies, *Stat Methods Med Res*, 8: 135-160.

Bland JM and Altman DG 2003, Applying the right statistics: analyses of measurement studies, *Ultrasound Obstet Gynecol*, 22: 85-93.

Blyth DI, Pedrick MS, Savage TJ, Hessel EM and Fattah D 1996, Lung inflammation and epithelial changes in a murine model of atopic asthma, *Am J Respir Cell Mol Biol*, 14: 425-438.

Boulet LP, Laviolette M, Turcotte H, Cartier A, Dugas M, Malo JL and Boutet M 1997, Bronchial subepithelial fibrosis correlates with airway responsiveness to methacholine, *Chest*, 112: 45-52.

Bourdin A, Neveu D, Vachier I, Paganin F, Godard P and Chanez P 2007, Specificity of basement membrane thickening in severe asthma, *J Allergy Clin Immunol*, 119: 1367-1374.

Bousquet J 2000, The use of biopsy to study airway inflammation, *Respir Med*, 94 Suppl F: S1-2.

Bousquet J, Jeffery PK, Busse WW, Johnson M and Vignola AM 2000, Asthma. From bronchoconstriction to airways inflammation and remodeling, *Am J Respir Crit Care Med*, 161: 1720-1745.

Bradley BL, Azzawi M, Jacobson M, Assoufi B, Collins JV, Irani Am, Schwartz LB, Durham SR, Jeffery PK and Kay AB 1991, Eosinophils, T-lymphocytes, mast cells, neutrophils, and macrophages in bronchial biopsy specimens from atopic subjects with asthma: Comparison with biopsy specimens from atopic subjects without asthma and normal control subjects and relationship to bronchial hyperresponsiveness, *J Allergy Clin Immunol*, 88: 661-674.

Brewster CE, Howarth PH, Djukanovic R, Wilson J, Holgate ST and Roche WR 1990, Myofibroblasts and subepithelial fibrosis in bronchial asthma, *Am J Respir Cell Mol Biol*, 3: 507-511.

British Standards Institution 1979, *Precision of test methods I: Guide for the determination and reproducibility for a standard test method*, BSI, London.

Carroll ML, Carroll NG and James AL 2006, Do bronchial biopsies represent mast cell density in airways? A stereological study, *Eur Respir J*, 28: 612-621.

Carroll N, Elliot J, Morton A and James A 1993, The structure of large and small airways in nonfatal and fatal asthma, *Am Rev Respir Dis*, 147: 405-410.

Cavalieri B 1635, *Geometria Indivisibilibus Continuorum*, Typis Clemetis Feronij, Bononi.

Chanez P, Vignola AM, O'Shaugnessy T, Enander I, Li D, Jeffery PK and Bousquet J 1997, Corticosteroid reversibility in COPD is related to features of asthma, *Am J Respir Crit Care Med*, 155: 1529-1534.

Chanez P, Vignola AM, Vic P, Guddo F, Bonsignore G, Godard P and Bousquet J 1999, Comparison between nasal and bronchial inflammation in asthmatic and control subjects, *Am J Respir Crit Care Med*, 159: 588-595.

Chu HW, Halliday JL, Martin RJ, Leung DY, Szefler SJ and Wenzel SE 1998, Collagen deposition in large airways may not differentiate severe asthma from milder forms of the disease, *Am J Respir Crit Care Med*, 158: 1936-1944.

Cruz-Orive LM and Weibel ER 1981, Sampling designs for stereology, *J Microsc*, 122: 235-257.

Cutz E, Levison H and Cooper DM 1978, Ultrastructure of airways in children with asthma, *Histopathology*, 2: 407-421.

Davies RJ and Devalia JL 1992, Asthma. Epithelial cells, *Br Med Bull*, 48: 85-96.

Di Stefano A, Caramori G, Ricciardolo FL, Capelli A, Adcock IM and Donner CF 2004, Cellular and molecular mechanisms in chronic obstructive pulmonary disease: an overview, *Clin Exp Allergy*, 34: 1156-1167.

Dorph-Petersen KA, Nyengaard JR and Gundersen HJ 2001, Tissue shrinkage and unbiased stereological estimation of particle number and size*, *J Microsc*, 204: 232-246.

Dunnill MS 1960, The pathology of asthma, with special reference to changes in the bronchial mucosa, *J Clin Pathol*, 13: 27-33.

Erjefalt JS, Korsgren M, Nilsson MC, Sundler F and Persson CG 1997, Prompt epithelial damage and restitution processes in allergen challenged guinea-pig trachea in vivo, *Clin Exp Allergy*, 27: 1458-1470.

Erpenbeck VJ, Hagenberg A, Dulkys Y, Elsner J, Balder R, Krentel H, Discher M, Braun A, Krug N and Hohlfeld JM 2004, Natural porcine surfactant augments airway inflammation after allergen challenge in patients with asthma, *Am J Respir Crit Care Med*, 169: 578-586.

Evans MJ and Plopper CG 1988, The role of basal cells in adhesion of columnar epithelium to airway basement membrane, *Am Rev Respir Dis*, 138: 481-483.

Fabbri LM, Romagnoli M, Corbetta L, Casoni G, Busljetic K, Turato G, Ligabue G, Ciaccia A, Saetta M and Papi A 2003, Differences in airway inflammation in patients with fixed airflow obstruction due to asthma or chronic obstructive pulmonary disease, *Am J Respir Crit Care Med*, 167: 418-424.

Fahy JV, Wong H, Liu J and Boushey HA 1995, Comparison of samples collected by sputum induction and bronchoscopy from asthmatic and healthy subjects, *Am J Respir Crit Care Med*, 152: 53-58.

Fahy JV 2001, Remodeling of the airway epithelium in asthma, *Am J Respir Crit Care Med*, 164: S46-51.

Faul JL, Demers EA, Burke CM and Poulter LW 1999, The reproducibility of repeat measures of airway inflammation in stable atopic asthma, *Am J Respir Crit Care Med*, 160: 1457-1461.

Fehrenbach H and Ochs M 1998, 'Studying lung ultrastructure', in *Methods in pulmonary research*, S Uhlig and AE Taylor, eds., Birkhäuser, Basel, pp. 429-454.

Fehrenbach H, Fehrenbach A, Erpenbeck VJ, Blocher S, Prinz R, Krug N and Hohlfeld JM 2006, 2D Morphometry overestimates large relative to small inflammatory cells in human bronchial biopsies, *Proc Am Thorac Soc*, 3: A619.

Ferrando RE, Nyengaard JR, Hays SR, Fahy JV and Woodruff PG 2003, Applying stereology to measure thickness of the basement membrane zone in bronchial biopsy specimens, *J Allergy Clin Immunol*, 112: 1243-1245.

Fixman ED, Stewart A and Martin JG 2007, Basic mechanisms of development of airway structural changes in asthma, *Eur Respir J*, 29: 379-389.

Folli C, Descalzi D, Scordamaglia F, Riccio AM, Gamalero C and Canonica GW 2008, New insights into airway remodelling in asthma and its possible modulation, *Curr Opin Allergy Clin Immunol*, 8: 367-375.

Foresi A, Bertorelli G, Pesci A, Chetta A and Olivieri D 1990, Inflammatory markers in bronchoalveolar lavage and in bronchial biopsy in asthma during remission, *Chest*, 98: 528-535.

Gallagher EJ 1996, Correlation versus agreement: Methods of measurement in medicine, *Ann Emerg Med*, 27: 236-238.

Gamble E, Qiu Y, Wang D, Zhu J, Vignola AM, Kroegel C, Morell F, Hansel TT, Pavord ID, Rabe KF, Barnes NC and Jeffery PK 2006, Variability of bronchial inflammation in chronic obstructive pulmonary disease: implications for study design, *Eur Respir J*, 27: 293-299.

Global Initiative for Chronic Obstructive Lung Disease, Guidelines: workshop report; global strategy for diagnosis, management, and prevention of COPD, updated December, 2007. *Available at www.goldcopd.com*, accessed August 2nd, 2008.

Glynn A and Michales L 1960, Bronchial biopsy in chronic bronchitis and asthma, *Istanbul Tip Fak Mecmuasi*, 15: 142-153.

Gundersen HJ 1978, Estimators of the number of objects per area unbiased by edge effects, *Microsc Acta*, 81: 107-117.

Gundersen HJG and Osterby R 1981, Optimizing sampling efficiency of stereological studies in biology: or 'Do more less well!', *J Microsc*, 121: 65-73.

Gundersen HJ and Jensen EB 1987, The efficiency of systematic sampling in stereology and its prediction, *J Microsc*, 147: 229-263.

Gundersen HJ, Jensen EB, Kieu K and Nielsen J 1999, The efficiency of systematic sampling in stereology--reconsidered, *J Microsc*, 193: 199-211.

Hackett TL and Knight DA 2007, The role of epithelial injury and repair in the origins of asthma, *Curr Opin Allergy Clin Immunol*, 7: 63-68.

Hedreen JC 1998a, What was wrong with the Abercrombie and empirical cell counting methods? A review, *Anat Rec*, 250: 373-380.

Hedreen JC 1998b, Lost caps in histological counting methods, *Anat Rec*, 250: 366-372.

Holgate ST, Wilson JR and Howarth PH 1992, New insights into airway inflammation by endobronchial biopsy, *Am Rev Respir Dis*, 145: S2-6.

Holgate ST, Lackie PM, Davies DE, Roche WR and Walls AF 1999, The bronchial epithelium as a key regulator of airway inflammation and remodelling in asthma, *Clin Exp Allergy*, 29 Suppl 2: 90-95.

Holgate ST, Lackie PM, Wilson S, Roche WR and Davies DE 2000, Bronchial Epithelium as a Key Regulator of Airway Allergen Sensitization and Remodeling in Asthma, *Am J Respir Crit Care Med*, 162: S113-117.

Holgate ST, Davies DE, Puddicombe S, Richter A, Lackie P, Lordan J and Howarth P 2003, Mechanisms of airway epithelial damage: epithelial-mesenchymal interactions in the pathogenesis of asthma, *Eur Respir J*, 44 Suppl: 24s-29s.

Holgate ST 2008, The airway epithelium is central to the pathogenesis of asthma, *Allergol Int*, 57: 1-10.

Howard V, Reid S, Baddeley A and Boyde A 1985, Unbiased estimation of particle density in the tandem scanning reflected light microscope, *J Microsc*, 138: 203-212.

Howard CV and Reed MG 1998, *Unbiased Stereology: Three-Dimensional Measurement in Microscopy*, 1st edn, BIOS Scientific Publishers Limited, New York.

Hsia CCW, Hyde DM, Ochs M and Weibel ER, Standards for quantitative assessment of lung structure: an official research policy statement of the ATS/ERS, submitted to *Am J Respir Crit Care Med* 2008.

Hunziker EB and Cruz-Orive LM 1986, Consistent and efficient delineation of reference spaces for light microscopical stereology using a laser microbeam system, *J Microsc*, 142: 95-99.

Hyde DM, Harkema JR, Tyler NK and Plopper CG 2006, Design-Based Sampling and Quantitation of the Respiratory Airways, *Toxicol Pathol*, 34: 286-295.

James AL, Maxwell PS, Pearce-Pinto G, Elliot JG and Carroll NG 2002, The relationship of reticular basement membrane thickness to airway wall remodeling in asthma, *Am J Respir Crit Care Med*, 166: 1590-1595.

Jeffery PK, Wardlaw AJ, Nelson FC, Collins JV and Kay AB 1989, Bronchial biopsies in asthma. An ultrastructural, quantitative study and correlation with hyperreactivity, *Am Rev Respir Dis*, 140: 1745-1753.

Jeffery PK 1992, Pathology of asthma, *Br Med Bull*, 48: 23-39.

Jeffery PK, Godfrey RW, Adelroth E, Nelson F, Rogers A and Johansson SA 1992, Effects of treatment on airway inflammation and thickening of basement membrane reticular collagen in asthma. A quantitative light and electron microscopic study., *Am Rev Respir Dis*, 145: 890-899.

Jeffery PK 1996, Bronchial biopsies and airway inflammation, *Eur Respir J*, 9: 1583-1587.

Jeffery PK 1998, Investigation and assessment of airway and lung inflammation: we now have the tools, what are the questions?, *Eur Respir J*, 11: 524-528.

Jeffery PK 1999, Differences and similarities between chronic obstructive pulmonary disease and asthma, *Clin Exp Allergy*, 29 Suppl 2: 14-26.

Jeffery PK, Laitinen A and Venge P 2000, Biopsy markers of airway inflammation and remodelling, *Respir Med*, 94 Suppl F: S9-15.

Jeffery PK 2001, Remodeling in Asthma and Chronic Obstructive Lung Disease, *Am J Respir Crit Care Med*, 164: S28-38.

Jeffery PK, Holgate S and Wenzel S 2003, Methods for the assessment of endobronchial biopsies in clinical research: application to studies of pathogenesis and the effects of treatment, *Am J Respir Crit Care Med*, 168: S1-17.

Jeffery PK 2004, Remodeling and inflammation of bronchi in asthma and chronic obstructive pulmonary disease, *Proc Am Thorac Soc*, 1: 176-183.

Kalisnik M, Blejec A., Pajer Z. and Majhenc J. 2001, Metric characteristics of various methods for numerical density estimation in transmission light microscopy - a computer simulation, *Image Anal Stereol*, 20: 15-25.

Keatings VM, Collins PD, Scott DM and Barnes PJ 1996, Differences in interleukin-8 and tumor necrosis factor-alpha in induced sputum from patients with chronic obstructive pulmonary disease or asthma, *Am J Respir Crit Care Med*, 153: 530-534.

Kim ES, Kim SH, Kim KW, Park JW, Kim YS, Sohn MH and Kim KE 2007, Basement membrane thickening and clinical features of children with asthma, *Allergy*, 62: 635-640.

Kirby JG, Hargreave FE, Gleich GJ and O'Byrne PM 1987, Bronchoalveolar cell profiles of asthmatic and nonasthmatic subjects, *Am Rev Respir Dis*, 136: 379-383.

Kühnel SM and Krebs D 2004, *Statistik für die Sozialwissenschaften*, Rowohlt Taschenbuch Verlag, Reinbek, Germany.

Lackie PM, Baker JE, Gunthert U and Holgate ST 1997, Expression of CD44 isoforms is increased in the airway epithelium of asthmatic subjects, *Am J Respir Cell Mol Biol*, 16: 14-22.

Lacoste JY, Bousquet J, Chanez P, Van VT, Simony-Lafontaine J, Lequeu N, Vic P, Enander I, Godard P and Michel FB 1993, Eosinophilic and neutrophilic inflammation in asthma, chronic bronchitis, and chronic obstructive pulmonary disease, *J Allergy Clin Immunol*, 92: 537-548.

Laitinen LA, Heino M, Laitinen A, Kava T and Haahtela T 1985, Damage of the airway epithelium and bronchial reactivity in patients with asthma, *Am Rev Respir Dis*, 131: 599-606.

LaMantia KR, O'Connor T and Barash PG 1990, Comparing Methods of Measurement: An Alternative Approach, *Anesthesiology*, 72: 781-783.

Lange P, Parner J, Vestbo J, Schnohr P and Jensen G 1998, A 15-year follow-up study of ventilatory function in adults with asthma, *N Engl J Med*, 339: 1194-1200.

Laprise C, Laviolette M, Boutet M and Boulet LP 1999, Asymptomatic airway hyperresponsiveness: relationships with airway inflammation and remodelling, *Eur Respir J*, 14: 63-73.

Lozewicz S, Wells C, Gomez E, Ferguson H, Richman P, Devalia J and Davies RJ 1990, Morphological integrity of the bronchial epithelium in mild asthma, *Thorax*, 45: 12-15.

Lundgren R, Soderberg M, Horstedt P and Stenling R 1988, Morphological studies of bronchial mucosal biopsies from asthmatics before and after ten years of treatment with inhaled steroids, *Eur Respir J*, 1: 883-889.

Madsen KM 1999, The art of counting, *J Am Soc Nephrol*, 10: 1124-1125.

Miller PB, Charleston JS, Battaglia DE, Klein NA and Soules MR 1997, An accurate, simple method for unbiased determination of primordial follicle number in the primate ovary, *Biol Reprod*, 56: 909-915.

Montefort S, Baker J, Roche WR and Holgate ST 1993a, The distribution of adhesive mechanisms in the normal bronchial epithelium, *Eur Respir J*, 6: 1257-1263.

Montefort S, Djukanovic R, Holgate ST and Roche WR 1993b, Ciliated cell damage in the bronchial epithelium of asthmatics and non-asthmatics, *Clin Exp Allergy*, 23: 185-189.

Montefort S, Roberts JA, Beasley R, Holgate ST and Roche WR 1992, The site of disruption of the bronchial epithelium in asthmatic and non-asthmatic subjects, *Thorax*, 47: 499-503.

Mouton PR 2002, *Principles and practices of unbiased stereology. An introduction for bioscientists.*, John Hopkins University Press, Baltimore.

Naylor B 1962, The shedding of the mucosa of the bronchial tree in asthma, *Thorax*, 17: 69-72.

NHLBI/NIAID/AAAI/ACCP/ATS, Workshop summary and guidelines: investigative use of bronchoscopy, lavage, and bronchial biopsies in asthma and other airway diseases 1991, *J Allergy Clin Immunol*, 88: 808-814.

O'Shaughnessy TC, Ansari TW, Barnes NC and Jeffery PK 1996, Reticular basement membrane thickness in moderately severe asthma and smokers' chronic bronchitis with and without airflow obstruction [abstract], *Am J Respir Crit Care Med*, 153: A879.

O'Shaughnessy TC, Ansari TW, Barnes NC and Jeffery PK 1997, Inflammation in bronchial biopsies of subjects with chronic bronchitis: inverse relationship of CD8+ T lymphocytes with FEV1, *Am J Respir Crit Care Med*, 155: 852-857.

Ochs M 2006, A brief update on lung stereology, *J Microscopy*, 222: 188-200.

Ordonez C, Ferrando R, Hyde DM, Wong HH and Fahy JV 2000, Epithelial desquamation in asthma: artifact or pathology?, *Am J Respir Crit Care Med*, 162: 2324-2329.

Pauwels RA, Buist AS, Calverley PMA, Jenkins CR and Hurd SS 2001, Global Strategy for the Diagnosis, Management, and Prevention of Chronic Obstructive Pulmonary Disease . NHLBI/WHO Global Initiative for Chronic Obstructive Lung Disease (GOLD) Workshop Summary, *Am J Respir Crit Care Med*, 163: 1256-1276.

Pauwels RA and Rabe KF 2004, Burden and clinical features of chronic obstructive pulmonary disease (COPD), *Lancet*, 364: 613-620.

Payne DN, Rogers AV, Adelroth E, Bandi V, Guntupalli KK, Bush A and Jeffery PK 2003, Early thickening of the reticular basement membrane in children with difficult asthma, *Am J Respir Crit Care Med*, 167: 78-82.

Payne DN, Qiu Y, Zhu J, Peachey L, Scallan M, Bush A and Jeffery PK 2004, Airway inflammation in children with difficult asthma: relationships with airflow limitation and persistent symptoms, *Thorax*, 59: 862-869.

Peterson DA 1999, Quantitative histology using confocal microscopy: implementation of unbiased stereology procedures, *Methods*, 18: 493-507.

Pohunek P, Warner JO, Turzikova J, Kudrmann J and Roche WR 2005, Markers of eosinophilic inflammation and tissue re-modelling in children before clinically diagnosed bronchial asthma, *Pediatr Allergy Immunol*, 16: 43-51.

Polito AJ and Proud D 1998, Epithelial cells as regulators of airway inflammation, , *J Allergy Clin Immunol*, 102: 714-718.

Poulter LW, Burke CM, Jarjour NN and Pyke SD 2000, Designing bronchial biopsy studies, *Respir Med*, 94 Suppl F: S3-8.

Puddicombe SM, Polosa R, Richter A, Krishna MT, Howarth PH, Holgate ST and Davies DE 2000, Involvement of the epidermal growth factor receptor in epithelial repair in asthma, *FASEB J*, 14: 1362-1374.

Redington AE, Springall DR, Ghatei MA, Lau LC, Bloom SR, Holgate ST, Polak JM and Howarth PH 1995, Endothelin in bronchoalveolar lavage fluid and its relation to airflow obstruction in asthma, *Am J Respir Crit Care Med*, 151: 1034-1039.

Robinson DS, Hamid Q, Ying S, Tsicopoulos A, Barkans J, Bentley AM, Corrigan C, Durham SR and Kay AB 1992, Predominant TH2-like bronchoalveolar T-lymphocyte population in atopic asthma, *N Engl J Med*, 326: 298-304.

Roche WR, Beasley R, Williams JH and Holgate ST 1989, Subepithelial fibrosis in the bronchi of asthmatics, *Lancet*, 1: 520-524.

Roche WR, Montefort S, Baker J and Holgate ST 1993, Cell adhesion molecules and the bronchial epithelium, *Am Rev Respir Dis*, 148: S79-82.

Saetta M, Di SA, Rosina C, Thiene G and Fabbri LM 1991, Quantitative structural analysis of peripheral airways and arteries in sudden fatal asthma, *Am Rev Respir Dis*, 143: 138-143.

Saetta M, Di SA, Maestrelli P, Ferraresso A, Drigo R, Potena A, Ciaccia A and Fabbri LM 1993, Activated T-lymphocytes and macrophages in bronchial mucosa of subjects with chronic bronchitis, *Am Rev Respir Dis*, 147: 301-306.

Saetta M, Di SA, Maestrelli P, Turato G, Ruggieri MP, Roggeri A, Calcagni P, Mapp CE, Ciaccia A and Fabbri LM 1994, Airway eosinophilia in chronic bronchitis during exacerbations, *Am J Respir Crit Care Med*, 150: 1646-1652.

Saetta M, Di SA, Maestrelli P, Turato G, Mapp CE, Pieno M, Zanguochi G, Del PG and Fabbri LM 1996, Airway eosinophilia and expression of interleukin-5 protein in asthma and in exacerbations of chronic bronchitis, *Clin Exp Allergy*, 26: 766-774.

Saetta M, Di SA, Turato G, Facchini FM, Corbino L, Mapp CE, Maestrelli P, Ciaccia A and Fabbri LM 1998, CD8+ T-lymphocytes in peripheral airways of smokers with chronic obstructive pulmonary disease, *Am J Respir Crit Care Med*, 157: 822-826.

Saper CB 1996, Any way you cut it: a new journal policy for the use of unbiased counting methods, *J Comp Neurol*, 364: 5.

Scherle W 1970, A simple method for volumetry of organs in quantitative stereology, *Mikroskopie*, 26: 57-60.

Silva JR, Jones JA, Cole PJ and Poulter LW 1989, The immunological component of the cellular inflammatory infiltrate in bronchiectasis, *Thorax*, 44: 668-673.

Soderberg M, Hellstrom S, Sandstrom T, Lundgren R and Bergh A 1990, Structural characterization of bronchial mucosal biopsies from healthy volunteers: a light and electron microscopical study, *Eur Respir J*, 3: 261-266.

Sohn SW, Chang YS, Lee HS, Chung DH, Lee CT, Kim YH, Kim YK, Min KU, Kim YY and Cho SH 2008, Atopy may be an important determinant of subepithelial fibrosis in subjects with asymptomatic airway hyperresponsiveness, *J Korean Med Sci*, 23: 390-396.

Sont JK, Willems LN, Evertse CE, Hooijer R, Sterk PJ and van Krieken JH 1997, Repeatability of measures of inflammatory cell number in bronchial biopsies in atopic asthma, *Eur Respir J*, 10: 2602-2608.

Sterio DC 1984, The unbiased estimation of number and sizes of arbitrary particles using the disector, *J Microsc*, 134: 127-136.

Stuart A 1984, *Basic ideas of scientific sampling*, Griffin, London.

Sullivan P, Stephens D, Ansari T, Costello J and Jeffery P 1998, Variation in the measurements of basement membrane thickness and inflammatory cell number in bronchial biopsies, *Eur Respir J*, 12: 811-815.

Tang ML, Wilson JW, Stewart AG and Royce SG 2006, Airway remodelling in asthma: current understanding and implications for future therapies, *Pharmacol Ther*, 112: 474-488.

ten Hacken NH, Aleva RM, Oosterhoff Y, Smith M, Kraan J, Postma DS and Timens W 1998, Submucosa 1.0 x 0.1 mm in size is sufficient to count inflammatory cell numbers in human airway biopsy specimens, *Mod Pathol*, 11: 292-294.

Thompson AB, Daughton D, Robbins RA, Ghafouri MA, Oehlerking M and Rennard SI 1989, Intraluminal airway inflammation in chronic bronchitis. Characterization and correlation with clinical parameters, *Am Rev Respir Dis*, 140: 1527-1537.

Thomson NC, Chaudhuri R and Livingston E 2004, Asthma and cigarette smoking, *Eur Respir J*, 24: 822-833.

Trifilieff A, El-Hashim A and Bertrand C 2000, Time course of inflammatory and remodeling events in a murine model of asthma: effect of steroid treatment, *Am J Physiol Lung Cell Mol Physiol*, 279: L1120-1128.

Vignola AM, Chanez P, Chiappara G, Merendino A, Pace E, Rizzo A, la Rocca AM, Bellia V, Bonsignore G and Bousquet J 1997, Transforming growth factor-beta expression in mucosal biopsies in asthma and chronic bronchitis, *Am J Respir Crit Care Med*, 156: 591-599.

Wang JH, Devalia JL, Xia C, Sapsford RJ and Davies RJ 1996, Expression of RANTES by human bronchial epithelial cells in vitro and in vivo and the effect of corticosteroids, *Am J Respir Cell Mol Biol*, 14: 27-35.

Ward C, Pais M, Bish R, Reid D, Feltis B, Johns D and Walters EH 2002, Airway inflammation, basement membrane thickening and bronchial hyperresponsiveness in asthma, *Thorax*, 57: 309-316.

Ward C, Reid DW, Orsida BE, Feltis B, Ryan VA, Johns DP and Walters EH 2005, Inter-relationships between airway inflammation, reticular basement membrane thickening and bronchial hyper-reactivity to methacholine in asthma; a systematic bronchoalveolar lavage and airway biopsy analysis, *Clin Exp Allergy*, 35: 1565-1571.

Weibel ER and Knight BW 1964, A morphometric study on the thickness of the pulmonary air-blood barrier, *J Cell Biol*, 21: 367-384.

Weibel ER 1990, 'Morphometry: stereological theory and practical methods', in *Models of lung disease: microscopy and structural methods*, J Gil, ed., Marcel Dekker, New York, pp. 199-252.

Weibel ER, Hsia CCW and Ochs M 2007, How much is there really? Why stereology is essential in lung morphometry, *J Appl Physiol*, 102: 459-467.

Wenzel SE, Schwartz LB, Langmack EL, Halliday JL, Trudeau JB, Gibbs RL and Chu HW 1999, Evidence that severe asthma can be divided pathologically into two inflammatory subtypes with distinct physiologic and clinical characteristics, *Am J Respir Crit Care Med*, 160: 1001-1008.

West MJ, Slomianka L and Gundersen HJ 1991, Unbiased stereological estimation of the total number of neurons in thesubdivisions of the rat hippocampus using the optical fractionator, *Anat Rec*, 231: 482-497.

West MJ, Ostergaard K, Andreassen OA and Finsen B 1996, Estimation of the number of somatostatin neurons in the striatum: an in situ hybridization study using the optical fractionator method, *J Comp Neurol*, 370: 11-22.

Wicksell SD 1925, The corpuscle problem. A mathematical study of a biometric problem., *Biometrika*, 17: 84-99.

Wilson JW and Li X 1997, The measurement of reticular basement membrane and submucosal collagen in the asthmatic airway, *Clin Exp Allergy*, 27: 363-371.

Wulfsohn D, Nyengaard JR and Tang Y 2004, Postnatal growth of cardiomyocytes in the left ventricle of the rat, *Anat Rec A Discov Mol Cell Evol Biol*, 277: 236-247.

Zar JH 1999, *Biostatistical analysis*, 4th edn, Prentice Hall, New Jersey.

Own Publications

This thesis appeared in part in the following publications:

Bratu V, Erpenbeck V, Fehrenbach A, Rausch T, Krug N, Hohlfeld J and Fehrenbach H 2007, Comparison of 3D versus 2D morphometry for cell counting in human endobronchial biopsies, *Eur Respir J*, 30 Suppl 51: P894.

Bratu V, Erpenbeck V, Fehrenbach A, Rausch T, Krug N, Hohlfeld J and Fehrenbach H 2008, Comparison of 3D versus 2D morphometry for cell counting in human endobronchial biopsies, 44 p, manuscript in preparation.

Table of Academic Teachers

My academic teachers were Ladies and Gentlemen

of Carol Davila University of Medicine and Pharmacy in Bucharest / Romania:
Albu, Ardeleanu, Bâră, Bălănescu, Boiangiu, Ciornei, Constantinescu, Debeleac, Dinu, Dorobanțu, Dumitrache, Eremia, Fulga, Georgescu, Ganea, Iamandescu, Marcu, Mohora, Naghi, Nicolescu, Rădulescu, Sfetea, Spircu, Voicu, Voiculescu

of Philipps University in Marburg / Germany:
Arnold, Baum, Bertalanffy, Bien, Christiansen, Czubayko, Dünne, Fehrenbach, Gotzen, Happle, Hertl, Hofmann, Kann, Krieg, Kroll, Kühnert, Maier, Maisch, Moosdorf, Mutters, Müller, Neubauer, Oertel, Remschmidt, Rothmund, Schmidt, Sekundo, Seyberth, Wagner, Werner, Wulf

of German Red Cross Hospital in Kassel / Germany (Teaching Hospital of Philipps University Marburg):
Braun, Del Barba, Franke, Hesterberg, Hillejan, Höpfner, Löser, Schrader, Spuck, Zeiger

of University Hospital in Basel / Switzerland:
Bongartz, Landmann, Müller, Radü, Steinbrich

Acknowledgements

It is a pleasure to thank the many people who made this thesis possible.

It is difficult to overstate my gratitude to my supervisor, Prof. Dr. Heinz Fehrenbach. With his enthusiasm, his inspiration and his great efforts to explain things clearly and simply, he helped me to discover and explore the fascinating field of microscopical morphometry. Throughout my professionally and personally cumbersome thesis-writing period he abundandtly provided encouragement, sound advice, an enormous patience, exemplary supervision, good company from afar and lots of good ideas. There are certainly many tempting wrong paths I would have gone without him and his ability to see things from a different angle.

I am especially grateful to the Department of Clinical Airway Research of Fraunhofer ITEM Hannover – Germany under the direction of Prof. Dr. Norbert Krug and Prof. Dr. Jens Hohlfeld for providing the bioptic material of this study.

I would like to thank Dr. Antonia Fehrenbach for the familiarisation with the practical implementation of stereological methods and the comprehensive CAST-Grid 2.01 training. To Dr. Ali Önder Yildirim I am thankful for his constructive remarks and suggestions during the histological assessment of the specimens. I wish to thank in addition Mr. Robert Prinz for the tutorial on the application of the physical disector.

I am indebted to Mrs. Tanja Rausch for the outstanding technical support and briefing on embedding, sectioning and staining of the specimens. In addition I wish to thank Mrs. Roswitha Naumann for the relaxing, entertaining and delicious breakfasts.

I am grateful to the Institute of Pathology of University Hospital Marburg and Gießen, Marburg – Germany for allowing the specimens to be embedded in their automated embedder Tissue-Tek VIP. I am also grateful to the Institute of Biometrics and

Epidemiology of Philipps University Marburg – Germany, especially to Mrs. Nina Timmesfeld for the suggestions on the statistical analyses of the data.

I would like to thank Prof. Dr. Hans Jørgen Gundersen, Prof. Dr. Jens Randel Nyengaard, Prof. Dr. Matthias Ochs and Prof. Dr. Dallas Hyde for the excellent stereological training during the 21st ISS-ERS European Stereology Course 2006 and the helpful pieces of advice on practical problems and the data processing.

I am grateful to Dr. Leopold Winter for his constructive remarks on the German summary of this thesis, his constant encouragement and support on a professional and personal level.

I am indebted to the many people who made huge contributions to my knowledge pack and professional education but especially to: my first math teacher Mrs. Georgeta Ghiciu, my high school chemistry teacher Mrs. Maria Ivanov Puzderică and my biochemistry teacher Prof. Dr. Maria Mohora.

I wish to thank my best friend as an undergraduate Elena Floareş for helping me to start learning German, the entertainment and support she provided, all without which my graduation and this doctoral thesis in Marburg would not have been possible.
I also wish to thank my best friend Anca Ciobanu Saadatkhah for helping me get through the difficult times, take the right decisions when in doubt and for all the emotional support, comraderie and caring she unconditionally provided.

Lastly and most importantly, I wish to thank my parents Viorica Bratu and Florentin Daniel Bratu for raising me, teaching me, loving me and supporting me to attain all my goals. Without them my university education in Bucharest, Marburg, Basel and this thesis would not have been possible.